bioRxiv preprint doi: https://doi.org/10.64898/2026.10.09.752918; this version posted October 16, 2026. The copyright holder for this preprint (which was not certified by peer review) is the author/funder, who has granted bioRxiv a license to display the preprint in perpetuity. It is made available under a CC-BY 4.0 International license.

The Hox code abolishes anatomical variation in an insect gonad

Jonchee A. Kao[1,2 #], Tarun Kumar[3,4 # *], Daniella A. Haber[1], Cassandra G. Extavour[1,3,4 *]

1. Department of Molecular and Cellular Biology, Harvard University, Cambridge MA, USA
2. Current address: Graduate School of Agriculture, Division of Applied Biosciences, Kyoto University, Japan
3. Department of Organismic and Evolutionary Biology, Harvard University, Cambridge MA, USA
4. Howard Hughes Medical Institute, Chevy Chase, MD, USA

# indicates equal contribution

* correspondence: tkumar@fas.harvard.edu, extavour@oeb.harvard.edu

bioRxiv preprint doi: https://doi.org/10.64898/2026.10.09.752918; this version posted October 16, 2026. The copyright holder for this preprint (which was not certified by peer review) is the author/funder, who has granted bioRxiv a license to display the preprint in perpetuity. It is made available under a CC-BY 4.0 International license.

Abstract

Phenotypic traits can vary based on genes or environment. Nevertheless, some quantitative traits remain invariant. Understanding the developmental mechanisms that generate such invariance can reveal how phenotypic robustness evolves. Insect reproductive capacity is largely determined by the number of gamete-producing subunits within the gonad, providing a tractable system to investigate these mechanisms as they operate on a quantitative trait that impacts fitness. In most insects, gonad subunit number varies within and between species. Here, we investigate gonad development in the milkweed bug *Oncopeltus fasciatus*, wherein subunit number is invariant. We show that subunit number is established during embryogenesis, when some abdominal segments, but not others, specify somatic gonad precursors. The position and number of these precursors depend on segment identity, and experimentally modified segment number or Hox-mediated segment identity changes the number of gonad subunits. Thus, *O. fasciatus* establishes invariant subunit number by coupling gonad development to segmental patterning machinery. We propose that co-option of the Hox code provides a developmental mechanism for generating robustness in gonad subunit number and may thereby contribute to the evolution of reproductive capacity in other insects.

Keywords: milkweed bug, *Oncopeltus fasciatus*, ovary, ovariole, testis, *Ultrabithorax*

bioRxiv preprint doi: https://doi.org/10.64898/2026.10.09.752918; this version posted October 16, 2026. The copyright holder for this preprint (which was not certified by peer review) is the author/funder, who has granted bioRxiv a license to display the preprint in perpetuity. It is made available under a CC-BY 4.0 International license.

Introduction

Developmental processes can produce highly stereotypic and reproducible anatomical structures despite genetic, environmental, and stochastic variation [1]. Standing variation is often considered a prerequisite for evolutionary change [2,3]. Likewise, evolvability can correlate positively with adaptability [4], leading to the prediction that some level of trait variation should be favoured by natural selection [5]. Nevertheless, some traits show remarkably little variation between or even within lineages [6,7], even traits that, if changed, might be predicted to increase organismal fitness [8].

Reproductive organ formation depends on multiple morphogenetic processes, including cell specification [9–12], migration [13–15], proliferation [16,17], and differentiation [9], each of which can vary within and between species [18–27]. Understanding how developmental mechanisms buffer variation and generate consistent phenotypes is central to understanding such phenotypic robustness [1]. Here we address this problem using a quantitative trait that can directly impact reproductive capacity and therefore fitness: insect ovariole and testiole number.

All insects have paired gonads composed of functional subunits called ovarioles in females and testioles, testicular follicles, or sperm tubes in males [28–30] . In this work, we collectively call these subunits “gonadioles”. Between species, the number of gonadioles varies from one to many hundreds per gonad [8] (Figure 1A). Within species, gonadiole number usually also exhibits species-specific variation, on the order of 10% of the mean [8,28,31]. However, some species show invariant gonadiole numbers [8] (Figure 1A), providing an example of phenotypic robustness. Gonadiole number therefore provides a tractable system for investigating how developmental mechanisms can either promote phenotypic variation, or constrain it, yielding robustness.

Most developmental studies of gonadiole number have focused on ovariole number in *Drosophila* (Diptera) species of fruit flies. Amongst these species, mean ovariole number, though genetically regulated and therefore heritable [18,32–39], also shows within-species variation, including species-specific phenotypic plasticity with temperature [40–42], altitudinal and latitudinal clines[42–48] and nutritional conditions [31,41,49].

The developmental regulation of ovariole number variation in *Drosophila melanogaster* begins with establishment of the embryonic gonad, which consists of both

bioRxiv preprint doi: https://doi.org/10.64898/2026.10.09.752918; this version posted October 16, 2026. The copyright holder for this preprint (which was not certified by peer review) is the author/funder, who has granted bioRxiv a license to display the preprint in perpetuity. It is made available under a CC-BY 4.0 International license.

germ cells and somatic gonadal precursors (SGPs) [9]. Primordial germ cells form at the posterior of the early embryo [50] and subsequently migrate through the embryo [13] to associate with SGPs derived principally from the mesoderm of parasegments 10–12 [9,51]. These cells coalesce to form the embryonic gonad [9,52,53]. During late larval development, a subset of somatic ovarian cells form multicellular structures called terminal filaments at the anterior of the ovary [54,55]. Each terminal filament leads to the establishment of one mature ovariole, making larval terminal filament number a determinant of adult ovariole number [55,56].

Variation in adult ovariole number in *Drosophila* can be caused by developmental variation in almost any stage of ovarian development, including the specification and proliferation of somatic gonadal precursors [19], the allocation of somatic cells to the terminal-filament lineage [18,19,41], and the number of cells incorporated into each terminal filament [38,41]. Differences in these processes contribute to ovariole-number variation within and between *Drosophila* lineages [18,19,31,38,41].

Much less is known about the developmental regulation of the invariant ovariole number seen in other insects. Classical embryological studies suggest that some ametabolous insects establish ovariole primordia in defined abdominal segments, such that the number of contributing segments corresponds to the adult ovariole number [57,58]. Similarly, in the European fire bug *Pyrrhocoris apterus* (Hemiptera), eight pairs of gonadiole primordia reportedly form in abdominal segments A1–A8 [59]. The A1 primordia subsequently degenerate, leaving seven gonadioles on each side [59]. These observations suggest a relationship between segmental organization and gonadiole number, but the mechanisms that might specify the identity and number of gonad-forming segments remain unknown.

The milkweed bug *Oncopeltus fasciatus* provides an opportunity to investigate these mechanisms genetically. Adult females possess seven ovarioles per ovary, and adult males possess seven testioles per testis [60,61], with no variation in gonadiole number reported in the literature [60,61], nor observed in our laboratory over hundreds of adult dissections. The gonadioles in both sexes are reported to be established by hatching, suggesting that their number is determined during embryogenesis [60,61].

bioRxiv preprint doi: https://doi.org/10.64898/2026.10.09.752918; this version posted October 16, 2026. The copyright holder for this preprint (which was not certified by peer review) is the author/funder, who has granted bioRxiv a license to display the preprint in perpetuity. It is made available under a CC-BY 4.0 International license.

Here, we examine germline and somatic gonad development in *O. fasciatus*. We provide evidence that instead of using the *D. melanogaster* mechanism of variable postembryonic cellular organisation within the gonad, *O. fasciatus* co-opts embryonic segment identity programs to produce an invariant number of gonadioles per gonad. We propose that this developmental coupling of body plan and gonadal organization provides robustness to this reproductive trait, and may represent a more general mechanism for establishing invariance in organ system anatomies.

Results

Gonadiole number in Oncopeltus fasciatus *is established during embryogenesis*

Adult *Oncopeltus fasciatus* have seven ovarioles per ovary and seven testioles per testis (Figure 1A–B), with no intra-species variation in gonadiole number [60,61] (Tables S1, S4). To determine when adult gonadiole number is established during development, we examined gonads at progressively earlier developmental stages, identifying nymphal instars based on characteristic wing morphology [62]. We observed seven testioles (Figure 1C) and seven ovarioles (Figure 1D) in all five nymphal instars, suggesting that gonadiole number is established during embryogenesis.

We next examined embryonic gonad development using previously defined developmental stages [63], further adapted for this study (Figure S1A; Table S2). By late stage 15 (approximately 60% of the way through embryogenesis, just over two days before hatching), seven distinct gonadiole primordia associated with primordial germ cells (PGCs) were evident (Figure 1E), confirming that the seven gonadioles are established during embryogenesis. We discovered that acetylated Tubulin, a post-translationally modified form of Tubulin associated with stable, long-lived microtubules [64,65], was enriched at the distal tips of each of the seven embryonic gonadiole primordia (Figure 1E). Using acetylated Tubulin as a marker of gonadioles, we then examined earlier embryonic stages. The earliest stage at which we detected acetylated Tubulin associated with these structures was stage 12, at which point individual gonadiole primordia were already distinguishable (Figure S1B, white arrowheads).

bioRxiv preprint doi: https://doi.org/10.64898/2026.10.09.752918; this version posted October 16, 2026. The copyright holder for this preprint (which was not certified by peer review) is the author/funder, who has granted bioRxiv a license to display the preprint in perpetuity. It is made available under a CC-BY 4.0 International license.

130 *Segment-specific mesodermal expression domains of* O. fasciatus traffic jam *and*
131 tinman *orthologs form the somatic gonad precursors.*
132 To identify potential molecular markers for the gonadiole primordia at earlier
133 stages, we examined the embryonic expression of the *O. fasciatus* homologs of genes
134 expressed in or near the embryonic somatic gonad in *D. melanogaster* (Figure 2, Figure
135 S1C–D, Table S3; also see Methods). In *D. melanogaster*, *tinman* (*tin*) expression is
136 required for the specification of the somatic gonad precursors (SGPs) from the
137 abdominal mesoderm of parasegments 10, 11 and 12 [53,66], and is also expressed in the
138 dorsal vessel spanning segments T2–A6 [67–69]. All embryonic SGPs in *D. melanogaster*
139 express Traffic jam (Tj) protein [70], and Tj-positive somatic cells are intermingled with the
140 germ cells throughout larval development [70,71]. We found that in *O. fasciatus* late stage
141 15 (S15l) embryos, each putative gonadiole primordium appeared to consist of
142 mesodermal regions with distinct gene expression profiles: a lateral domain expressing
143 *Ofas-tin* and a medial domain expressing *Ofas-tj* (Figure 2M–M”). To characterize the
144 emergence and morphogenesis of these domains, we examined *Ofas-tin* and *Ofas-tj*
145 expression throughout embryogenesis (Figure 2).
146 We first detected *Ofas-tin* expression at stage 8 in segmentally repeated
147 domains along the lateral margins of the mesoderm (Figure 2A; white arrowheads),
148 coincident with the formation of coelomic cavities. These primary expression domains
149 appeared sequentially from anterior to posterior, beginning in the labial segment (Figure
150 S2A, A′; white arrowheads). During stage 8, a second *Ofas-tin*-expressing domain
151 emerged sequentially only in abdominal segments A1–A7 (Figure 2A′; white
152 arrowhead), positioned anterior and medial to the primary *Ofas-tin* domain within each
153 segment. At the same stage, we detected mesodermal *Ofas-tj* expression appearing
154 sequentially in the posterior compartments based on co-expression with the *O. fasciatus*
155 ortholog of *invected* (*Ofas-inv*) [72] of segments A1–A6 (Figure 2A′; white arrow), but not
156 in the head or thoracic segments (Figure S2A, A″). By early stage 9, secondary *Ofas-tj*-
157 expressing domains emerged immediately adjacent to the secondary *Ofas-tin* domains
158 (Figure 2B, B′–B″; white arrows). By the end of stage 9, the initially separated medial
159 secondary *Ofas-tj*- and lateral *Ofas-tin*-expressing domains formed seven repeated

bioRxiv preprint doi: https://doi.org/10.64898/2026.10.09.752918; this version posted October 16, 2026. The copyright holder for this preprint (which was not certified by peer review) is the author/funder, who has granted bioRxiv a license to display the preprint in perpetuity. It is made available under a CC-BY 4.0 International license.

160 *Ofas-tin* and *Ofas-tj* units along the anteroposterior (AP) axis in segments A1–A7
161 (Figure 2C, C′; white arrowhead).
162 At stage 10, the *Ofas-tj*-expressing domains in A2–A7 expanded anteriorly and
163 appeared contiguous along the AP axis (Figure 2D–D′; white arrows). In contrast, the
164 A1 *Ofas-tj* domain was not comparably anteriorly expanded (Figure 2D–D′). At stage 11,
165 the secondary *Ofas-tin*-expressing domains also appeared expanded and were
166 connected with each other, resulting in contiguous *Ofas-tin*- and *Ofas-tj*-expressing
167 domains associated with seven repeated structures, one in each of segments A1 to A7
168 (Figure 2E, E′; white arrowheads).
169 At stage 12, we detected *Ofas-tin* expression along each lateral side of the
170 embryo from the labial segment to the posterior abdomen (Figure 2F; DV). We refer to
171 these as longitudinal *Ofas-tin*-expressing domains, and interpret them as being derived
172 from the primary *Ofas-tin* domains first observed at stage 8 (Figure 2A; white
173 arrowheads). We speculate that these longitudinal *Ofas-tin*-expressing domains may
174 correspond to the developing dorsal vessel (Figure 2F–G; DV). In addition, seven tube-
175 like *Ofas-tin*-expressing structures, corresponding spatially to the earlier secondary
176 *Ofas-tin* domains, extended medially from the longitudinal *tin*-expressing domains
177 (Figure 2F, F′; asterisks).
178 During stages 13–14, as the embryo further shortened and widened, the lateral
179 ends of the tube-like *Ofas-tin* expression domains became tapered while remaining
180 connected laterally to the longitudinal *Ofas-tin*-expressing domain (Figure 2G–I; white
181 arrowheads in G–G′). We interpret these tube-like *Ofas-tin*-expressing domains as
182 gonadiole primordia, noting that they are associated with PGCs and also correspond
183 spatially to the region enriched in acetylated Tubulin in each segment (Figure 2M–M″).
184 We therefore considered this connected group of tube-like *Ofas-tin* and *Ofas-tj*-
185 expressing cells to be the embryonic gonad primordium.
186 The embryonic gonad primordium initially formed in the dorsal mesoderm of the
187 embryo (Figure 2A’’–F’’) and extended across abdominal segments A1–A7 up to stage
188 12 (Figure 2F). Following katatrepsis (stage 13) and during dorsal closure (stage 14
189 onward), it progressively condensed along the AP axis (Figure 2G–J). During this
190 process, the lateral ends of the *Ofas-tin*-positive structures appeared to shift anteriorly

bioRxiv preprint doi: https://doi.org/10.64898/2026.10.09.752918; this version posted October 16, 2026. The copyright holder for this preprint (which was not certified by peer review) is the author/funder, who has granted bioRxiv a license to display the preprint in perpetuity. It is made available under a CC-BY 4.0 International license.

and converge (Figure 2K). The morphology and final position of these structures are consistent with their contribution to the previously described suspensory ligaments that connect the gonads to the thoracic body wall [61]. Concurrently, the seven gonadiole primordia became bundled and reoriented approximately parallel to the AP axis (Figure 2K). Nearly two days prior to hatching (stage 16l), each embryonic gonad had condensed to lie almost entirely within segment A2, excluding the suspensory ligaments and primordial gonoduct (Figure 2L). We detected no consistent differences in morphology or in *Ofas-tin* or *Ofas-tj* expression that were suggestive of sexual dimorphism from stage 8 through late stage 16 (nearly two days before hatching), consistent with previous reports that sexual differentiation of the gonads is not apparent during these embryonic stages [73].

Ofas-tin *and* Ofas-tj *expression patterns are mutually independent in gonadiole-forming domains, and neither is required for gonadiole formation.*

Because gonadiole primordia comprise cells associated with both the *Ofas-tin* and *Ofas-tj* expression domains (Figure 2), we wished to determine whether reduction of one or both genes would disrupt gonadiole primordia formation. We therefore performed embryonic RNA interference (eRNAi) targeting *Ofas-tin* and *Ofas-tj* individually (Figure 3A–C″) or simultaneously (Figure 3D–G″), and confirmed reduction of target transcript with hybridisation chain reaction (HCR) (Figure S3). These experiments yielded two major results relevant to gonadiole number determination. First, we found that expression of these two genes in gonadiole primordia was mutually independent. Following *Ofas-tin* RNAi, the *Ofas-tj* expression domains, organized into seven primordia, remained detectable at stage 13 in all embryos examined (*n* = 135/135; Figures 3B, S6A; Tables S4, S5), and formed primordia comparable to those observed in eRNAi control embryos (*n* = 209/209; Figures 3A, S6A; Tables S4, S5). Similarly, *Ofas-tin* expression remained detectable following *Ofas-tj* eRNAi (*n* = 41/41; Figures 3C, S6A; Tables S4, S5), organized into seven primordia. In both eRNAi conditions, however, knockdown appeared incomplete, based on faint expression of the targeted gene detected with HCR (Figure 3B′–C″; white arrowheads). Thus, these results indicate that partial reduction of *Ofas-tin* or *Ofas-tj* expression does not abolish

bioRxiv preprint doi: https://doi.org/10.64898/2026.10.09.752918; this version posted October 16, 2026. The copyright holder for this preprint (which was not certified by peer review) is the author/funder, who has granted bioRxiv a license to display the preprint in perpetuity. It is made available under a CC-BY 4.0 International license.

the expression domain of the other gene, although the incomplete knockdown precludes us from excluding a requirement for *Ofas-tin* or *Ofas-tj* in establishing or maintaining the respective expression domains.

Second, we observed that in both single knockdown conditions, seven gonadiole primordia remained identifiable (Figure 3E–E″, F–F″; S5). In the double knockdown condition, expression of both genes remained detectable with HCR, albeit at lower levels than in controls, and we could also still detect formed gonadiole structures (Figure 3G–G’’). However, because of the residual expression noted above (Figure 3E’, F”, G’–G″; white arrowheads), we cannot rule out the possibility that complete loss of *Ofas-tin* and *Ofas-tj* would disrupt gonadiole primordia specification or formation.

Germ cells populate the gonad after gonadiole primordia formation.

The *O. fasciatus* embryonic gonad at stage 15 comprises two cell populations: the somatic gonad precursors and the PGCs (Figure 2M–M”). PGCs are first observed at the cellular blastoderm stage (Table S2; stage 3). We [21] and others [74] previously described the location of PGC emergence as being immediately inside the posterior pit, which is an indentation at the ventral posterior of the blastoderm into which the germ band invaginates during its formation. PGCs then migrate towards the anterior, along the dorsal side of the germ band [21,63,74,75]. By stage 8, most PGCs are organised into segmental clusters, with one cluster located in each of abdominal segments A4–A6; many embryos also have an additional cluster in A7 (Figure 4A). At stage 9, coincident with neuroectodermal invagination, each cluster separates bilaterally along the ventral midline, to yield a total of six to eight clusters, one in each hemisegment of A4 through A6 or A7 (Figure 4B–C). During stages 10–12, the clusters on each of the left and right sides of the embryo merge to form two longitudinal groups of PGCs oriented parallel to the AP axis (Figure 4D–F), spanning abdominal segments A4–A6. By stage 13, small numbers of cells from these longitudinal groups begin to appear in columnar formations perpendicular to the AP axis of the embryo (Figure 4G; asterisks). By early stage 15, seven distinct such columnar groups of PGCs are distinguishable (Figure 4H; asterisks). In contrast, the seven somatic gonadiole primordia are already established by late stage 9, including in segments A1–A3 (Figure 2C), where PGCs are not present (Figure 4C).

bioRxiv preprint doi: https://doi.org/10.64898/2026.10.09.752918; this version posted October 16, 2026. The copyright holder for this preprint (which was not certified by peer review) is the author/funder, who has granted bioRxiv a license to display the preprint in perpetuity. It is made available under a CC-BY 4.0 International license.

Thus, the seven somatic gonadiole primordia are established before PGCs become organised into seven corresponding groups. This temporal sequence suggests that PGCs are unlikely to determine gonadiole number.

To ask whether PGCs influenced gonadiole morphogenesis or final gonadiole number determination, we used RNAi to abrogate the function of the *O. fasciatus* homolog of the *vasa* gene (*Ofas-vas*), which is required for survival of many [76,77] (but not all; see [22,78]) studied animal germ cells [24]. *Ofas-vas* is expressed throughout embryonic development (Figure S4A), with its transcript detectable at low levels in most embryonic cells, and at somewhat higher levels in PGCs [21,75]. Ofas-Vas protein is specifically detectable in PGCs during their formation, migration, and gonad coalescence [63]. We found that depletion of *Ofas-vas*, either embryonically (eRNAi; efficacy confirmed by assessment of Ofas-Vas protein expression; Figure S6B; Table S6) or maternally (through depletion in adult parental females, pRNAi; efficacy confirmed by Ofas-Vas protein expression; Figure S6B; Table S6), did not appear to alter PGC organisation (Figures 4J–J′, S4C–C′), and did not change gonadiole number (eRNAi *n* = 32/32; pRNAi *n* = 12/12; Figures 4J–J’, S4C–C’, S6A; Tables S4, S7). Though we did not detect Ofas-Vas expression in *Ofas-vas* RNAi embryos (Figures 4J’, S4C,S6B; Table S6), we were nonetheless able to identify PGCs based on their low levels of acetylated Tubulin expression (Figure S4C-C’). *Ofas-vas* function therefore appears dispensable for the correct establishment of seven gonadiole primordia. However, because, as previously reported [79], PGCs were not eliminated by *Ofas-vas* RNAi (Figure S4C–C’), we cannot formally exclude a role for PGCs in this process.

Reduction of gonadiole-producing segments leads to fewer gonadiole primordia.

Our observation of *Ofas-tin* and *Ofas-tj* expression in segmentally repeated groups of somatic gonadiole primordia suggested that the number of gonadiole-producing segments might determine the number of gonadioles formed. We therefore hypothesised that reducing the number of these segments would reduce gonadiole primordium number. To test this hypothesis, we examined somatic gonad development following two distinct perturbations of the segmentation gene regulatory network.

bioRxiv preprint doi: https://doi.org/10.64898/2026.10.09.752918; this version posted October 16, 2026. The copyright holder for this preprint (which was not certified by peer review) is the author/funder, who has granted bioRxiv a license to display the preprint in perpetuity. It is made available under a CC-BY 4.0 International license.

First, we knocked down the *O. fasciatus* homolog of the gap gene *giant* (*gt*) [80]. Gap genes are expressed in and required for the specification of contiguous regions of the insect body plan, and disruption of their function can result in the loss of groups of adjacent segments [81–83]. In *O. fasciatus*, the first four abdominal segments (A1–A4) are missing in *Ofas-gt* knockdown embryos [80]. Because A1–A4 normally contribute four of the seven segmentally repeated gonadiole primordia, we predicted that their loss would reduce the number of gonadiole primordia. Consistent with this prediction, stage 13 *Ofas-gt* dsRNA-injected embryos (eRNAi) showed both reduced numbers of abdominal segments (Figures 5B–C, S6B; Table S6) as previously reported [80], and a reduction in gonadiole primordium number that corresponded to the reduced number of abdominal segments (*n* = 40/91; Figures 5A–C, S6A; Tables S4, S5).

Second, we examined gonadiole primordium number in *O. fasciatus* mutants homozygous for a previously generated hypomorphic *Ofas-Blimp1*$^{22\text{-}12}$ allele, which is predicted to yield a non-functional protein product missing the zinc finger domains [84]. In embryos of these mutants, the segment pairs T1/T2, T3/A1, A2/A3, A4/A5 and A7–A10 are consistently fused, while A6 is sometimes unaffected, and sometimes incorporated into the A7–A10 fusion [84]. We found that at stage 13, homozygous *Ofas-Blimp1* mutant embryos contained only two to four gonadiole primordia (*n* = 56/56; Figures 5D–F, S6A; Table S4), and had reduced numbers of abdominal segments (Figures 5E-F, S6B; Table S6) as previously reported [84]. The relationship between the number of morphologically distinguishable segments and gonadiole number was less pronounced in *Ofas-Blimp1* mutants (Figure 5F) than following *Ofas-gt* knockdown (Figure 5C). One possible explanation is that fusion between adjacent segments alters or produces variable segmental identities, such that the number of morphologically distinguishable segments does not directly reflect the number or identity of segmental domains competent to produce gonadiole primordia. Together these findings support a model in which the segmental organisation of the embryo establishes the repeated somatic gonadal units that determine the final number of gonadioles. Thus, loss of any of segments A1–A7 results in correspondingly fewer gonadiole primordia.

bioRxiv preprint doi: https://doi.org/10.64898/2026.10.09.752918; this version posted October 16, 2026. The copyright holder for this preprint (which was not certified by peer review) is the author/funder, who has granted bioRxiv a license to display the preprint in perpetuity. It is made available under a CC-BY 4.0 International license.

Posterior Hox genes regulate gonadiole primordium formation.

Our observations of wild type embryos and of embryos with abnormal numbers of abdominal segments suggested that the segmental organisation of the embryo establishes the repeated somatic gonadal units that determine the final number of gonadioles. Further, the restriction of gonadiole primordia to A1–A7 suggested that segmental identity may determine whether a segment is competent to form a gonadiole primordium. The conserved role of Hox genes in specifying regional identity along the AP axis of animals [85] led us to hypothesise that they might be involved in conferring this competence upon some, but not all, abdominal segments in *O. fasciatus*. Previous work showed that , the posterior Hox genes *Ultrabithorax* (*Ofas-Ubx*), *abdominal A* (*Ofas-abd-A*) and *Abdominal B* (*Ofas-Abd-B*) pattern the *O. fasciatus* abdomen [86], and we detected their expression in the abdominal mesoderm before and during gonadiole primordium formation (Figures 6A, S5A–B). We therefore asked whether these genes regulate the segment-specific formation of gonadiole primordia.

We individually depleted *Ofas-Ubx*, *Ofas-abd-A* and *Ofas-Abd-B* using eRNAi. We confirmed the efficacy of eRNAi based on homeotic transformations observed in the RNAi embryos (Figure S6B; Table S6). In *Ofas-Ubx* knockdown embryos, the secondary *Ofas-tin* and both *Ofas-tj* domains were not detected at early stage 9 in A1 or A2 (Figure 6G), and gonadiole primordia were also absent from A1 and A2 at stage 13, resulting in five gonadiole primordia (*n* = 34/56; Figures 6C, S6A; Tables S4, S5). In contrast, *Ofas-Abd-B* knockdown resulted in ectopic *Ofas-tin* and *Ofas-tj* expression domains in A8 and A9 at stage 9 (Figure 6I), and ectopic gonadiole primordia in A8–A10 at stage 13, producing a total of ten gonadiole primordia (*n* = 23/60; Figures 6E, S6A; Tables S4). Despite their abnormal gonadiole numbers, however, the primordial gonads of *Ofas-Ubx* and *Ofas-Abd-B* eRNAi embryos underwent normal coalescence (Figure 6J–L).

Depletion of *Ofas-abd-A* alone had little apparent effect on gonadiole primordium formation, with seven gonadiole primordia observed in nearly all embryos (*n* = 86/87; Figures 6D, S6A; Tables S4). A previous study provided evidence that *Ofas-abd-A* knockdown leads to expansion of *Ofas-Ubx* expression domain into posterior abdominal segments, a phenomenon known as posterior prevalence [87–90] This results in formation

bioRxiv preprint doi: https://doi.org/10.64898/2026.10.09.752918; this version posted October 16, 2026. The copyright holder for this preprint (which was not certified by peer review) is the author/funder, who has granted bioRxiv a license to display the preprint in perpetuity. It is made available under a CC-BY 4.0 International license.

of ectopic legs (which are normally only formed in the thorax) in abdominal segments A2–A8 [86]. We therefore hypothesised that *Ofas-abd-A* RNAi embryos generate gonadiole primordia in A2–A7 because *Ofas-Ubx* expression expands posteriorly and promotes their development. This hypothesis predicts that *Ofas-abd-A* and *Ofas-Ubx* might play overlapping or redundant functions in promoting gonadiole primordium formation. To test this prediction, we performed double eRNAi for *Ofas-Ubx* and *Ofas-abd-A* simultaneously. In contrast to either single knockdown, combined depletion of these two genes resulted in complete loss of the secondary *Ofas-tin* and *Ofas-tj* expression domains at stage 11 (Figure S5O–R), and loss of gonadiole primordia at stage 13 (*n* = 102/112; Figures 6M–P, S6A; Tables S4). However, the longitudinal *Ofas-tin* expression domain that likely corresponds to the developing dorsal vessel appeared unaffected (Figures 6M–P, S5O–R; Tables S4). We conclude that *Ofas-Ubx* and *Ofas-abd-A* are specifically required for the *Ofas-tin* and *Ofas-tj*-expressing domains associated with gonadiole primordium formation, but not for the primary *Ofas-tin*-expressing domain.

The results of parental RNAi (pRNAi) experiments were consistent with those of the embryonic RNAi experiments with respect to the segments in which gonadiole primordium formation was affected (Figures S5C–F, S6A; Table S4, S7). In nymphs produced by injected mothers, we observed morphological defects consistent with the homeotic transformations reported in previous studies of Hox genes using pRNAi (Figure S5G–L) [86]. These transformations were weaker than those observed with eRNAi (Figures S5C–F, S6A-B; Tables S4 S6). Accordingly, for example, in A1 of *Ofas-Ubx* pRNAi embryos, we observed gonadiole primordia that appeared incomplete, or disconnected from the rest of the primordia at stages when control embryos had all seven primordia linked through their *Ofas-tj* domain (*n* = 25/25 had seven gonadioles that were at least partially formed, but 11/25 of these were disconnected in A1; Figures S5D, S6A; Table S4). Similarly, in A8 and A9 of *Ofas-Abd-B* pRNAi embryos, we observed gonadiole primordia in 5/16 embryos, but in all of these embryos, the gonadiole primordia appeared incomplete (Figures S5F, S6A; Table S4).

The *O. fasciatus* ortholog of the Hox gene *Antennapedia* (*Ofas-Antp*) is expressed predominantly in the thoracic segments immediately anterior to the *Ofas-Ubx*

bioRxiv preprint doi: https://doi.org/10.64898/2026.10.09.752918; this version posted October 16, 2026. The copyright holder for this preprint (which was not certified by peer review) is the author/funder, who has granted bioRxiv a license to display the preprint in perpetuity. It is made available under a CC-BY 4.0 International license.

domain [86]. Based on the principle of posterior prevalence, *Ofas-Antp* expression is predicted to expand into segments A1–A2 upon *Ofas-Ubx* knockdown. Thus, the loss of gonadiole primordia from A1–A2 in the *Ofas-Ubx* condition (Figure 6C, G) could result either from the loss of a primordium-promoting function of *Ofas-Ubx* in A1–A2, or to the gain of a primordium-suppressing function of *Ofas-Antp* in those segments. To try to distinguish between these alternatives, we knocked down *Ofas-Antp* with eRNAi. We found that depletion of *Ofas-Antp* did not affect gonadiole primordium formation, either alone (*n* = 35/35; Figures S5M-N, S6A; Tables S4), or in combination with *Ofas-Ubx* knockdown (*n* = 7/42 had seven gonadioles, while n = 35/42 had five gonadioles, recapitulating the *Ofas-Ubx* single eRNAi phenotype; Figures S5S–V, S6A; Table S4). These data suggest that loss of *Ofas-Antp* activity is not sufficient to confer gonadiole-forming identity upon thoracic segments.

Discussion

We have shown that unlike in *Drosophila*, where adult ovariole number is determined through larval proliferation and terminal filament assembly, the number of gonadioles in *O. fasciatus* is established through the segmental specification of discrete primordia during embryogenesis. Our results further suggest that posterior Hox genes determine the abdominal segments that are competent to produce gonadioles. Under this model, one or both of *Ofas-Ubx* and *Ofas-abd-A* are required for formation of the secondary *Ofas-tin* and *Ofas-tj* expression domains in A1–A7 that prefigure gonadiole primordium formation, and *Ofas-Abd-B* restricts gonadiole formation posteriorly, either by repressing *Ofas-tin* and *Ofas-tj* transcription in these domains, or by failing to promote it.

Hox genes in somatic gonad precursor specification

Our Hox gene knockdown experiments suggest that *Ofas-Ubx* and *Ofas-abd-A* promote gonadiole primordium formation in their respective expression domains (Figure 6), suggesting that they regulate the same target genes in these positions. There is ample precedent for such a regulatory paradigm: these two Hox genes can occupy common binding sites [91], and share regulatory targets during body-wall and alary

bioRxiv preprint doi: https://doi.org/10.64898/2026.10.09.752918; this version posted October 16, 2026. The copyright holder for this preprint (which was not certified by peer review) is the author/funder, who has granted bioRxiv a license to display the preprint in perpetuity. It is made available under a CC-BY 4.0 International license.

muscle determination [92,93] and appendage formation [91] in *D. melanogaster*, and abdominal trachea formation of *O. fasciatus* [94].

As we report here for *O. fasciatus*, somatic gonad precursor (SGP) specification in *D. melanogaster* also depends on the Hox genes *abd-A* and *Abd-B*. In *D. melanogaster*, Abd-A alone specifies an anterior SGP population in parasegments 10 and 11, whereas Abd-A and Abd-B jointly specify a posterior SGP population in parasegment 12 [9]. These SGP populations are molecularly distinct: *escargot* (*esg*) is expressed only in the anterior population, whereas *eyes-absent* (*eya*) is expressed only in the posterior population [9]. In the adult ovary, *esg* is expressed in escort cells [95], whereas *eya* is expressed in follicle stem cells [96], suggesting the possibility that the two embryonic cell populations might give rise to distinct cell types in *D. melanogaster* adult ovaries. In *O. fasciatus*, however, we observed no morphological differences between adult gonadioles whose specification required *Ofas-Ubx* (A1–A2) and those specified by *Ofas-abd-A* alone (A3–A7).

Formation of both primary and secondary *Ofas-tj*-expressing domains depends on *Ofas-Ubx* or *Ofas-abd-A*, whereas the two *Ofas-tin*-expressing domains are differentially regulated - Following *Ofas-Ubx* and *Ofas-abd-A* double knockdown, which transforms the affected segments towards more anterior identities, the primary *Ofas-tin* domains still form and give rise to the presumptive dorsal vessel (Figures 6P, S5R). However, the secondary *Ofas-tin* domains, which contribute to the somatic gonadiole precursors, fail to form (Figures 6P, S5R). These results suggest that *Ofas-Ubx* and *Ofas-abd-A* are specifically required for the formation of the somatic gonad-associated *Ofas-tj* and secondary *Ofas-tin* domains, but not for the primary *Ofas-tin* domain that is putatively associated with the dorsal vessel.

We find that depletion of either *Ofas-tin* or *Ofas-tj* does not abolish expression of the other gene, and that gonadiole precursors still form even if both are depleted. This could be because we were unable to achieve complete knockdown, such that the low levels of residual *Ofas-tin* and *Ofas-tj* expression remaining were sufficient to support gonadiole precursor formation. Alternatively, these genes may not be required for gonadiole precursor specification, but may instead act following specification to regulate the morphogenesis or function of these cells. This possibility is consistent with findings

bioRxiv preprint doi: https://doi.org/10.64898/2026.10.09.752918; this version posted October 16, 2026. The copyright holder for this preprint (which was not certified by peer review) is the author/funder, who has granted bioRxiv a license to display the preprint in perpetuity. It is made available under a CC-BY 4.0 International license.

in *D. melanogaster*, where *traffic jam* is not required for SGP specification [70], but is expressed in SGPs as they come into contact with PGCs [70,97], and is required for intermingling of somatic and germ cells during embryogenesis [70]. Similarly, *raw*, a negatively regulator of JNK signaling, is expressed in SGPs and required for the extension of SGP protrusions that surround the germ cells during gonad coalescence, but is dispensable for SGP specification [98].

The initial mesodermal domains of *Ofas-tj* expression in segments A1–A7 directly overlie ectodermal stripes of *Ofas-inv* expression (Figure 2A–B), which also express *Ofas-hedgehog* [99]. Similarly, somatic gonad precursors in *D. melanogaster* arise from mesoderm overlying ectodermal stripes of *engrailed* and *hedgehog* expression [100]. Future studies should investigate the hypothesis that Hedgehog signaling contributes to the specification of *tj*-expressing somatic gonad precursors in *O. fasciatus*, as it does in *D. melanogaster* [100].

By contrast, no mesodermal expression domain analogous to the secondary *Ofas-tin* domain that produces *Ofas-tin*-expressing somatic gonad precursors has, to our knowledge, been described in *D. melanogaster*. Future studies could also test the role of Hedgehog signalling in specifying the *Ofas-tj*-expressing population and identify the signals that specify the *Ofas-tin*-expressing population. Such experiments, however, will likely require spatial or temporal control of gene knockdown or overexpression to minimize the pleiotropic effects of manipulating Hedgehog and other candidate pathways [101,102]. To our knowledge, such methods have not yet been established for *O. fasciatus* (but see [103]). These studies should clarify how the genetic pathways specifying distinct mesodermal cell types have evolved across insects.

Adult gonad development and function

Wick and Bonhag [60] identified four distinct regions of each ovariole in first-instar *O. fasciatus* nymphs: the anterior ovarian strand, posterior ovarian strand, epithelial sheath, and germ cells. Comparison of our embryonic expression data (Figure 2M–M″) with their descriptions leads us to hypothesise that the anterior ovarian strand corresponds to the *Ofas-tin*-expressing domain, whereas the posterior ovarian strand corresponds to the *Ofas-tj*-expressing domain.

bioRxiv preprint doi: https://doi.org/10.64898/2026.10.09.752918; this version posted October 16, 2026. The copyright holder for this preprint (which was not certified by peer review) is the author/funder, who has granted bioRxiv a license to display the preprint in perpetuity. It is made available under a CC-BY 4.0 International license.

The anterior ovarian strand ultimately forms the terminal filament, which in *O. fasciatus* is reported to be a syncytial structure at the anterior tip of each adult ovariole [60,61]. The embryonic *Ofas-tin*-expressing domain that gives rise to the terminal filament is directly associated with the dorsal vessel (Figure 2G′) and is enriched in acetylated Tubulin (Figures 1E, 2M'), a marker of stable microtubules [64,65]. Together with the observation that the *Ofas-tin* expressing domain elongates and becomes more filamentous as development progresses (Figure 2E'', G'), these features suggest the possibility that the anterior ovarian strand may be subject to mechanical tension. We speculate that during dorsal closure, the cardioblasts migrate and coalesce medially [104], thereby exerting force on the terminal filaments. Testing this model in future studies will require direct analysis of tissue movements and mechanical interactions between the dorsal vessel and developing ovary.

The testes and ovaries of first-instar *O. fasciatus* differ in morphology. In the testis, germ cells surround an apical complex that is thought to provide a niche for germline stem cells in adults [105]. We found that the apical complex expresses *Ofas-tin* in adult testioles (Figure S2G–H'), consistent with the possibility that it is derived from the same embryonic cell population as the anterior ovarian strand. Alternatively, adult *Ofas-tin* expression may be unrelated to its embryonic expression, and the apical complex may arise from another, unidentified cell population. We also detected *Ofas-tj* and *Ofas-tin* in regions of the adult testis that house primary spermatogonia and secondary spermatocytes, respectively (Figure S2H–J′). The specific functions of these genes during spermatogenesis, if any, remain unknown.

Ofas-tj is also expressed in follicle cells in the adult ovary (Figure S2B–F'). In *D. melanogaster*, *tj* is expressed in intermingled cells, and loss of *tj* disrupts germ-cell ensheathment and differentiation [70]. The adult expression pattern of *Ofas-tj* in *O. fasciatus* suggests that it may perform a similar function in gonadal somatic cells. Furthermore, the failure in oogenesis observed following *Ofas-tj* knockdown suggests an additional role in this process (Figure S3A–C).

bioRxiv preprint doi: https://doi.org/10.64898/2026.10.09.752918; this version posted October 16, 2026. The copyright holder for this preprint (which was not certified by peer review) is the author/funder, who has granted bioRxiv a license to display the preprint in perpetuity. It is made available under a CC-BY 4.0 International license.

Developmental basis of gonadiole number across insects

Since gonadioles are the functional subunits of the adult gonad, their number can constrain an individual's maximum capacity for gamete production [8,106]. Here we have provided evidence that the invariant gonadiole number of *O. fasciatus* is determined by the spatial distribution of the specified somatic gonadal precursors, rather than by the PGCs. Similarly, in *Drosophila*, variable ovariole numbers are determined by the number, specification and organization of somatic cells, in this case called terminal filament cells [18,19,38,41,55]. Thus, in both systems, irrespective of the variability or lack thereof in gonadiole number, this potentially significant component of reproductive fitness appears to be regulated by cellular behaviours within the developing somatic gonad rather than the germ line itself.

Most Heteroptera have an invariant number of seven gonadioles per gonad [8,107], and ancestral reconstruction studies have suggested seven as the ancestral gonadiole number for true bugs [107]. We hypothesise that the developmental and genetic mechanisms establishing this number in *O. fasciatus* may be conserved across the suborder. However, unlike *O. fasciatus*, embryos of the European firebug *P. apterus* are reported to form eight gonadiole primordia, with the anteriormost primordium subsequently degenerating before hatching [59]. In embryos of the kissing bug *Rhodnius prolixus*, Heming and Huebner [108] reported that seven gonadiole primordia form as in *O. fasciatus*, but across segments A3–A6. We hypothesise that evolutionary changes in the Hox-mediated regulation of segmental identity within the Heteroptera could determine segment competence to form, maintain or eliminate SGPs and gonadiole primordia, while still maintaining invariance in adult gonadiole number. This hypothesis is consistent with another instance of Hox-mediated morphological invariance: the case of the number of cervical vertebrae in mammals. In this case, almost all studied mammals have exactly seven vertebrae in the neck [109–111], a phenomenon attributed by some authors to Hox-mediated identity regulation of these vertebrae [110,but see 112,113]. In sloths, which are one of the two reported exceptions to this rule [114,115] (the other being manatees [109,111,116–118]), a correlative study suggests that changes in Hox gene expression boundaries may promote formation, maintenance or elimination of cervical vertebrae, while maintaining their number invariant within a lineage [119].

bioRxiv preprint doi: https://doi.org/10.64898/2026.10.09.752918; this version posted October 16, 2026. The copyright holder for this preprint (which was not certified by peer review) is the author/funder, who has granted bioRxiv a license to display the preprint in perpetuity. It is made available under a CC-BY 4.0 International license.

Invariant ovariole number evolved independently in multiple insect orders [8]. In the firebrat *Thermobia domestica* (Zygentoma), Woodland [57] reported that an invariant number of segmentally organized gonad rudiments first appear during the third nymphal instar. Whether similar mechanisms operate in other lineages with invariant ovariole numbers, such as butterflies and moths (Lepidoptera), which typically have four ovarioles per ovary, or weevils (Curculionoidea: Coleoptera), which typically have two, remains unknown [8,120]. Notably, to our knowledge no insect species with an invariant ovariole number has been reported to possess more than seven ovarioles per ovary [8]. Thus, we speculate that the maximum observed invariant ovariole number could potentially be constrained by segmental mechanisms within the 10–12 abdominal segments that characterise the insect body plan.

Evolutionary implications of invariant morphologies

The timing of gonadiole number specification may influence its sensitivity to environmental conditions, including whether it displays phenotypic plasticity. In *D. melanogaster*, ovariole number is variable, established during larval development [55,56], and can display phenotypic plasticity in response to non-genetic factors including nutrition and temperature [38,41,48,121,122]. The larval stage is a feeding stage, and variation in nutritional input is sensed by larval tissues via the insulin and TOR signaling pathways [123–127]. The activity levels of these pathways regulate proliferation of most cell types [128–130], including somatic gonad cells [31]. This in turn alters the number of terminal filament cells, the number of terminal filaments formed, and ultimately the number of ovarioles in the adult [31]. By contrast, gonadiole number in *O. fasciatus* is invariant [60,61], and specified during embryogenesis, a non-feeding embryonic stage that by definition is not sensing nutritional inputs. Even if *O. fasciatus* mothers were to experience different nutritional regimes, we predict that the gonadiole number of their offspring would be unaffected, since that number is tied to the Hox code that establishes the invariant body plan. The offspring of starved females can be smaller than those of well-fed mothers, but they still have the same body plan for their species [121,131,132]. Comparative developmental genetic studies across a broader range of species with invariant and variable gonadiole numbers will be needed going forward, to test the correlation

bioRxiv preprint doi: https://doi.org/10.64898/2026.10.09.752918; this version posted October 16, 2026. The copyright holder for this preprint (which was not certified by peer review) is the author/funder, who has granted bioRxiv a license to display the preprint in perpetuity. It is made available under a CC-BY 4.0 International license.

562 between gonadiole number variability and the developmental stage during which that
563 number is determined. Such work will be relevant to the long-standing question of why
564 some traits display more phenotypic plasticity than others [133–135]. We suggest that the
565 specific developmental stages during which traits are established may have predictive
566 value in this regard, because different developmental stages interact in distinct ways
567 with the environment.
568 Among female insects, there is strong evidence that ovariole number correlates
569 positively with reproductive output in some clades, including but not limited to
570 *Drosophila* [34,136–138,but see 139]. Ovariole number can also evolve independently of body
571 size [18,140], such that insects could in principle evolve higher reproductive outputs without
572 having to evolve larger bodies. Further, when accounting for body size, there is a
573 negative correlation between ovariole number and egg size, which is weak across all
574 studied insect groups [140], but very strong in others, including Drosophilidae fruit flies
575 [136,140]. In some animals, larger eggs can give rise to offspring with higher fitness by
576 metrics including hatching rate [141], nutrient contents [142] and juvenile size and survival
577 [143–146]. We previously showed that there is no universal correlation between egg
578 morphology and duration of embryogenesis across all insects [140], and studies in some
579 vertebrates and invertebrates show that there is not always a predictable relationship
580 between egg size and offspring fitness metrics [147–150]. However, this does not preclude
581 the possibility that for specific insect clades, there could be a positive relationship
582 between egg volume and offspring fitness [151–154]. Although it could seem counter-
583 intuitive to potentially limit offspring number by both reducing ovariole number and
584 eliminating its variance, and thereby its evolvability, we speculate that convergent
585 evolution of invariant gonadiole numbers across insects – rather than simply evolution
586 of lower ovariole numbers [8] – might be linked to increased egg size, and in turn,
587 increased offspring fitness. A thorough, phylogenetically informed investigation of the
588 evolutionary and genetic mechanistic relationships between ovariole number, lifetime
589 reproductive capacity, egg size, and offspring fitness across clades showing
590 independent evolution of gonadiole number invariance, would be a valuable avenue for
591 future studies.
592

bioRxiv preprint doi: https://doi.org/10.64898/2026.10.09.752918; this version posted October 16, 2026. The copyright holder for this preprint (which was not certified by peer review) is the author/funder, who has granted bioRxiv a license to display the preprint in perpetuity. It is made available under a CC-BY 4.0 International license.

Materials and Methods

Animal rearing

O. fasciatus were maintained as previously described [21,63,155,156] on sunflower seeds in the laboratory on a 12h:12h light/dark cycle at 28°C with 70% relative humidity. Since the *Ofas-Blimp1*$^{22\text{-}12}$ allele is homozygous lethal, bugs carrying this allele were maintained as a heterozygous stock. Every two or three generations, individual bugs were genotyped using PCR as previously described [84] to ensure the mutant allele was maintained. Homozygous mutant embryos were identified in experiments as embryos that had fewer segments and were shorter than wild type embryos; we have independently verified by PCR that all such embryos are indeed homozygous mutant.

Generation of cladogram with ovariole number in different species of insects

Ovariole and testiole counts from multiple insect species were collated from the literature (Table S1). The evolutionary relationships between the species were drawn using the Interactive Tree of Life v7 [157] using the relationships reported by Misof and colleagues [158].

Adult and nymphal dissection and fixation

Adult gonads were dissected from seven-day old adults, a stage by which oogenesis and spermatogenesis have commenced. Gonads were dissected in 1X PBS (phosphate buffered saline) and then imaged in droplets of 1X PBS under white light using a Zeiss SteREO Discovery.V12 or a Zeiss Axio Zoom.V16 stereomicroscope. For immunohistochemistry and *in situ* hybridisation, the sheath surrounding the adult gonads was removed before the gonads were fixed in 4% PFA (paraformaldehyde) in 1X PBS (4% PFA in PBS).

Nymphal instars were identified using characteristic wing morphology as previously described [159]. Nymphs were pinned, opened along the dorsal midline, eviscerated and fixed in 4% PFA in PBS. Following fixation, gonads were removed from the body cavity for subsequent whole mount immunohistochemistry.

bioRxiv preprint doi: https://doi.org/10.64898/2026.10.09.752918; this version posted October 16, 2026. The copyright holder for this preprint (which was not certified by peer review) is the author/funder, who has granted bioRxiv a license to display the preprint in perpetuity. It is made available under a CC-BY 4.0 International license.

Embryo collection, fixation and dissection

O. fasciatus were allowed to lay eggs in dry cotton for four hours, after which eggs were picked out of the cotton with plastic insect forceps and aged under the same environmental conditions as the animal cultures, until they reached the appropriate stage for analysis. Embryonic staging was based on the developmental series previously described [63], expanded and adapted for the present study (Figure S1A; Table S2). All embryonic stages described herein are defined by the range of hours after egg laying (h AEL). Thus, embryos given the same stage number can show all, or only some, of the morphological features described for that stage in Table S2, as they may be up to four hours different in chronological age. *O. fasciatus* eggs of desired ages were stuck to the bottom of a 60 mm Petri dish with double-sided tape and a slit was created in the eggshell with a microscalpel. 4% PFA in PBS was then poured into the dish to fix the embryos for 30 minutes at room temperature, followed by at least three washes with PBT (1X PBS with 0.1% Triton X-100). Embryos were then dissected free of their yolk in PBT with fine forceps. Embryos were washed at least three times with PBT at room temperature before continuing with staining or dehydration in methanol.

Gene identification

Genes of interest were identified from the *O. fasciatus* genome assembly [160] according to existing annotations or based on tBLASTn searches of the genome using homologs from *D. melanogaster* as queries. In all cases, genes for study were considered *O. fasciatus* homologs of the *D. melanogaster* queries, if these sequences were returned as the top hit in reciprocal BLASTp searches. All genes were also amplified from mixed stage embryonic cDNA to verify their sequences using Sanger sequencing (data not shown). When full-length coding sequence was not available, RACE was performed using the SMARTer RACE 5′/3′ Kit (Takara Bio 634859) on mixed stage embryonic cDNA following manufacturer's instructions. See Table S3.

Molecular biology

For RNA extraction and cDNA synthesis, embryos or tissues of interest were homogenized in TRIzol (Invitrogen 15596026), and RNA was extracted with phenol–

bioRxiv preprint doi: https://doi.org/10.64898/2026.10.09.752918; this version posted October 16, 2026. The copyright holder for this preprint (which was not certified by peer review) is the author/funder, who has granted bioRxiv a license to display the preprint in perpetuity. It is made available under a CC-BY 4.0 International license.

chloroform extraction and isopropanol precipitation. cDNA was synthesized with SuperScript III First-Strand Synthesis SuperMix for qRT-PCR (Invitrogen 11752250) following manufacturer's instructions.

For cloning and *in vitro* transcription, fragments of genes of interest were PCR-amplified from embryonic cDNA and each cloned into the pGEM-T Easy vector (Promega A137A) using manufacturer's instructions. A fragment of *GFP* was subcloned from an existing plasmid containing the *GFP* sequence. Insertion was confirmed by Sanger sequencing. Primers used are listed in Table S8.

For *in situ* probe synthesis, gene fragments were PCR-amplified from plasmids using T7 and Sp6 primers. *In vitro* transcription was performed using T7 RNA polymerase (Promega P2075) or Sp6 RNA polymerase (Roche 10810274001) with DIG RNA labelling mix (Roche 11277073910). 100 ng of template was used for a 20-µl reaction run at 37°C overnight. RNA was purified with LiCl/ethanol precipitation, then resuspended in 20 µl DEPC-treated water. Concentration was measured using a NanoDrop Spectrophotometer (Thermo Fisher), and the sample was diluted to 100 ng/µl with hybridisation buffer (50% formamide, 1X PBS, 5x SSC (saline–sodium citrate), 0.1% Triton X-100, 0.1% CHAPS ((3-((3-cholamidopropyl) dimethylammonio)-1-propanesulfonate), 5 mM EDTA (ethylenediaminetetraacetic acid), 50 µg/mL heparin, 1 µg/mL yeast tRNA). Probes were stored at −20°C.

For double-stranded RNA (dsRNA) synthesis, gene fragments were PCR-amplified from plasmids using T7 and T7-Sp6 primers to generate a template for *in vitro* transcription with T7 promoter sequences on both ends. *In vitro* transcription was performed using the MEGAscript T7 Transcription Kit (Invitrogen AM13345). 100 ng of template was used for an 80-µl reaction run at 37°C overnight. RNA was purified with LiCl/ethanol precipitation, then resuspended in 100 µl DEPC (diethyl pyrocarbonate)-treated water. To anneal the two strands, this solution was heated to 95°C on a heat block for 5 minutes, then allowed to cool slowly by leaving the tube on the heat block with the power switched off. A 1:10 dilution of annealed RNA was analysed using a NanoDrop Spectrophotometer (Thermo Fisher) to measure its concentration and purity, then run on a 1% agarose gel to confirm its size and integrity. For RNAi, dsRNA was

bioRxiv preprint doi: https://doi.org/10.64898/2026.10.09.752918; this version posted October 16, 2026. The copyright holder for this preprint (which was not certified by peer review) is the author/funder, who has granted bioRxiv a license to display the preprint in perpetuity. It is made available under a CC-BY 4.0 International license.

685 diluted in DEPC-treated water with 0.05% Texas-Red. Concentrations of injected
686 dsRNA used in each experiment are shown in Tables S5 and S7.
687
688 *Search for somatic gonad markers*
689 Somatic gonad precursors in *D. melanogaster* form distinct subpopulations: an anterior
690 population expressing *escargot* (*esg*) and a posterior population expressing *eyes*
691 *absent* (*eya*) [9]. *escargot* is one of three *snail*-type transcription factors in *D.*
692 *melanogaster* [161,162161,162]. Our search of the *O. fasciatus* genome [160] yielded only one
693 gene in this family. This gene, *Ofas-snail*, was expressed most highly in the embryonic
694 nervous system (Figure S1C). These data are consistent with previous studies in other
695 arthropods suggesting that the three *D. melanogaster snail*-type family members are the
696 result of gene duplications specific to Diptera [163–165]. We found that *Ofas-eya* was
697 expressed most strongly in the embryonic optic lobes (Figure S1D). Although both *Ofas-*
698 *snail* and *Ofas-eya* were also expressed in a segmental pattern in the thorax and
699 abdomen in *O. fasciatus*, neither of these expression patterns obviously corresponded
700 to the embryonic gonad, so we did not pursue these candidate genes further.
701
702 *Microinjection and RNA interference (RNAi)*
703 *O. fasciatus* were allowed to lay eggs in dry cotton for four hours, after which eggs were
704 picked out of the cotton for injection. Two glass microscope slides were taped together
705 with double-sided tape to create a ledge with exposed double-sided tape against which
706 embryos were lined up. Eggs were then submerged in tap water for at least 20 minutes
707 to soften the eggshell before injection. Slides with injected eggs were kept at 28°C in a
708 humidified dish to continue development until the desired age. Needles for embryonic
709 injection were made by pulling glass capillaries (World Precision Instruments 1B100-4)
710 with a Sutter P-97 Flaming/Brown micropipette puller. Needle tips were manually
711 opened with fine forceps just prior to injection. Eggs were injected with a Narishige
712 IM300 microinjector.
713 Adult *O. fasciatus* six or more days after the final moult were anesthetised with
714 CO_2 and injected between the fourth and fifth abdominal segments using a Hamilton
715 syringe and then reared with same-age adults of the opposite sex. Adult RNAi gonad

bioRxiv preprint doi: https://doi.org/10.64898/2026.10.09.752918; this version posted October 16, 2026. The copyright holder for this preprint (which was not certified by peer review) is the author/funder, who has granted bioRxiv a license to display the preprint in perpetuity. It is made available under a CC-BY 4.0 International license.

716 phenotypes were scored five days after injection (Figure S3). Embryonic pRNAi
717 phenotypes were scored in embryos collected within a 24-hour window seven or eight
718 days after injection, and aged until the desired stage of analysis. Concentration of
719 injected dsRNA used in each experiment is shown in Tables S5 and S7.
720
721 *Quantitative RT-PCR*
722 Quantitative RT-PCR was performed on an AriaMx Real-time PCR system (Agilent)
723 using PerfeCTa SYBR Green SuperMix, Low ROX (Quantabio 95056). Fold-change
724 differences were calculated using log-transformed relative normalised expression [166] for
725 gene expression changes over time. Expression levels were normalised against *Ofas-*
726 *Gapdh1* and *Ofas-δ-Tubulin* (See Table S3). All primers used are listed in Table S8.
727
728 *Colorimetric* in situ *hybridisation*
729 Dissected embryos were stored in methanol at −20°C overnight or longer before
730 *in situ* hybridisation. After rehydration in PBT and washing in hybridisation buffer,
731 embryos were hybridised overnight in a 70°C water bath with 1 ng/µl probe in
732 hybridisation buffer. The next day, the following series of 20-minute washes were
733 performed at 70°C: once in hybridisation buffer, three times in wash 1 (2X SSC, 0.1%
734 CHAPS) and three times in wash 2 (0.2X SSC, 0.1% CHAPS). Embryos were then
735 washed three times for ten minutes each at room temperature in KTBT (1X Tris-
736 buffered saline with KCl and 0.1% Triton X-100) followed by an hour-long incubation at
737 room temperature in *in situ* blocking solution (1X PBS, 0.1% Tween-20, 5% normal goat
738 serum, 2 mg/mL bovine serum albumin, 1% dimethyl sulfoxide). Embryos were
739 incubated for two hours at room temperature with sheep anti-digoxigenin–AP (Roche
740 11093274910), diluted 1:2000 in *in situ* blocking solution, then washed at least four
741 times over two hours with KTBT and incubated in KTBT overnight at 4°C. The following
742 day, embryos were washed with NTMT (100 mM Tris pH 9.5, 100 mM NaCl, 50 mM
743 $MgCl_2$, 0.1% Tween-20), then developed in the dark at 37°C with NBT (nitro blue
744 tetrazolium)/BCIP (5-bromo-4-chloro-3-indolyl phosphate) in NTMT with 5% polyvinyl
745 alcohol. Development was monitored at least every hour under a dissection microscope.
746 To stop development of the enzymatic reaction, embryos were washed in PBT, post-

bioRxiv preprint doi: https://doi.org/10.64898/2026.10.09.752918; this version posted October 16, 2026. The copyright holder for this preprint (which was not certified by peer review) is the author/funder, who has granted bioRxiv a license to display the preprint in perpetuity. It is made available under a CC-BY 4.0 International license.

fixed in 4% PFA in PBS, then incubated in 70% glycerol before mounting in 100% glycerol.

Fluorescent hybridisation chain reaction (HCR)

All HCR probes except *Ofas-inv* were designed using HCR Probe Maker (Özpolat lab, Washington University St. Louis [167]) and ordered from IDT as oPools (oligo pools) (Table S9). The *Ofas-inv* probes were obtained from Molecular Instruments by submitting a partial cDNA sequence (Table S9). Dissected samples were stored in methanol at −20°C overnight or longer before *in situ* hybridisation. After rehydration in PBT and washing in probe hybridisation buffer (Molecular Instruments), samples were hybridised overnight in a 37°C water bath with 10 nM probe in probe hybridisation buffer. The following day, samples were washed four times for 15 minutes each in probe wash buffer (Molecular Instruments) at 37°C followed by two five-minute washes in SSCT (5X SSC, 0.1% Tween-20) and at least 30 minutes in amplification buffer (Molecular Instruments) at room temperature. Samples were then incubated overnight with 60 nM hairpins (Molecular Instruments) in amplification buffer at room temperature in the dark. On the third day, samples were washed four times for 15 minutes each in SSCT. If applicable, samples were then immunostained as described below. Otherwise, samples were incubated with 2 ng/µl Hoechst 33342 in PBT at room temperature for one hour, post-fixed for 30 minutes in 4% PFA in PBS, then incubated in 70% glycerol before mounting in 100% glycerol.

Immunohistochemistry

Immunohistochemistry was performed on embryos as previously described [63]. Primary antibodies used were rabbit anti-Ofas-Vasa (1:100; [63]), mouse Monoclonal anti-Acetylated Tubulin (6-11B-1, 1:1000; Sigma-Aldrich catalog number T6793) and mouse anti-*Schistocerca gregaria* Pairberry (Pax3/7, DP312, 1:10; [168]; see also Key Resources Table).

bioRxiv preprint doi: https://doi.org/10.64898/2026.10.09.752918; this version posted October 16, 2026. The copyright holder for this preprint (which was not certified by peer review) is the author/funder, who has granted bioRxiv a license to display the preprint in perpetuity. It is made available under a CC-BY 4.0 International license.

Imaging and image analysis

Fluorescently labelled tissues were imaged on a Nikon CSU-W1 spinning disc inverted confocal microscope or a Zeiss LSM 980 with Airyscan. Colorimetric *in situ*s were imaged on a Zeiss Axio Observer 7 inverted or a Zeiss Axio Imager Z1 upright compound microscope. Whole mounted adults and dissected and unstained adult gonads were imaged on a Zeiss SteREO Discovery.V12 or a Zeiss Axio Zoom.V16 stereomicroscope. Images were analysed in Fiji v1.54 [169] and figures were edited in Inkscape v. 1.1 (retrieved from https://inkscape.org). The SNT Plugin [170] in Fiji was used to highlight segments in both the *Ofas-gt* RNAi and *Ofas-Blimp1* mutant experiments as described below. Zen Blue v. 3.4 (Zeiss) and NIS Elements Viewer v. 5.21.00 (Nikon) were used to visualise data.

Segment counts in Ofas-gt *RNAi and* Ofas-Blimp1 *experiments*

Segment counts were based on *Ofas-inv* signal, which marks posterior segment boundaries [72]. The *Ofas-inv* stripe defining the posterior boundary of T3 was used as the reference point for abdominal segment identification and was identified by the presence of legs anterior to the stripe. All *Ofas-inv* stripes posterior to T3 were considered abdominal and traced toward the posterior end of the embryo. The final analysis focused on the number of segments present within the A1–A7 region, with A7 defined as the most posterior gonadiole-bearing segment. Individual segments were not otherwise assigned specific identities. The total number of segments present was recorded independently for each side of each embryo, along with the corresponding number of gonadiole primordia. Only embryos with clearly visibly thoracic and abdominal morphology and segment boundaries, based on *Ofas-inv* signal, were used for analyses.

bioRxiv preprint doi: https://doi.org/10.64898/2026.10.09.752918; this version posted October 16, 2026. The copyright holder for this preprint (which was not certified by peer review) is the author/funder, who has granted bioRxiv a license to display the preprint in perpetuity. It is made available under a CC-BY 4.0 International license.

Key Resources Table

REAGENT or RESOURCE	SOURCE/CITATION	IDENTIFIER
Antibodies		
Rabbit anti-*Oncopeltus fasciatus* Vasa (1:100)	[63]	
Mouse Monoclonal anti-Acetylated Tubulin (6-11B-1; 1:1000)	Sigma-Aldrich	T6793
Mouse anti-*Schistocerca americana* Pairberry (Pax 3/7; 1:10)	[168]	DP312
Chemicals, peptides, and recombinant proteins		
TRIzol	Invitrogen	15596026
Phalloidin Alexa 647-conjugate (1:50)	Thermo Fisher	A34054
Hoechst 33342 (2 ng/µl)	Sigma-Aldrich	B2261
Critical commercial assays		
PerfeCTa SYBR Green SuperMix, Low ROX	Quantabio	95056-02K
SuperScript III First-Strand Synthesis SuperMix for qRT-PCR	Invitrogen	11752250
pGEM-T Easy vector	Promega	A137A
DIG RNA Labelling Mix	Roche	11277073910
MEGAscript T7 Transcription Kit	Invitrogen	AM13345
SMARTer RACE 5′/3′ Kit	Takara Bio	634859
Experimental models: Organisms/strains		
Oncopeltus fasciatus wild type strain	Carolina Biological Supply Company (Burlington, NC)	
Oncopeltus fasciatus Blimp1$^{22\text{-}12}$ *strain*	[84]	
Software and algorithms		
Fiji with SNT Plugin	[169,170]	1.54p
Zen Blue	Zeiss	3.4
Agilent Aria 2.0	Agilent	2.0
NIS Elements Viewer	Nikon	5.21.00
Inkscape	https://inkscape.org	1.1

bioRxiv preprint doi: https://doi.org/10.64898/2026.10.09.752918; this version posted October 16, 2026. The copyright holder for this preprint (which was not certified by peer review) is the author/funder, who has granted bioRxiv a license to display the preprint in perpetuity. It is made available under a CC-BY 4.0 International license.

Acknowledgements

The authors thank Extavour lab members for helpful discussions, Katie Reding and Leslie Pick (University of Maryland, College Park, MD, USA) for the *Ofas-Blimp1*$^{22\text{-}12}$ mutant line, and Nipam Patel (Marine Biological Laboratory, Woods Hole, MA, USA) for the anti-Pax3/7 (DP312) antibody. This work was supported by National Science Foundation award IOS-2220747, funds from Harvard University, and funds from the Howard Hughes Medical Institute (HHMI) to CGE. CGE is an HHMI Investigator.

Author Contributions

TK and CGE conceived of the study. JAK, TK and DAH performed experiments. All authors analysed data. JAK and TK wrote the first draft of the manuscript. All authors reviewed and edited the manuscript. CGE obtained funding for and oversaw the study.

Disclosures

The authors have nothing to disclose.

Generative AI Use Statement

Chat GPT (5.6 Sol Light) was used occasionally as an initial literature search engine to find scientific papers, which were then manually verified for veracity by the authors. It was also used as an interface to ask about clarity of text that had been manually written by the authors. No generative AI was used to generate content of any kind.

bioRxiv preprint doi: https://doi.org/10.64898/2026.10.09.752918; this version posted October 16, 2026. The copyright holder for this preprint (which was not certified by peer review) is the author/funder, who has granted bioRxiv a license to display the preprint in perpetuity. It is made available under a CC-BY 4.0 International license.

References

1. Félix, M.-A., and Barkoulas, M. (2015). Pervasive robustness in biological systems. Nat. Rev. Genet. *16*, 483–496. https://doi.org/10.1038/nrg3949.

2. Barrett, R.D.H., and Schluter, D. (2008). Adaptation from standing genetic variation. Trends Ecol. Evol. *23*, 38–44. https://doi.org/10.1016/j.tree.2007.09.008.

3. Orr, H.A., and Betancourt, A.J. (2001). Haldane's Sieve and Adaptation From the Standing Genetic Variation. Genetics *157*, 875–884. https://doi.org/10.1093/genetics/157.2.875.

4. Barnett, M., Meister, L., and Rainey, P.B. (2025). Experimental evolution of evolvability. Science *387*, eadr2756. https://doi.org/10.1126/science.adr2756.

5. Simons, A.M. (2011). Modes of response to environmental change and the elusive empirical evidence for bet hedging. Proc. R. Soc. B: Biol. Sci. *278*, 1601–1609. https://doi.org/10.1098/rspb.2011.0176.

6. Rendel, J.M., Sheldon, B.L., and Finlay, D.E. (1965). Canalisation of development of scutellar bristles in Drosophila by control of the scute locus. Genetics *52*, 1137–1151. https://doi.org/10.1093/genetics/52.6.1137.

7. Galis, F., Dooren, T.J.M.V., Feuth, J.D., Metz, J.A.J., Witkam, A., Ruinard, S., Steigenga, M.J., and Wunaendts, L.C.D. (2006). Extreme selection in humans against homeotic transformations of cervical vertebrae. Evolution *60*, 2643–2654. https://doi.org/10.1111/j.0014-3820.2006.tb01896.x.

8. Church, S.H., Medeiros, B.A.S. de, Donoughe, S., Reyes, N.L.M., and Extavour, C.G. (2021). Repeated loss of variation in insect ovary morphology highlights the role of development in life-history evolution. Proc Royal Soc B *288*, 20210150. https://doi.org/10.1098/rspb.2021.0150.

9. Boyle, M., and DiNardo, S. (1995). Specification, migration and assembly of the somatic cells of the Drosophila gonad. Development *121*, 1815–1825.

10. Extavour, C.G.M. (2007). Evolution of the bilaterian germ line: lineage origin and modulation of specification mechanisms. Integr. Comp. Biol. *47*, 770–785. https://doi.org/10.1093/icb/icm027.

11. Extavour, C.G.M. (2007). Gray anatomy: phylogenetic patterns of somatic gonad structures and reproductive strategies across the Bilateria. Integr Comp Biol *47*, 420–426. https://doi.org/10.1093/icb/icm052.

bioRxiv preprint doi: https://doi.org/10.64898/2026.10.09.752918; this version posted October 16, 2026. The copyright holder for this preprint (which was not certified by peer review) is the author/funder, who has granted bioRxiv a license to display the preprint in perpetuity. It is made available under a CC-BY 4.0 International license.

12. Ephrussi, A., and Lehmann, R. (1992). Induction of germ cell formation by oskar. Nature *358*, 387–392. https://doi.org/10.1038/358387a0.

13. Sonnenblick, B.P. (1941). Germ cell movements and sex differentiation of the gonads in the Drosophila embryo. Proc. Natl. Acad. Sci. *27*, 484–489. https://doi.org/10.1073/pnas.27.10.484.

14. Kuyyamudi, C., Ghosh, S., and Extavour, C.G. (2026). Heterotypic intercellular adhesion tunes efficiency of cell-on-cell migration. Proc. Natl. Acad. Sci. *123*, e2524496123. https://doi.org/10.1073/pnas.2524496123.

15. Jaglarz, M.K., and Howard, K.R. (1995). The active migration of Drosophila primordial germ cells. Development *121*, 3495–3503. https://doi.org/10.1242/dev.121.11.3495.

16. Gilboa, L., and Lehmann, R. (2004). Repression of Primordial Germ Cell Differentiation Parallels Germ Line Stem Cell Maintenance. Curr Biol *14*, 981–986. https://doi.org/10.1016/j.cub.2004.05.049.

17. Sarikaya, D.P., and Extavour, C.G. (2015). The Hippo Pathway Regulates Homeostatic Growth of Stem Cell Niche Precursors in the Drosophila Ovary. Plos Genet *11*, e1004962. https://doi.org/10.1371/journal.pgen.1004962.

18. Sarikaya, D.P., Church, S.H., Lagomarsino, L.P., Magnacca, K.N., Montgomery, S.L., Price, D.K., Kaneshiro, K.Y., and Extavour, C.G. (2019). Reproductive Capacity Evolves in Response to Ecology through Common Changes in Cell Number in Hawaiian Drosophila. Curr Biol *29*, 1877-1884.e6. https://doi.org/10.1016/j.cub.2019.04.063.

19. Green, D.A., and Extavour, C.G. (2012). Convergent evolution of a reproductive trait through distinct developmental mechanisms in Drosophila. Dev Biol *372*, 120–130. https://doi.org/10.1016/j.ydbio.2012.09.014.

20. Ewen-Campen, B., Srouji, J.R., Schwager, E.E., and Extavour, C.G. (2012). oskar Predates the Evolution of Germ Plasm in Insects. Curr Biol *22*, 2278–2283. https://doi.org/10.1016/j.cub.2012.10.019.

21. Ewen-Campen, B., Jones, T.E.M., and Extavour, C.G. (2013). Evidence against a germ plasm in the milkweed bug Oncopeltus fasciatus, a hemimetabolous insect. Biol. Open *2*, 556–568. https://doi.org/10.1242/bio.20134390.

22. Ewen-Campen, B., Donoughe, S., Clarke, D.N., and Extavour, C.G. (2013). Germ cell specification requires zygotic mechanisms rather than germ plasm in a basally branching insect. Curr. Biol. *23*, 835–842. https://doi.org/10.1016/j.cub.2013.03.063.

bioRxiv preprint doi: https://doi.org/10.64898/2026.10.09.752918; this version posted October 16, 2026. The copyright holder for this preprint (which was not certified by peer review) is the author/funder, who has granted bioRxiv a license to display the preprint in perpetuity. It is made available under a CC-BY 4.0 International license.

23. Gupta, T., and Extavour, C.G. (2013). Identification of a putative germ plasm in the amphipod Parhyale hawaiensis. EvoDevo *4*, 34. https://doi.org/10.1186/2041-9139-4-34.

24. Ewen-Campen, B., Schwager, E.E., and Extavour, C.G.M. (2010). The molecular machinery of germ line specification. Mol. Reprod. Dev. *77*, 3–18. https://doi.org/10.1002/mrd.21091.

25. Srouji, J., and Extavour, C.G. (2010). Redefining Stem Cells and Assembling Germ Plasm: Key Transitions in the Evolution of the Germ Line. In Key Innovations in Animal Evolution, R. DeSalle and B. Schierwater, eds. (CRC Press), pp. 360–397. https://doi.org/10.1201/b10425-20.

26. Donoughe, S., Nakamura, T., Ewen-Campen, B., Green, D.A., Henderson, L., and Extavour, C.G. (2014). BMP signaling is required for the generation of primordial germ cells in an insect. Proc. Natl. Acad. Sci. *111*, 4133–4138. https://doi.org/10.1073/pnas.1400525111.

27. Schwager, E.E., Meng, Y., and Extavour, C.G. (2015). vasa and piwi are required for mitotic integrity in early embryogenesis in the spider Parasteatoda tepidariorum. Dev. Biol. *402*, 276–290. https://doi.org/10.1016/j.ydbio.2014.08.032.

28. Snodgrass, R.E. (1935). Principles Of Insect Morphology (McGRaw-Hill Book Company).

29. Büning, J. (1994). The Insect Ovary: Ultrastructure, previtellogenic growth and evolution (Chapman & Hall) https://doi.org/10.1007/978-94-011-0741-9.

30. Heming, B.S. (2003). Insect Development and Evolution (Cornell University Press).

31. Green, D.A., and Extavour, C.G. (2014). Insulin signalling underlies both plasticity and divergence of a reproductive trait in Drosophila. Proc Royal Soc B Biological Sci *281*, 20132673. https://doi.org/10.1098/rspb.2013.2673.

32. Kumar, T., Blondel, L., and Extavour, C.G. (2020). Topology-driven protein-protein interaction network analysis detects genetic sub-networks regulating reproductive capacity. eLife *9*, e54082. https://doi.org/10.7554/elife.54082.

33. Lobell, A.S., Kaspari, R.R., Negron, Y.L.S., and Harbison, S.T. (2017). The Genetic Architecture of Ovariole Number in Drosophila melanogaster: Genes with Major, Quantitative, and Pleiotropic Effects. G3 Genes Genomes Genetics *7*, 2391–2403. https://doi.org/10.1534/g3.117.042390.

34. Wayne, M.L., Hackett, J.B., and Mackay, T.F.C. (1997). Quantitative Genetics of Ovariole Number in Drosophila melanogaster. I. Segregating Variation and Fitness. Evolution *51*, 1156–1163. https://doi.org/10.1111/j.1558-5646.1997.tb03963.x.

bioRxiv preprint doi: https://doi.org/10.64898/2026.10.09.752918; this version posted October 16, 2026. The copyright holder for this preprint (which was not certified by peer review) is the author/funder, who has granted bioRxiv a license to display the preprint in perpetuity. It is made available under a CC-BY 4.0 International license.

931 35. Telonis-Scott, M., McIntyre, L.M., and Wayne, M.L. (2005). Genetic Architecture of
932 Two Fitness-related Traits in Drosophila melanogaster: Ovariole Number and Thorax
933 Length. Genetica *125*, 211–222. https://doi.org/10.1007/s10709-005-8549-4.

934 36. Wayne, M.L., Korol, A., and Mackay, T.F.C. (2004). Microclinal variation for ovariole
935 number and body size in Drosophila melanogaster in 'Evolution Canyon.' Genetica *123*,
936 263. https://doi.org/10.1007/s10709-004-5056-y.

937 37. Wayne, M.L., and Mackay, T.F.C. (1998). Quantitative Genetics of Ovariole Number
938 in Drosophila melanogaster. II. Mutational Variation and Genotype-Environment
939 Interaction. Genetics *148*, 201–210. https://doi.org/10.1093/genetics/148.1.201.

940 38. Hodin, J., and Riddiford, L.M. (2000). Different Mechanisms Underlie Phenotypic
941 Plasticity and Interspecific Variation for a Reproductive Character in Drosophilids
942 (Insecta:Diptera). Evolution *54*, 1638–1653. https://doi.org/10.1111/j.0014-
943 3820.2000.tb00708.x.

944 39. Orgogozo, V., Broman, K.W., and Stern, D.L. (2006). High-Resolution Quantitative
945 Trait Locus Mapping Reveals Sign Epistasis Controlling Ovariole Number Between Two
946 Drosophila Species. Genetics *173*, 197–205.
947 https://doi.org/10.1534/genetics.105.054098.

948 40. Delpuech, J., Moreteau, B., Chiche, J., Pla, E., Vouidibio, J., and David, J.R. (1995).
949 Phenotypic Plasticity and Reaction Norms in Temperate and Tropical Populations of
950 Drosophila melanogaster: Ovarian Size and Developmental Temperature. Evolution *49*,
951 670–675. https://doi.org/10.1111/j.1558-5646.1995.tb02303.x.

952 41. Sarikaya, D.P., Belay, A.A., Ahuja, A., Dorta, A., Green, D.A., and Extavour, C.G.
953 (2012). The roles of cell size and cell number in determining ovariole number in
954 Drosophila. Dev Biol *363*, 279–289. https://doi.org/10.1016/j.ydbio.2011.12.017.

955 42. Azevedo, R.B.R., French, V., and Partridge, L. (1996). Thermal evolution of egg size
956 in Drosophila melanogaster. Evolution *50*, 2338–2345. https://doi.org/10.1111/j.1558-
957 5646.1996.tb03621.x.

958 43. Gibert, P., Capy, P., Imasheva, A., Moreteau, B., Morin, J.P., Pétavy, G., and David,
959 J.R. (2004). Comparative Analysis of Morphological Traits Among Drosophila
960 Melanogaster and D. Simulans: Genetic Variability, Clines and Phenotypic Plasticity.
961 Genetica *120*, 165–179. https://doi.org/10.1023/b:gene.0000017639.62427.8b.

962 44. Capy, P., Pla, E., and David, J. (1993). Phenotypic and genetic variability of
963 morphometrical traits in natural populations of Drosophila melanogaster and D
964 simulans. I. Geographic variations. Genet Sel Evol *25*, 517.
965 https://doi.org/10.1186/1297-9686-25-6-517.

bioRxiv preprint doi: https://doi.org/10.64898/2026.10.09.752918; this version posted October 16, 2026. The copyright holder for this preprint (which was not certified by peer review) is the author/funder, who has granted bioRxiv a license to display the preprint in perpetuity. It is made available under a CC-BY 4.0 International license.

966 45. Chakir, M., Moreteau, B., Capy, P., and David, J.R. (2007). Phenotypic variability of
967 wild living and laboratory grown Drosophila: Consequences of nutritional and thermal
968 heterogeneity in growth conditions. J Therm Biol *32*, 1–11.
969 https://doi.org/10.1016/j.jtherbio.2006.06.001.

970 46. David, J.R., and Bocquet, C. (1975). Similarities and differences in latitudinal
971 adaptation of two Drosophila sibling species. Nature *257*, 588–590.
972 https://doi.org/10.1038/257588a0.

973 47. Klepsatel, P., Gáliková, M., Huber, C.D., and Flatt, T. (2014). Similarities and
974 differences in altitudinal versus latitudinal variation for morphological traits in Drosophila
975 melanogaster. Evolution *68*, 1385–1398. https://doi.org/10.1111/evo.12351.

976 48. Klepsatel, P., Gáliková, M., Maio, N., Huber, C.D., Schlötterer, C., and Flatt, T.
977 (2013). Variation in thermal performance and reaction norms among populations of
978 Drosophila melanogaster. Evolution *67*, 3573–3587. https://doi.org/10.1111/evo.12221.

979 49. Bergland, A.O., Genissel, A., Nuzhdin, S.V., and Tatar, M. (2008). Quantitative Trait
980 Loci Affecting Phenotypic Plasticity and the Allometric Relationship of Ovariole Number
981 and Thorax Length in Drosophila melanogaster. Genetics *180*, 567–582.
982 https://doi.org/10.1534/genetics.108.088906.

983 50. Huettner, A.F. (1923). The origin of the germ cells in Drosophila melanogaster. J.
984 Morphol. *2*, 385–423.

985 51. Gehring, W.J., Wieschaus, E., and Holliger, M. (1976). The use of “normal” and
986 “transformed” gynandromorphs in mapping the primordial germ cells and the gonadal
987 mesoderm in Drosophila. J. Embryol. Exp. Morphol. *35*, 607–616.

988 52. Doren, M.V., Mathews, W.R., Samuels, M., Moore, L.A., Broihier, H.T., and
989 Lehmann, R. (2003). fear of intimacy encodes a novel transmembrane protein required
990 for gonad morphogenesis in Drosophila. Development *130*, 2355–2364.
991 https://doi.org/10.1242/dev.00454.

992 53. Brookman, J.J., Toosy, A.T., Shashidhara, L.S., and White, R.A. (1992). The 412
993 retrotransposon and the development of gonadal mesoderm in Drosophila.
994 Development *116*, 1185–1192.

995 54. Sahut-Barnola, I., Godt, D., Laski, F.A., and Couderc, J.-L. (1995). Drosophila Ovary
996 Morphogenesis: Analysis of Terminal Filament Formation and Identification of a Gene
997 Required for This Process. Dev Biol *170*, 127–135.
998 https://doi.org/10.1006/dbio.1995.1201.

999 55. Godt, D., and Laski, F.A. (1995). Mechanisms of cell rearrangement and cell
1000 recruitment in Drosophila ovary morphogenesis and the requirement of bric a brac.
1001 Development *121*, 173–187.

bioRxiv preprint doi: https://doi.org/10.64898/2026.10.09.752918; this version posted October 16, 2026. The copyright holder for this preprint (which was not certified by peer review) is the author/funder, who has granted bioRxiv a license to display the preprint in perpetuity. It is made available under a CC-BY 4.0 International license.

1002 56. King, R.C., Aggarwal, S.K., and Aggarwal, U. (1968). The development of the
1003 female Drosophila reproductive system. J Morphol *124*, 143–165.
1004 https://doi.org/10.1002/jmor.1051240203.

1005 57. Woodland, J.T. (1957). A contribution to our knowledge of lepismatid development.
1006 J. Morphol. *101*, 523–577. https://doi.org/10.1002/jmor.1051010306.

1007 58. Weyda, F. (1989). Female reproductive system of the first-instar nymphs of Machilis
1008 helleri (verh.) (Thysanura : Machilidae) with special reference to the segmental
1009 arrangement of ovarioles in arthropods. Int J Insect Morphol Embryology *18*, 85–96.
1010 https://doi.org/10.1016/0020-7322(89)90018-4.

1011 59. Seidel, F. (1924). Die geschlechtsorgane in der Embryonalen Entwicklung von
1012 Pyrrhocoris apterus L. Z. Morphol. Ökol. Tiere *1*, 429–506.
1013 https://doi.org/10.1007/bf00407470.

1014 60. Wick, J.R., and Bonhag, P.F. (1955). Postembryonic development of the ovaries of
1015 Oncopeltus fasciatus (Dallas). J Morphol *96*, 31–59.
1016 https://doi.org/10.1002/jmor.1050960103.

1017 61. Bonhag, P.F., and Wick, J.R. (1953). The functional anatomy of the male and
1018 female reproductive systems of the milkweed bug, Oncopeltus fasciatus (Dallas)
1019 (Heteroptera: Lygaeidae). J Morphol *93*, 177–283.
1020 https://doi.org/10.1002/jmor.1050930202.

1021 62. Chesebro, J., Hrycaj, S., Mahfooz, N., and Popadić, A. (2009). Diverging functions
1022 of Scr between embryonic and post-embryonic development in a hemimetabolous
1023 insect, Oncopeltus fasciatus. Dev Biol *329*, 142–151.
1024 https://doi.org/10.1016/j.ydbio.2009.01.032.

1025 63. Kao, J.A., Ewen-Campen, B., and Extavour, C.G. (2025). Divergence of germ cell-
1026 less roles in germ line development across insect species. Dev. Biol. *525*, 93–101.
1027 https://doi.org/10.1016/j.ydbio.2025.05.004.

1028 64. Li, L., and Yang, X.-J. (2015). Tubulin acetylation: responsible enzymes, biological
1029 functions and human diseases. Cell. Mol. Life Sci. *72*, 4237–4255.
1030 https://doi.org/10.1007/s00018-015-2000-5.

1031 65. Piperno, G., LeDizet, M., and Chang, X.J. (1987). Microtubules containing
1032 acetylated alpha-tubulin in mammalian cells in culture. J. Cell Biol. *104*, 289–302.
1033 https://doi.org/10.1083/jcb.104.2.289.

1034 66. Boyle, M., Bonini, N., and DiNardo, S. (1997). Expression and function of clift in the
1035 development of somatic gonadal precursors within the Drosophila mesoderm.
1036 Development *124*, 971–982.

bioRxiv preprint doi: https://doi.org/10.64898/2026.10.09.752918; this version posted October 16, 2026. The copyright holder for this preprint (which was not certified by peer review) is the author/funder, who has granted bioRxiv a license to display the preprint in perpetuity. It is made available under a CC-BY 4.0 International license.

1037 67. Azpiazu, N., and Frasch, M. (1993). tinman and bagpipe: two homeo box genes that
1038 determine cell fates in the dorsal mesoderm of Drosophila. Genes Dev. *7*, 1325–1340.
1039 https://doi.org/10.1101/gad.7.7b.1325.

1040 68. Rugendorff, A., Younossi-Hartenstein, A., and Hartenstein, V. (1994). Embryonic
1041 origin and differentiation of the Drosophila heart. Roux's Arch. Dev. Biol. *203*, 266–280.
1042 https://doi.org/10.1007/bf00360522.

1043 69. Bodmer, R., Jan, L.Y., and Jan, Y.N. (1990). A new homeobox-containing gene,
1044 msh-2, is transiently expressed early during mesoderm formation of Drosophila.
1045 Development *110*, 661–669. https://doi.org/10.1242/dev.110.3.661.

1046 70. Li, M.A., Alls, J.D., Avancini, R.M., Koo, K., and Godt, D. (2003). The large Maf
1047 factor Traffic Jam controls gonad morphogenesis in Drosophila. Nat Cell Biol *5*, 994–
1048 1000. https://doi.org/10.1038/ncb1058.

1049 71. Gilboa, L., and Lehmann, R. (2006). Soma–germline interactions coordinate
1050 homeostasis and growth in the Drosophila gonad. Nature *443*, 97–100.
1051 https://doi.org/10.1038/nature05068.

1052 72. Peel, A.D., Telford, M.J., and Akam, M. (2006). The evolution of hexapod engrailed-
1053 family genes: evidence for conservation and concerted evolution. Proc Royal Soc B
1054 Biological Sci *273*, 1733–1742. https://doi.org/10.1098/rspb.2006.3497.

1055 73. Paz, J. de la (1958). Studies on the embryogeny of Oncopeltus fasciatus. Doctoral
1056 dissertation, Cornell University.

1057 74. Butt, F.H. (1949). Embryology of the Milkweed Bug, Oncopeltus fasciatus
1058 (Hemiptera). Cornell Experiment Station Memoir, 3–43.

1059 75. Lochab, A. (2022). Early germ line development in the hemipteran insect
1060 Oncopeltus fasciatus. Doctoral dissertation, Harvard University.

1061 76. Lasko, P.F., and Ashburner, M. (1990). Posterior localization of vasa protein
1062 correlates with, but is not sufficient for, pole cell development. Genes Dev. *4*, 905–921.
1063 https://doi.org/10.1101/gad.4.6.905.

1064 77. Tanaka, S.S., Toyooka, Y., Akasu, R., Katoh-Fukui, Y., Nakahara, Y., Suzuki, R.,
1065 Yokoyama, M., and Noce, T. (2000). The mouse homolog of Drosophila Vasa is
1066 required for the development of male germ cells. Genes & Development *14*, 841–853.

1067 78. Li, M., Hong, N., Xu, H., Yi, M., Li, C., Gui, J., and Hong, Y. (2009). Medaka vasa is
1068 required for migration but not survival of primordial germ cells. Mech Develop *126*, 366–
1069 381. https://doi.org/10.1016/j.mod.2009.02.004.

bioRxiv preprint doi: https://doi.org/10.64898/2026.10.09.752918; this version posted October 16, 2026. The copyright holder for this preprint (which was not certified by peer review) is the author/funder, who has granted bioRxiv a license to display the preprint in perpetuity. It is made available under a CC-BY 4.0 International license.

79. Ewen-Campen, B., Jones, T.E.M., and Extavour, C.G. (2013). Evidence against a germ plasm in the milkweed bug Oncopeltus fasciatus, a hemimetabolous insect. Biol. Open *2*, 556–568. https://doi.org/10.1242/bio.20134390.

80. Liu, P.Z., and Patel, N.H. (2010). giant is a bona fide gap gene in the intermediate germband insect, Oncopeltus fasciatus. Development *137*, 835–844. https://doi.org/10.1242/dev.045948.

81. Brent, A.E., Yucel, G., Small, S., and Desplan, C. (2007). Permissive and Instructive Anterior Patterning Rely on mRNA Localization in the Wasp Embryo. Science *315*, 1841–1843. https://doi.org/10.1126/science.1137528.

82. Petschek, J.P., and Mahowald, A.P. (1990). Different requirements for l(1)giant in two embryonic domains of Drosophila melanogaster. Dev. Genet. *11*, 88–96. https://doi.org/10.1002/dvg.1020110110.

83. Wilson, M.J., Havler, M., and Dearden, P.K. (2010). Giant, Krüppel, and caudal act as gap genes with extensive roles in patterning the honeybee embryo. Dev Biol *339*, 200–211. https://doi.org/10.1016/j.ydbio.2009.12.015.

84. Reding, K., Chung, M., Heath, A., Hotopp, J.D., and Pick, L. (2024). Same rule, different genes: Blimp1 is a pair-rule gene in the milkweed bug Oncopeltus fasciatus. Science Advances *10*. https://doi.org/10.1126/sciadv.adq9045.

85. McGinnis, W., and Krumlauf, R. (1992). Homeobox genes and axial patterning. Cell *68*, 283–302. https://doi.org/10.1016/0092-8674(92)90471-n.

86. Angelini, D.R., Liu, P.Z., Hughes, C.L., and Kaufman, T.C. (2005). Hox gene function and interaction in the milkweed bug Oncopeltus fasciatus (Hemiptera). Dev Biol *287*, 440–455. https://doi.org/10.1016/j.ydbio.2005.08.010.

87. Yekta, S., Tabin, C.J., and Bartel, D.P. (2008). MicroRNAs in the Hox network: an apparent link to posterior prevalence. Nat. Rev. Genet. *9*, 789–796. https://doi.org/10.1038/nrg2400.

88. Hafen, E., Levine, M., and Gehring, W.J. (1984). Regulation of Antennapedia transcript distribution by the bithorax complex in Drosophila. Nature *307*, 287–289. https://doi.org/10.1038/307287a0.

89. Struhl, G., and White, R.A.H. (1985). Regulation of the Ultrabithorax Gene of Drosophila by Other Bithorax Complex Genes. Cell *43*, 507–519. https://doi.org/10.1016/0092-8674(85)90180-1.

90. Beachy, P.A., Krasnow, M.A., Gavis, E.R., and Hogness, D.S. (1988). An Ultrabithorax protein binds sequences near its own and the Antennapedia P1 promoters. Cell *55*, 1069–1081. https://doi.org/10.1016/0092-8674(88)90251-6.

bioRxiv preprint doi: https://doi.org/10.64898/2026.10.09.752918; this version posted October 16, 2026. The copyright holder for this preprint (which was not certified by peer review) is the author/funder, who has granted bioRxiv a license to display the preprint in perpetuity. It is made available under a CC-BY 4.0 International license.

1105 91. Gebelein, B., McKay, D.J., and Mann, R.S. (2004). Direct integration of Hox and
1106 segmentation gene inputs during Drosophila development. Nature *431*, 653–659.
1107 https://doi.org/10.1038/nature02946.

1108 92. Enriquez, J., Boukhatmi, H., Dubois, L., Philippakis, A.A., Bulyk, M.L., Michelson,
1109 A.M., Crozatier, M., and Vincent, A. (2010). Multi-step control of muscle diversity by Hox
1110 proteins in the Drosophila embryo. Development *137*, 457–466.
1111 https://doi.org/10.1242/dev.045286.

1112 93. LaBeau, E.M., Trujillo, D.L., and Cripps, R.M. (2009). Bithorax Complex genes
1113 control alary muscle patterning along the cardiac tube of Drosophila. Mech. Dev. *126*,
1114 478–486. https://doi.org/10.1016/j.mod.2009.01.001.

1115 94. Hanna, L., and Popadić, A. (2020). A hemipteran insect reveals new genetic
1116 mechanisms and evolutionary insights into tracheal system development. Proc. Natl.
1117 Acad. Sci. *117*, 4252–4261. https://doi.org/10.1073/pnas.1908975117.

1118 95. Rust, K., Byrnes, L.E., Yu, K.S., Park, J.S., Sneddon, J.B., Tward, A.D., and Nystul,
1119 T.G. (2020). A single-cell atlas and lineage analysis of the adult Drosophila ovary. Nat
1120 Commun *11*, 5628. https://doi.org/10.1038/s41467-020-19361-0.

1121 96. Slaidina, M., Gupta, S., Banisch, T.U., and Lehmann, R. (2021). A single-cell atlas
1122 reveals unanticipated cell type complexity in Drosophila ovaries. Genome Res. *31*,
1123 gr.274340.120. https://doi.org/10.1101/gr.274340.120.

1124 97. Okegbe, T.C., and DiNardo, S. (2011). The endoderm specifies the mesodermal
1125 niche for the germline in Drosophila via Delta-Notch signaling. Development *138*, 1259–
1126 1267. https://doi.org/10.1242/dev.056994.

1127 98. Jemc, J.C., Milutinovich, A.B., Weyers, J.J., Takeda, Y., and Doren, M.V. (2012).
1128 raw Functions through JNK signaling and cadherin-based adhesion to regulate
1129 Drosophila gonad morphogenesis. Dev. Biol. *367*, 114–125.
1130 https://doi.org/10.1016/j.ydbio.2012.04.027.

1131 99. Auman, T., and Chipman, A.D. (2018). Growth zone segmentation in the milkweed
1132 bug Oncopeltus fasciatus sheds light on the evolution of insect segmentation. BMC
1133 Evol. Biol. *18*, 178. https://doi.org/10.1186/s12862-018-1293-z.

1134 100. Riechmann, V., Rehorn, K.-P., Reuter, R., and Leptin, M. (1998). The genetic
1135 control of the distinction between fat body and gonadal mesoderm in Drosophila.
1136 Development *125*, 713–723. https://doi.org/10.1242/dev.125.4.713.

1137 101. Pakvasa, M., Tucker, A.B., Shen, T., He, T.-C., and Reid, R.R. (2021). The
1138 Pleiotropic Intricacies of Hedgehog Signaling: From Craniofacial Patterning to
1139 Carcinogenesis. FACE *2*, 260–274. https://doi.org/10.1177/27325016211024326.

bioRxiv preprint doi: https://doi.org/10.64898/2026.10.09.752918; this version posted October 16, 2026. The copyright holder for this preprint (which was not certified by peer review) is the author/funder, who has granted bioRxiv a license to display the preprint in perpetuity. It is made available under a CC-BY 4.0 International license.

1140 102. Petrova, R., and Joyner, A.L. (2014). Roles for Hedgehog signaling in adult organ
1141 homeostasis and repair. Development *141*, 3445–3457.
1142 https://doi.org/10.1242/dev.083691.

1143 103. Shirai, Y., Hashmi, Y., Watts, A., Kao, J.A., and Extavour, C.G. (2026). A nuclear
1144 targeting approach enables efficient transgenesis in the milkweed bug Oncopeltus
1145 fasciatus. bioRxiv : Prepr. Serv. Biol., 741915.
1146 https://doi.org/10.64898/2026.07.30.741915.

1147 104. Medioni, C., Astier, M., Zmojdzian, M., Jagla, K., and Sémériva, M. (2008). Genetic
1148 control of cell morphogenesis during Drosophila melanogaster cardiac tube formation. J.
1149 Cell Biol. *182*, 249–261. https://doi.org/10.1083/jcb.200801100.

1150 105. Schmidt, E.D., Papanikolaou, A., and Dorn, A. (2001). The relationship between
1151 germline cells and apical complex in the testes of the milkweed bug throughout
1152 postembryonic development. Invertebr Reprod Dev *39*, 109–126.
1153 https://doi.org/10.1080/07924259.2001.9652474.

1154 106. Klepsatel, P., Gáliková, M., Maio, N., Ricci, S., Schlötterer, C., and Flatt, T. (2013).
1155 Reproductive and post-reproductive life history of wild-caught Drosophila melanogaster
1156 under laboratory conditions. J Evolution Biol *26*, 1508–1520.
1157 https://doi.org/10.1111/jeb.12155.

1158 107. Grozeva, S., Stoianova, D., Konstantinov, F., Simov, N., Kuznetsova, V.G.,
1159 Grozeva, S., Stoianova, D., Simov, N., and Kuznetsova, V.G. (2022). A synopsis of the
1160 numbers of testicular follicles and ovarioles in true bugs (Heteroptera, Hemiptera) –
1161 sixty-five years of progress after J. Pendergrast's review. ZooKeys *1136*, 71–123.
1162 https://doi.org/10.3897/zookeys.1136.96431.

1163 108. Heming, B.S., and Huebner, E. (1994). Development of the germ cells and
1164 reproductive primordia in male and female embryos of Rhodnius prolixus Stål
1165 (Hemiptera: Reduviidae). Can. J. Zool. *72*, 1100–1119. https://doi.org/10.1139/z94-148.

1166 109. Owen, R. (1855). Art. XXII.—The Principal Forms of the Skeleton and of the Teeth.
1167 Am. J. Méd. Sci. *27*, 197. https://doi.org/10.1097/00000441-185527570-00022.

1168 110. Galis, F. (1999). Why do almost all mammals have seven cervical vertebrae?
1169 Developmental constraints, Hox genes, and cancer. J. Exp. Zoöl. *285*, 19–26.
1170 https://doi.org/10.1002/(sici)1097-010x(19990415)285:1<19::aid-jez3>3.3.co;2-q.

1171 111. Narita, Y., and Kuratani, S. (2005). Evolution of the vertebral formulae in
1172 mammals: A perspective on developmental constraints. J. Exp. Zoöl. Part B: Mol. Dev.
1173 Evol. *304B*, 91–106. https://doi.org/10.1002/jez.b.21029.

bioRxiv preprint doi: https://doi.org/10.64898/2026.10.09.752918; this version posted October 16, 2026. The copyright holder for this preprint (which was not certified by peer review) is the author/funder, who has granted bioRxiv a license to display the preprint in perpetuity. It is made available under a CC-BY 4.0 International license.

1174 112. Buchholtz, E.A. (2014). Crossing the frontier: a hypothesis for the origins of
1175 meristic constraint in mammalian axial patterning. Zoology *117*, 64–69.
1176 https://doi.org/10.1016/j.zool.2013.09.001.

1177 113. Buchholtz, E.A., Bailin, H.G., Laves, S.A., Yang, J.T., Chan, M.-Y., and Drozd, L.E.
1178 (2012). Fixed cervical count and the origin of the mammalian diaphragm. Evol. Dev. *14*,
1179 399–411. https://doi.org/10.1111/j.1525-142x.2012.00560.x.

1180 114. Buchholtz, E.A., and Stepien, C.C. (2009). Anatomical transformation in mammals:
1181 developmental origin of aberrant cervical anatomy in tree sloths. Evol. Dev. *11*, 69–79.
1182 https://doi.org/10.1111/j.1525-142x.2008.00303.x.

1183 115. Hautier, L., Weisbecker, V., Sánchez-Villagra, M.R., Goswami, A., and Asher, R.J.
1184 (2010). Skeletal development in sloths and the evolution of mammalian vertebral
1185 patterning. Proc. Natl. Acad. Sci. *107*, 18903–18908.
1186 https://doi.org/10.1073/pnas.1010335107.

1187 116. Varela-Lasheras, I., Bakker, A.J., Mije, S.D. van der, Metz, J.A., Alphen, J. van,
1188 and Galis, F. (2011). Breaking evolutionary and pleiotropic constraints in mammals: On
1189 sloths, manatees and homeotic mutations. EvoDevo *2*, 11. https://doi.org/10.1186/2041-
1190 9139-2-11.

1191 117. Giffin, E.B., and Gillett, M. (1996). Neurological and Osteological Definitions of
1192 Cervical Vertebrae in Mammals. Brain, Behav. Evol. *47*, 214–218.
1193 https://doi.org/10.1159/000113241.

1194 118. Galis, F., Wagner, G.P., and Jockusch, E.L. (2003). Why is limb regeneration
1195 possible in amphibians but not in reptiles, birds, and mammals? Evol Dev *5*, 208–220.
1196 https://doi.org/10.1046/j.1525-142x.2003.03028.x.

1197 119. Böhmer, C., Amson, E., Arnold, P., Heteren, A.H. van, and Nyakatura, J.A. (2018).
1198 Homeotic transformations reflect departure from the mammalian 'rule of seven' cervical
1199 vertebrae in sloths: inferences on the Hox code and morphological modularity of the
1200 mammalian neck. BMC Evol. Biol. *18*, 84. https://doi.org/10.1186/s12862-018-1202-5.

1201 120. Virkki, N. (1961). Ovariole Numbers in two Puerto Rican Oedionychina
1202 (Coleoptera). 1978, 50–56. https://doi.org/10.1139/z61-028.

1203 121. Deas, J.B., Blondel, L., and Extavour, C.G. (2019). Ancestral and offspring nutrition
1204 interact to affect life-history traits in Drosophila melanogaster. Proc Royal Soc B *286*,
1205 20182778. https://doi.org/10.1098/rspb.2018.2778.

1206 122. Mendes, C.C., and Mirth, C.K. (2016). Stage-Specific Plasticity in Ovary Size Is
1207 Regulated by Insulin/Insulin-Like Growth Factor and Ecdysone Signaling in Drosophila.
1208 Genetics *202*, 703–719. https://doi.org/10.1534/genetics.115.179960.

bioRxiv preprint doi: https://doi.org/10.64898/2026.10.09.752918; this version posted October 16, 2026. The copyright holder for this preprint (which was not certified by peer review) is the author/funder, who has granted bioRxiv a license to display the preprint in perpetuity. It is made available under a CC-BY 4.0 International license.

123. Katewa, S.D., and Kapahi, P. (2011). Role of TOR signaling in aging and related biological processes in Drosophila melanogaster. Exp. Gerontol. *46*, 382–390. https://doi.org/10.1016/j.exger.2010.11.036.

124. Kapahi, P., and Zid, B. (2004). TOR Pathway: Linking Nutrient Sensing to Life Span. Sci. Aging Knowl. Environ. *2004*, PE34. https://doi.org/10.1126/sageke.2004.36.pe34.

125. Colombani, J., Raisin, S., Pantalacci, S., Radimerski, T., Montagne, J., and Léopold, P. (2003). A Nutrient Sensor Mechanism Controls Drosophila Growth. Cell *114*, 739–749. https://doi.org/10.1016/s0092-8674(03)00713-x.

126. Kim, J., and Neufeld, T.P. (2015). Dietary sugar promotes systemic TOR activation in Drosophila through AKH-dependent selective secretion of Dilp3. Nat. Commun. *6*, 6846. https://doi.org/10.1038/ncomms7846.

127. Mirth, C.K., and Riddiford, L.M. (2007). Size assessment and growth control: how adult size is determined in insects. Bioessays *29*, 344–355. https://doi.org/10.1002/bies.20552.

128. Suzawa, M., and Bland, M.L. (2023). Insulin signaling in development. Development *150*. https://doi.org/10.1242/dev.201599.

129. Schmelzle, T., and Hall, M.N. (2000). TOR, a Central Controller of Cell Growth. Cell *103*, 253–262. https://doi.org/10.1016/s0092-8674(00)00117-3.

130. Gonzalez, S., and Rallis, C. (2017). The TOR Signaling Pathway in Spatial and Temporal Control of Cell Size and Growth. Front. Cell Dev. Biol. *5*, 61. https://doi.org/10.3389/fcell.2017.00061.

131. Vijendravarma, R.K., Narasimha, S., and Kawecki, T.J. (2010). Effects of parental larval diet on egg size and offspring traits in Drosophila. Biol Letters *6*, 238–241. https://doi.org/10.1098/rsbl.2009.0754.

132. Naguib, M., and Gil, D. (2005). Transgenerational body size effects caused by early developmental stress in zebra finches. Biol. Lett. *1*, 95–97. https://doi.org/10.1098/rsbl.2004.0277.

133. Scheiner, S.M. (1993). Genetics and Evolution of Phenotypic Plasticity. Annu Rev Ecol Syst *24*, 35–68. https://doi.org/10.1146/annurev.es.24.110193.000343.

134. Bateson, P., Gluckman, P., and Hanson, M. (2014). The biology of developmental plasticity and the Predictive Adaptive Response hypothesis. J. Physiol. *592*, 2357–2368. https://doi.org/10.1113/jphysiol.2014.271460.

bioRxiv preprint doi: https://doi.org/10.64898/2026.10.09.752918; this version posted October 16, 2026. The copyright holder for this preprint (which was not certified by peer review) is the author/funder, who has granted bioRxiv a license to display the preprint in perpetuity. It is made available under a CC-BY 4.0 International license.

135. DeWitt, T.J., Sih, A., and Wilson, D.S. (1998). Costs and limits of phenotypic plasticity. Trends Ecol Evol *13*, 77–81. https://doi.org/10.1016/s0169-5347(97)01274-3.

136. Montague, J.R., Mangan, R.L., and Starmer, W.T. (1981). Reproductive Allocation in the Hawaiian Drosophilidae: Egg Size and Number. Am Nat *118*, 865–871. https://doi.org/10.1086/283877.

137. David, J. (1970). Le nombre d'ovarioles chez Drosophila melanogaster: relation avec la fécondité et valeur adaptative. Archives de Zoologie experimentale et generale *111*, 357–370.

138. Boulétreau-Merle, J., Allemand, R., Cohet, Y., and David, J.R. (1982). Reproductive strategy in Drosophila melanogaster: Significance of a genetic divergence between temperate and tropical populations. Oecologia *53*, 323–329. https://doi.org/10.1007/bf00389008.

139. Schmidt, P.S., Matzkin, L., Ippolito, M., and Eanes, W.F. (2005). Geographic variation in diapause incidence, life-history traits, and climatic adaptation in Drosophila melanogaster. Evolution *59*, 1721–1732. https://doi.org/10.1554/05-115.1.

140. Church, S.H., Donoughe, S., Medeiros, B.A.S. de, and Extavour, C.G. (2019). Insect egg size and shape evolve with ecology but not developmental rate. Nature *571*, 58–62. https://doi.org/10.1038/s41586-019-1302-4.

141. Grant, M.C. (1991). Relationships between egg size, chick size at hatching, and chick survival in the Whimbrel Numenius phaeopus. Ibis *133*, 127–133. https://doi.org/10.1111/j.1474-919x.1991.tb04823.x.

142. Badzinski, S.S., Ankney, C.D., Leafloor, J.O., and Abraham, K.F. (2002). Egg size as a predictor of nutrient composition of eggs and neonates of Canada Geese (Branta canadensis interior) and Lesser Snow Geese (Chen caerulescens caerulescens). Can. J. Zoöl. *80*, 333–341. https://doi.org/10.1139/z02-010.

143. Krist, M. (2011). Egg size and offspring quality: a meta-analysis in birds. Biol Rev *86*, 692–716. https://doi.org/10.1111/j.1469-185x.2010.00166.x.

144. Liu, T.-H., Lee, C.-Y.D., Tu, C.-W., Lin, P.-H., Chen, C.A., Jeng, M.-S., and Ko, C.-Y. (2025). Shaping hatchling fitness through maternal and environmental influences in green sea turtles. Sci. Rep. *15*, 20268. https://doi.org/10.1038/s41598-025-01142-8.

145. Segers, F.H.I.D., and Taborsky, B. (2011). Egg size and food abundance interactively affect juvenile growth and behaviour. Funct. Ecol. *25*, 166–176. https://doi.org/10.1111/j.1365-2435.2010.01790.x.

bioRxiv preprint doi: https://doi.org/10.64898/2026.10.09.752918; this version posted October 16, 2026. The copyright holder for this preprint (which was not certified by peer review) is the author/funder, who has granted bioRxiv a license to display the preprint in perpetuity. It is made available under a CC-BY 4.0 International license.

146. Xu, F., Yang, W., and Li, Y. (2019). Enlarged Egg Size Increases Offspring Fitness of a Frog Species on the Zhoushan Archipelago of China. Sci. Rep. *9*, 11653. https://doi.org/10.1038/s41598-019-48147-8.

147. Wilson, H.R. (1991). Interrelationships of egg size, chick size, posthatching growth and hatchability. World's Poult. Sci. J. *47*, 5–20. https://doi.org/10.1079/wps19910002.

148. Williams, T.D. (1994). Intraspecific variation in egg size and egg composition in birds: effects on offspring fitness. Biol. Rev. *69*, 35–59. https://doi.org/10.1111/j.1469-185x.1994.tb01485.x.

149. Williams, T.D., Lank, D.B., Cooke, F., and Rockwell, R.F. (1993). Fitness consequences of egg-size variation in the lesser snow goose. Oecologia *96*, 331–338. https://doi.org/10.1007/bf00317502.

150. Fox, C.W. (1994). The Influence of Egg Size on Offspring Performance in the Seed Beetle, Callosobruchus maculatus. Oikos *71*, 321. https://doi.org/10.2307/3546280.

151. Stewart, L.A., Hemptinne, J.-L., and Dixon, A.F.G. (1991). Reproductive Tactics of Ladybird Beetles: Relationships Between Egg Size, Ovariole Number and Developmental Time. Funct Ecol *5*, 380. https://doi.org/10.2307/2389809.

152. Gooding, R.H., and McIntyre, G.S. (2000). Egg size, contents, and quality. Can J Zool *78*, 1544–1551.

153. Fischer, K., Bot, A.N.M., Brakefield, P.M., and Zwaan, B.J. (2003). Fitness consequences of temperature-mediated egg size plasticity in a butterfly. Funct Ecol *17*, 803–810. https://doi.org/10.1111/j.1365-2435.2003.00798.x.

154. Boivin, G., and Gauvin, M.-J. (2009). Egg size affects larval performance in a coleopteran parasitoid. Ecol. Entomol. *34*, 240–245. https://doi.org/10.1111/j.1365-2311.2008.01063.x.

155. Hughes, C.L., and Kaufman, T.C. (2000). RNAi analysis of Deformed, proboscipedia and Sex combs reduced in the milkweed bug Oncopeltus fasciatus: novel roles for Hox genes in the Hemipteran head. Development *127*, 3683–3694. https://doi.org/10.1242/dev.127.17.3683.

156. Ewen-Campen, B., Shaner, N., Panfilio, K.A., Suzuki, Y., Roth, S., and Extavour, C.G. (2011). The maternal and early embryonic transcriptome of the milkweed bug Oncopeltus fasciatus. BMC Genomics *12*, 61. https://doi.org/10.1186/1471-2164-12-61.

157. Letunic, I., and Bork, P. (2024). Interactive Tree of Life (iTOL) v6: recent updates to the phylogenetic tree display and annotation tool. Nucleic Acids Res. *52*, W78–W82. https://doi.org/10.1093/nar/gkae268.

bioRxiv preprint doi: https://doi.org/10.64898/2026.10.09.752918; this version posted October 16, 2026. The copyright holder for this preprint (which was not certified by peer review) is the author/funder, who has granted bioRxiv a license to display the preprint in perpetuity. It is made available under a CC-BY 4.0 International license.

158. Misof, B., Liu, S., Meusemann, K., Peters, R.S., Donath, A., Mayer, C., Frandsen, P.B., Ware, J., Flouri, T., Beutel, R.G., et al. (2014). Phylogenomics resolves the timing and pattern of insect evolution. Science *346*, 763–767. https://doi.org/10.1126/science.1257570.

159. Hrycaj, S., Chesebro, J., and Popadić, A. (2010). Functional analysis of Scr during embryonic and post-embryonic development in the cockroach, Periplaneta americana. Dev Biol *341*, 324–334. https://doi.org/10.1016/j.ydbio.2010.02.018.

160. Panfilio, K.A., Jentzsch, I.M.V., Benoit, J.B., Erezyilmaz, D., Suzuki, Y., Colella, S., Robertson, H.M., Poelchau, M.F., Waterhouse, R.M., Ioannidis, P., et al. (2019). Molecular evolutionary trends and feeding ecology diversification in the Hemiptera, anchored by the milkweed bug genome. Genome Biol. *20*, 64. https://doi.org/10.1186/s13059-019-1660-0.

161. Ashraf, S.I., Hu, X., Roote, J., and Ip, Y.T. (1999). The mesoderm determinant Snail collaborates with related zinc-finger proteins to control Drosophila neurogenesis. EMBO J. *18*, 6426–6438. https://doi.org/10.1093/emboj/18.22.6426.

162. Whiteley, M., Noguchi, P.D., Sensabaugh, S.M., Odenwald, W.F., and Kassis, J.A. (1992). The Drosophila gene escargot encodes a zinc finger motif found in snail-related genes. Mech. Dev. *36*, 117–127. https://doi.org/10.1016/0925-4773(92)90063-p.

163. Kerner, P., Hung, J., Béhague, J., Gouar, M.L., Balavoine, G., and Vervoort, M. (2009). Insights into the evolution of the snail superfamily from metazoan wide molecular phylogenies and expression data in annelids. BMC Evol Biol *9*, 94. https://doi.org/10.1186/1471-2148-9-94.

164. Sommer, R.J., Retzlaff, M., Goerlich, K., Sander, K., and Tautz, D. (1992). Evolutionary conservation pattern of zinc-finger domains of Drosophila segmentation genes. Proc. Natl. Acad. Sci. *89*, 10782–10786. https://doi.org/10.1073/pnas.89.22.10782.

165. Sommer, R.J., and Tautz, D. (1994). Expression patterns of twist and snail in Tribolium (Coleoptera) suggest a homologous formation of mesoderm in long and short germ band insects. Dev. Genet. *15*, 32–37. https://doi.org/10.1002/dvg.1020150105.

166. Taylor, S.C., Nadeau, K., Abbasi, M., Lachance, C., Nguyen, M., and Fenrich, J. (2019). The Ultimate qPCR Experiment: Producing Publication Quality, Reproducible Data the First Time. Trends Biotechnol. *37*, 761–774. https://doi.org/10.1016/j.tibtech.2018.12.002.

167. Kuehn, E., Clausen, D.S., Null, R.W., Metzger, B.M., Willis, A.D., and Özpolat, B.D. (2022). Segment number threshold determines juvenile onset of germline cluster expansion in Platynereis dumerilii. J. Exp. Zoöl. Part B, Mol. Dev. Evol. *338*, 225–240. https://doi.org/10.1002/jez.b.23100.

bioRxiv preprint doi: https://doi.org/10.64898/2026.10.09.752918; this version posted October 16, 2026. The copyright holder for this preprint (which was not certified by peer review) is the author/funder, who has granted bioRxiv a license to display the preprint in perpetuity. It is made available under a CC-BY 4.0 International license.

168. Davis, G.K., D'Alessio, J.A., and Patel, N.H. (2005). Pax3/7 genes reveal conservation and divergence in the arthropod segmentation hierarchy. Dev. Biol. *285*, 169–184. https://doi.org/10.1016/j.ydbio.2005.06.014.

169. Schindelin, J., Arganda-Carreras, I., Frise, E., Kaynig, V., Longair, M., Pietzsch, T., Preibisch, S., Rueden, C., Saalfeld, S., Schmid, B., et al. (2012). Fiji: an open-source platform for biological-image analysis. Nat. Methods *9*, 676–682. https://doi.org/10.1038/nmeth.2019.

170. Arshadi, C., Günther, U., Eddison, M., Harrington, K.I.S., and Ferreira, T.A. (2021). SNT: a unifying toolbox for quantification of neuronal anatomy. Nat. Methods *18*, 374–377. https://doi.org/10.1038/s41592-021-01105-7.

171. Schmidt, E.D., and Dorn, A. (2004). Structural polarity and dynamics of male germline stem cells in the milkweed bug (Oncopeltus fasciatus). Cell Tissue Res *318*, 383–394. https://doi.org/10.1007/s00441-004-0983-6.

172. Washington, J.T., Cavender, K.R., Amukamara, A.U., McKinney, E.C., Schmitz, R.J., and Moore, P.J. (2021). The essential role of Dnmt1 in gametogenesis in the large milkweed bug Oncopeltus fasciatus. eLife *10*, e62202. https://doi.org/10.7554/elife.62202.

173. Kisiel, E., and Klag, J. (2001). Development of terminal filaments and ovariole envelopes in Thermobia domestica (Insecta, Zygentoma) larvae. Folia Biol. *49*, 199–204.

174. Tworzydlo, W., Kisiel, E., Jankowska, W., and Bilinski, S.M. (2014). Morphology and ultrastructure of the germarium in panoistic ovarioles of a basal "apterygotous" insect, Thermobia domestica. Zoology *117*, 200–206. https://doi.org/10.1016/j.zool.2014.01.002.

175. Bitsch, J., and Bitsch, C. (1982). Les etapes de la vitellogenese chez Thermobia Domestica (Packard) (Thysanura: Lepismatidae). Int. J. Insect Morphol. Embryol. *11*, 197–212. https://doi.org/10.1016/s0020-7322(82)80005-6.

176. Bawa, S.R. (1974). Epithelium of the male reproductive duct of Thermobia domestica (Packard) (Thysanura: Lepismatidae). Int. J. Insect Morphol. Embryol. *3*, 87–100. https://doi.org/10.1016/s0020-7322(74)81009-3.

177. Soldán, T. (1979). The structure and development of the female internal reproductive system in six European species of Ephemeroptera. Acta Entomologica Bohemoslovaca *76*, 353–365.

178. Gottanka, J., and Büning, J. (1993). Mayflies (ephemeroptera), the most "primitive" winged insects, have telotrophic meroistic ovaries. Roux's Arch. Dev. Biol. *203*, 18–27. https://doi.org/10.1007/bf00539886.

bioRxiv preprint doi: https://doi.org/10.64898/2026.10.09.752918; this version posted October 16, 2026. The copyright holder for this preprint (which was not certified by peer review) is the author/funder, who has granted bioRxiv a license to display the preprint in perpetuity. It is made available under a CC-BY 4.0 International license.

179. Fink, T.J., Soldn, T., Peters, J.G., and Peters, W.L. (1991). The reproductive life history of the predacious, sand-burrowing mayfly Dolania americana (Ephemeroptera: Behningiidae) and comparisons with other mayflies. Can. J. Zoöl. *69*, 1083–1093. https://doi.org/10.1139/z91-153.

180. Soldán, T. (1979). The structure and development of the male internal reproductive organs in six European species of Ephemeroptera. Acta Entomologica Bohemoslovaca *76*, 22–33.

181. Reinhardt, K., Köhler, G., Maas, S., and Detzel, P. (2005). Low dispersal ability and habitat specificity promote extinctions in rare but not in widespread species: the Orthoptera of Germany. Ecography *28*, 593–602. https://doi.org/10.1111/j.2005.0906-7590.04285.x.

182. Bayram, G.G., and Candan, S. (2021). Morphology and Histology of Male Reproductive System of Gryllus campestris Linnaeus, 1758 (Orthoptera: Gryllidae). Commagene J. Biol. *Erken Görünüm*, 63–72. https://doi.org/10.31594/commagene.869116.

183. Spann, L. (1934). Studies on the Reproductive Systems of Gryllus assimilis Fabr. Trans. Kans. Acad. Sci. (1903-) *37*, 299. https://doi.org/10.2307/3625312.

184. Zinsmeister, P.P. (1969). A Histochemical and Autoradiographic Study of the Ovarioles of the Cockroach, Periplaneta americana, and the Milkweed Bug, Oncopeltus fasciatus. Doctoral dissertation, University of Illinois.

185. Muschio, H.M. (1957). A Study of Spermatogenesis in the American Cockroach, Periplaneta americana Linnaeus. Masters dissertation, Fordham University.

186. Jervis, M.A., and Kidd, N.A.C. (1986). Host-feeding strategies in hymenopteran parasitoids. Biol. Rev. *61*, 395–434. https://doi.org/10.1111/j.1469-185x.1986.tb00660.x.

187. Liu, N.-Y., Wu, G.-X., Ze, S.-Z., Yang, B., and Zhu, J.-Y. (2017). Morphology and ultrastructure of the male reproductive system of the jewel wasp, Nasonia vitripennis (Walker) (Hymenoptera: Pteromalidae). J. Asia-Pac. Entomol. *20*, 577–582. https://doi.org/10.1016/j.aspen.2017.03.017.

188. Srivastava, U.S. (1956). On the Post-embryonic Development of the Female Reproductive Organs of Tribolium castaneum Herbst. Beitrage zur Entomologie *6*, 274–284.

189. Hodin, J. (2009). Chapter 11. She Shapes Events As They Come: Plasticity in Female Insect Reproduction. In Phenotypic Plasticity of Insects, D. W. Whitman, ed.

190. Trauner, J., and Büning, J. (2007). Germ-cell cluster formation in the telotrophic meroistic ovary of Tribolium castaneum (Coleoptera, Polyphaga, Tenebrionidae) and its

bioRxiv preprint doi: https://doi.org/10.64898/2026.10.09.752918; this version posted October 16, 2026. The copyright holder for this preprint (which was not certified by peer review) is the author/funder, who has granted bioRxiv a license to display the preprint in perpetuity. It is made available under a CC-BY 4.0 International license.

1417 implication on insect phylogeny. Dev Genes Evol *217*, 13–27.
1418 https://doi.org/10.1007/s00427-006-0114-3.

1419 191. Tungjitwitayakul, J., Suppasat, T., and Tatun, N. (2022). Adverse effects of UV-C
1420 irradiation on the morphology of reproductive organs, fecundity, and fertility of the red
1421 flour beetle, Tribolium castaneum Herbst (Coleoptera; Tenebrionidae). Pol J
1422 Entomology *91*, 56–67. https://doi.org/10.5604/01.3001.0015.8555.

1423 192. Vommaro, M.L., Donato, S., Caputo, S., Agostino, R.G., Montali, A., Tettamanti,
1424 G., and Giglio, A. (2024). Anatomical changes of Tenebrio molitor and Tribolium
1425 castaneum during complete metamorphosis. Cell Tissue Res. *396*, 19–40.
1426 https://doi.org/10.1007/s00441-024-03877-8.

1427 193. Vommaro, M.L., Donato, S., Lo, L.K., Brandmayr, P., and Giglio, A. (2022).
1428 Anatomical study of the red flour beetle using synchrotron radiation X-ray phase-
1429 contrast micro-tomography. J Anat. https://doi.org/10.1111/joa.13796.

1430 194. Fishman, E.L., Jo, K., Ha, A., Royfman, R., Zinn, A., Krishnamurthy, M., and
1431 Avidor-Reiss, T. (2017). Atypical centrioles are present in Tribolium sperm. Open
1432 Biology *7*, 160334. https://doi.org/10.1098/rsob.160334.

1433 195. Hopkins, J.D., Steelman, C.D., and Carlton, C.E. (1992). Anatomy of the Adult
1434 Female Lesser Mealworm Alphitobius diaperinus (Coleoptera: Tenebrionidae)
1435 Reproductive system. Journal of the Kansas Entomological Society *65*, 299–307.

1436 196. Sakai, H., Kirino, Y., Katsuma, S., Aoki, F., and Suzuki, M.G. (2016).
1437 Morphological and histomorphological structures of testes and ovaries in early
1438 developmental stages of the silkworm, Bombyx mori. J. Insect Biotechnol. Sericology
1439 *85*, 15–20. https://doi.org/10.11416/jibs.85.1_015.

1440 197. Dai, F.-Y., Wang, X.-Y., Tan, D., Lu, C., and Xiang, Z.-H. (2006). Variation in
1441 ovariole number of diverse lines and its relationship with egg productivity in the
1442 silkworm, Bombyx mori. Acta Entomologica Sinica *49*, 903–907.

1443 198. Ômura, S. (1936). Studies on the reproductive system of the male of Bombyx mori:
1444 I. Structure of the testis and the intratesticular behaviour of the spermatozoa. Journal of
1445 the Faculty of Agriculture, Hokkaido Imperial University *38*, 151–181.

1446 199. Fiil, A. (1976). Oogenesis in the malaria mosquito Anopheles gambiae. Cell Tissue
1447 Res. *167*, 23–35. https://doi.org/10.1007/bf00220157.

1448 200. Huho, B.J., Ng'habi, K.R., Killeen, G.F., Nkwengulila, G., Knols, B.G., and
1449 Ferguson, H.M. (2006). A reliable morphological method to assess the age of male
1450 Anopheles gambiae. Malar. J. *5*, 62. https://doi.org/10.1186/1475-2875-5-62.

bioRxiv preprint doi: https://doi.org/10.64898/2026.10.09.752918; this version posted October 16, 2026. The copyright holder for this preprint (which was not certified by peer review) is the author/funder, who has granted bioRxiv a license to display the preprint in perpetuity. It is made available under a CC-BY 4.0 International license.

201. Bader, C.A., and Williams, C.R. (2012). Mating, ovariole number and sperm production of the dengue vector mosquito Aedes aegypti (L.) in Australia: broad thermal optima provide the capacity for survival in a changing climate. Physiol. Entomol. *37*, 136–144. https://doi.org/10.1111/j.1365-3032.2011.00818.x.

202. Zhang, H., Goh, F.G., Ng, L.C., Chen, C.H., and Cai, Y. (2023). Aedes aegypti exhibits a distinctive mode of late ovarian development. BMC Biol. *21*, 11. https://doi.org/10.1186/s12915-023-01511-7.

203. Hodapp, C.J., and Jones, J.C. (1961). The Anatomy of the Adult Male Reproduction System of Aedes aegypti (Linnaeus) (Diptera, Culicidae)1. Ann. Entomol. Soc. Am. *54*, 832–844. https://doi.org/10.1093/aesa/54.6.832.

204. Silva, H.B. da, Barbosa, R.C., Rezende, P.H., Ayala-Costa, D., and Lino-Neto, J. (2025). New findings on the male reproductive system and spermatozoa of Aedes aegypti (Diptera: Culicidae). Parasites Vectors *18*, 246. https://doi.org/10.1186/s13071-025-06808-w.

205. R'Kha, S., Moreteau, B., Coyne, J.A., and David, J.R. (1997). Evolution of a lesser fitness trait: egg production in the specialist Drosophila sechellia. Genet Res *69*, 17–23. https://doi.org/10.1017/s0016672396002546.

206. Hodin, J. (2000). Plasticity and constraints in development and evolution. J Exp Zool *288*, 1–20. https://doi.org/10.1002/(sici)1097-010x(20000415)288:1<1::aid-jez1>3.0.co;2-7.

207. Calise, C.L. (2024). Characterization of the Apical Testis and Fusome Patterning in Drosophila melanogaster, Drosophila simulans, Drosophila pseduoobscura, Drosophila affinis, and Drosophila sechellia. Masters dissertation, Cornell University.

208. Hardy, R.W., Tokuyasu, K.T., Lindsley, D.L., and Garavito, M. (1979). The germinal proliferation center in the testis of Drosophila melanogaster. J. Ultrastruct. Res. *69*, 180–190. https://doi.org/10.1016/s0022-5320(79)90108-4.

209. Starmer, W.T., Polak, M., Pitnick, S., McEvey, S.F., Barker, J.S.F., and Wolf, L.L. (2003). Phylogenetic, Geographical, and Temporal Analysis of Female Reproductive Trade-Offs in Drosophilidae. 139–171. https://doi.org/10.1007/978-1-4757-5190-1_3.

210. Chapman, R.F. (2012). The Insects. https://doi.org/10.1017/cbo9781139035460.

211. Bustin, S.A., Benes, V., Garson, J.A., Hellemans, J., Huggett, J., Kubista, M., Mueller, R., Nolan, T., Pfaffl, M.W., Shipley, G.L., et al. (2009). The MIQE Guidelines: Minimum Information for Publication of Quantitative Real-Time PCR Experiments. Clin. Chem. *55*, 611–622. https://doi.org/10.1373/clinchem.2008.112797.

bioRxiv preprint doi: https://doi.org/10.64898/2026.10.09.752918; this version posted October 16, 2026. The copyright holder for this preprint (which was not certified by peer review) is the author/funder, who has granted bioRxiv a license to display the preprint in perpetuity. It is made available under a CC-BY 4.0 International license.

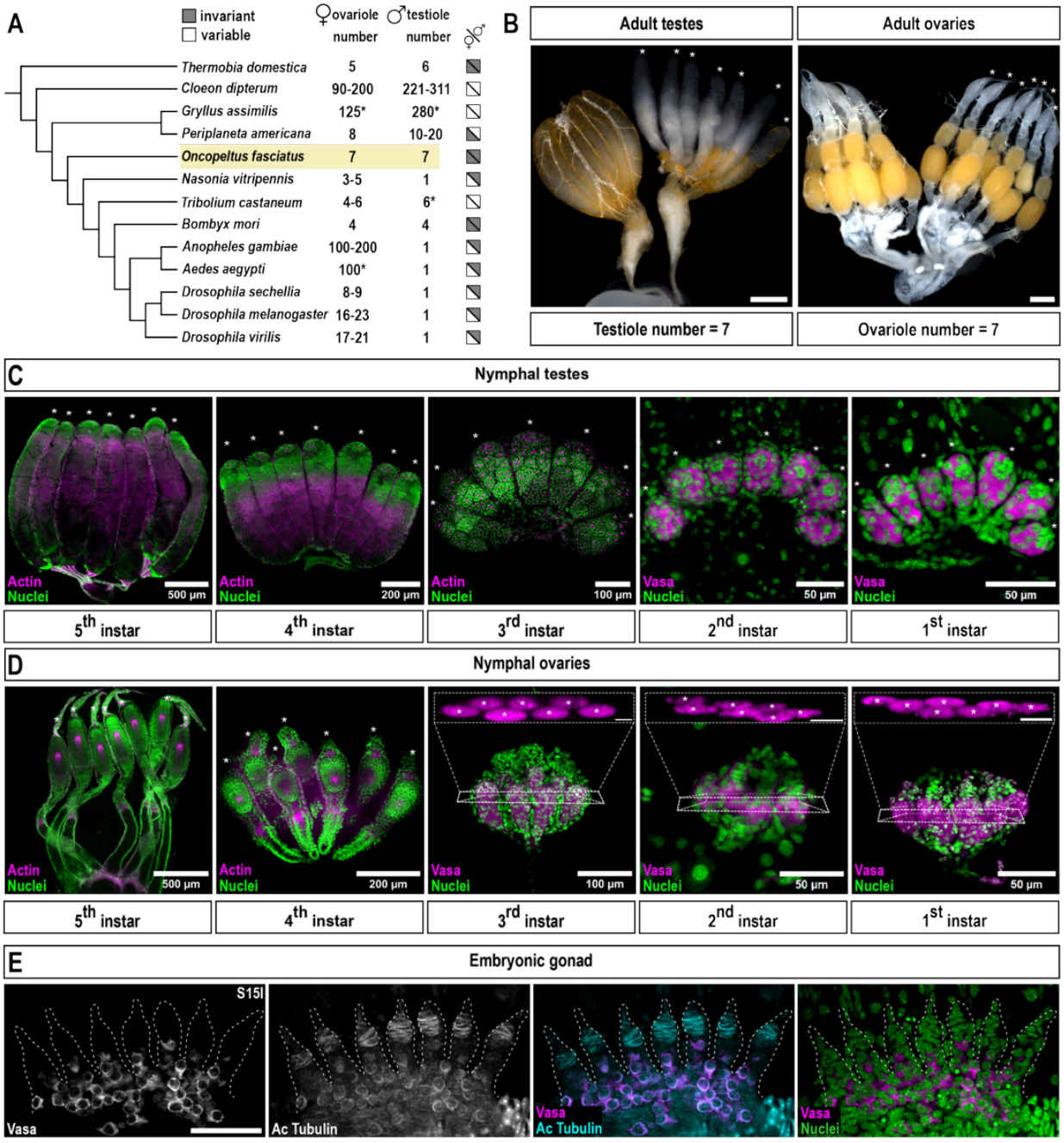


Figure 1. *O. fasciatus* gonadiole number is established in the embryo. (A) Cladogram illustrating the phylogenetic relationships amongst previously studied insect species. Ovariole number per ovary and testiole number per testis for each species (Table S1) are shown as a single value, a reported range (minimum – maximum), or an approximate mean (indicated by *). **(B)** Paired gonads of the adult hemipteran bug *O. fasciatus*. Gonads on the left are shown intact, whereas those on the right are dissected to reveal individual gonadioles. Asterisks denote each individual gonadiole, totalling seven ovarioles per ovary in females (n=20) and seven testioles per testis in males (n=20). Scale bars = 500 µm. **(C-D)** Gonad development across five nymphal stages. Individual testes (C) or ovaries (D) from each nymphal stage are shown, with asterisks denoting individual gonadioles. In later stage gonads, tissue architecture is visualised using phalloidin staining which labels filamentous actin (magenta). In earlier stage gonads, immunostaining against Ofas-Vas (magenta) is used to identify germ cells. Scale bar lengths are 500, 200, 100, 50 and 50 µm for 5th, 4th, 3rd, 2nd and 1st instar panels respectively. Insets above 3rd, 2nd and 1st instar ovary panels show transverse sections of the ovary where each ovariole is clearly resolved (inset scale bars = 20 µm). Nuclei are stained with Hoechst 33342 (green). **(E)** Embryonic gonad in a late-stage 15 embryo. Seven embryonic gonadiole primordia are outlined by dotted lines. Ofas-Vasa (magenta) labels the germ cells, while acetylated Tubulin (Ac Tubulin, cyan) highlights somatic gonadal structures and is detectable at low levels in the germ cells. Nuclei are stained with Hoechst 33342 (green). Scale bars = 50 µm.

bioRxiv preprint doi: https://doi.org/10.64898/2026.10.09.752918; this version posted October 16, 2026. The copyright holder for this preprint (which was not certified by peer review) is the author/funder, who has granted bioRxiv a license to display the preprint in perpetuity. It is made available under a CC-BY 4.0 International license.

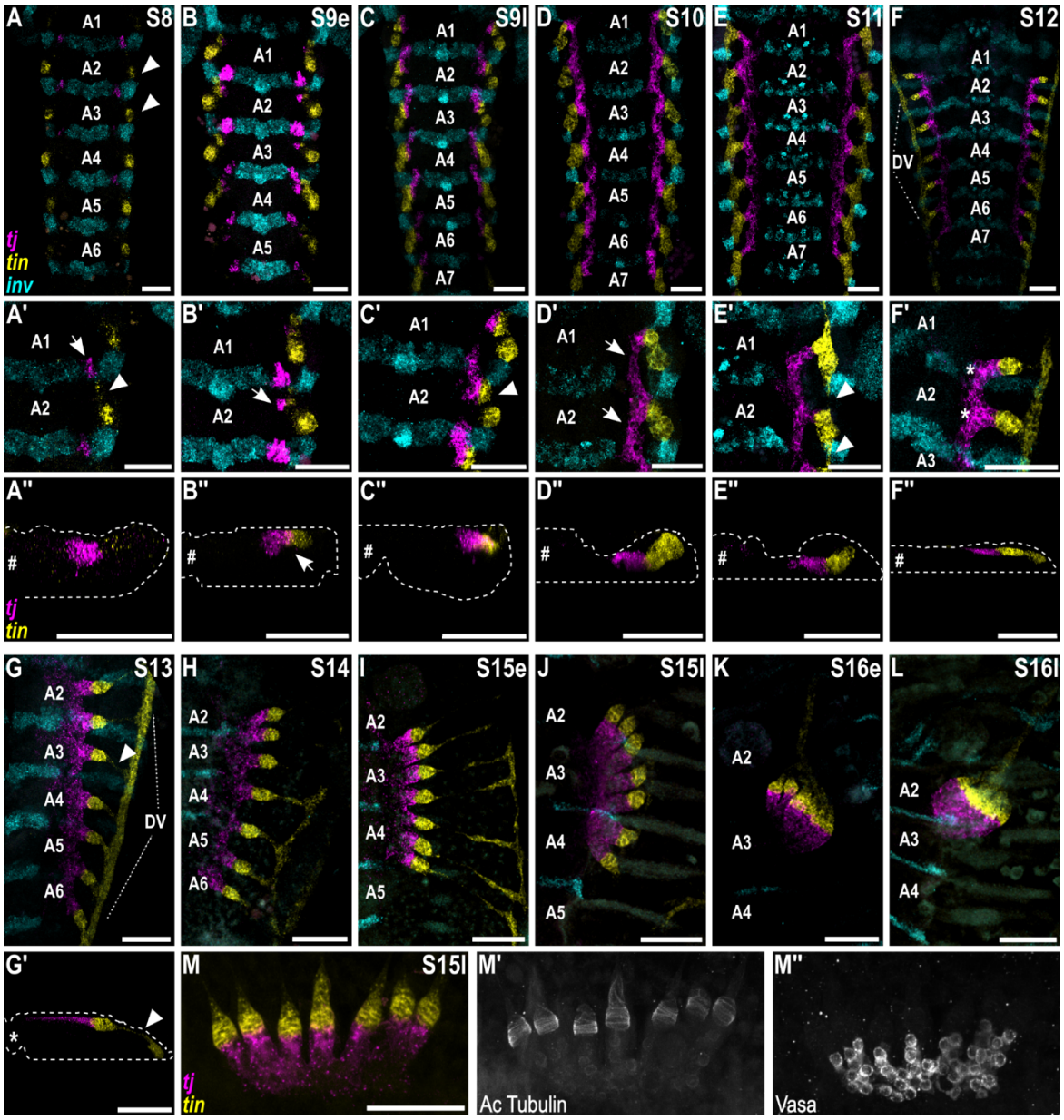


Figure 2. Segment-specific domains of *Ofas-traffic jam* and *Ofas-tinman* expression form the somatic gonad precursors. **(A-L)** Selected abdominal regions where *Ofas-tin* and *Ofas-tj* expression are detected across sequential stages of *O. fasciatus* embryonic development. *Ofas-tj* (magenta) and *Ofas-tin* (yellow) mark somatic gonad precursors. *Ofas-inv* (cyan) marks the posterior compartment of each segment. Segment identity is indicated in each panel. In (A), arrowheads indicate the primary and lateral *Ofas-tin* domain. In (F-G), the dorsal vessel (DV) is indicated with dotted lines. Tapered regions of *Ofas-tin* expression are highlighted with arrowheads in (G). **(A'-F')** Magnified views of the right hemisegment of segments A1 and A2 from the embryos shown in (A-F). In (A'), arrowhead shows the secondary domain of *Ofas-tin* expression while the arrow points out the primary *Ofas-tj* expression domain. In (B'), the secondary domain of *Ofas-tj* is highlighted with a white arrow. In (C'), the adjacent *Ofas-tin*/*Ofas-tj* units are indicated with a white arrowhead. White arrows and arrowheads in (D') and (E') show the expansion of the *Ofas-tj* and *Ofas-tin* domains leading the formation of a contiguous expression domain from A1-A7. Asterisks in (F') show individual *Ofas-tin*/*Ofas-tj* gonadiole precursors. **(A''-F'' and G')** Transverse sections through the right hemisegment of segment A2. Only *Ofas-tin* and *Ofas-tj* are visualized in these panels. Dotted lines indicate the embryonic surface while the hash denotes the midline. In (B''), the arrowhead shows the adjacent expression of *Ofas-tin* and *Ofas-tj*. In (G'), the arrowhead highlights the tapering *Ofas-tin* domain. **(M-M'')** show a coalesced embryonic gonad in a late-stage 15 embryo. *Ofas*-Vas labels the germ cells which are present in the *Ofas-tj* -positive (magenta) region of the gonad. Acetylated Tubulin (Ac Tubulin) is detected in the *Ofas-tin* -positive (yellow) region of the gonad and at lower levels in the germ cells. Scale bars = 50 μm.

bioRxiv preprint doi: https://doi.org/10.64898/2026.10.09.752918; this version posted October 16, 2026. The copyright holder for this preprint (which was not certified by peer review) is the author/funder, who has granted bioRxiv a license to display the preprint in perpetuity. It is made available under a CC-BY 4.0 International license.

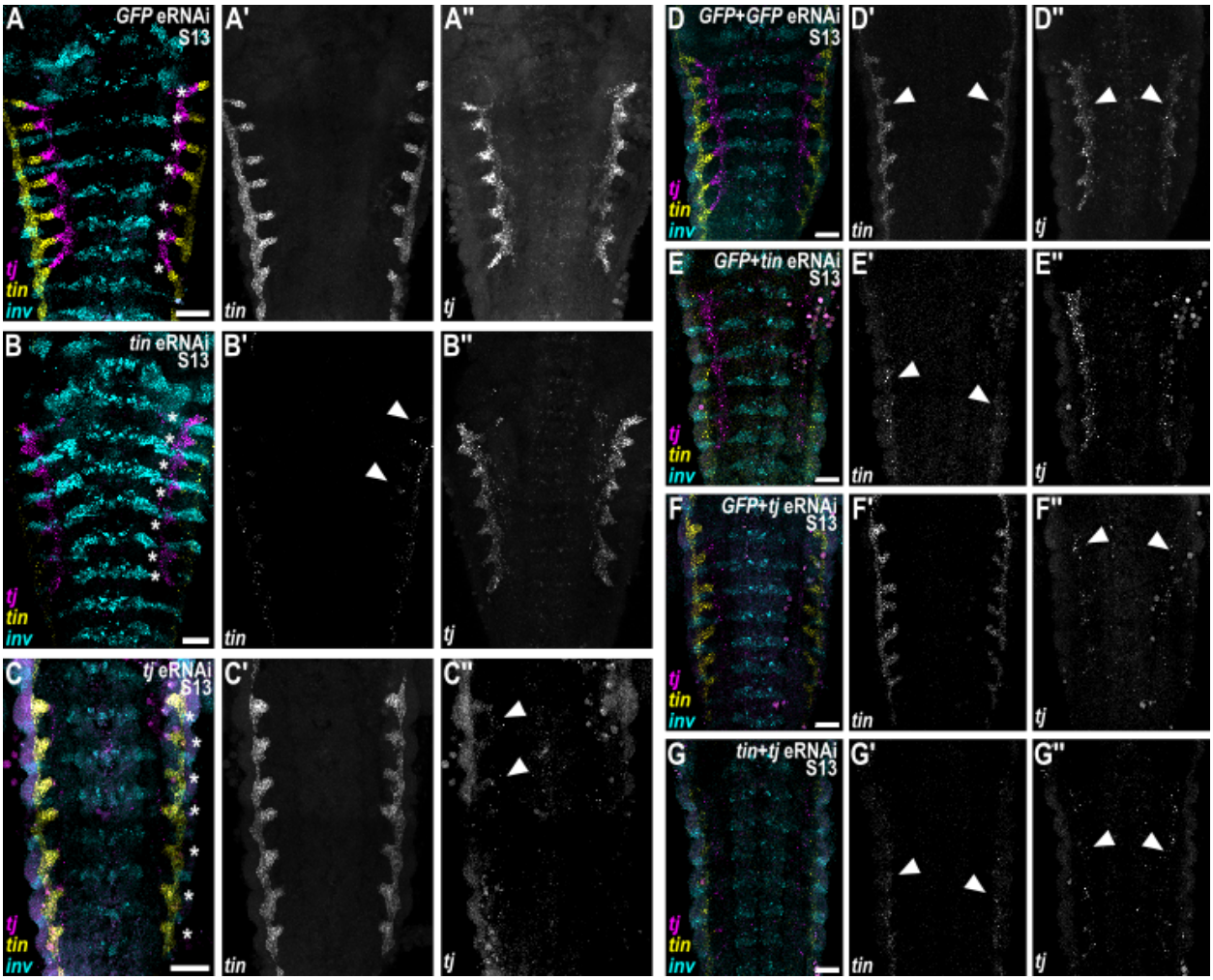


Figure 3. *Ofas-tin* and *Ofas-tj* are expressed independently of each other. **(A-C'')** Representative images of selected abdominal segments of embryos from double eRNAi experiments. (A-A'') A *GFP* dsRNA-injected (*GFP* eRNAi) embryo (n=209/209); (B-B'') an *Ofas-tin* dsRNA-injected (*tin* eRNAi) embryo (n=135/135). *Ofas-traffic jam* (*tj*) expression is still detectable, and seven gonadiole primordia still form. *Ofas-tin* expression is still present weakly (B'; white arrowheads); (C-C'') *Ofas-tj* dsRNA-injected (*tj* eRNAi) embryo (n=41/41). *Ofas-tin* expression does not appear to be affected while *Ofas-tj* continues to be weakly expressed (C''; white arrowheads). **(D-G'')** Representative images of selected abdominal segments of embryos from double eRNAi experiments. (D-D'') A *GFP+GFP* double eRNAi (*GFP+GFP* eRNAi) embryo (n=14/14); (E-E'') *GFP+ Ofas-tin* dsRNA-injected (*GFP+tin* eRNAi) embryo (n=17/19). *Ofas-traffic jam* (*tj*) expression does not appear to be affected and forms seven precursors (E''). *Ofas-*tinman (*tin*) expression is still present weakly (E'; white arrowheads); (F-F'') a *GFP+ Ofas-tj* -dsRNA-injected (*GFP+tj* eRNAi) embryo (n=15/16). *Ofas-tin* expression does not appear to be affected (F') while *Ofas-tj* continues to be weakly expressed (F''; white arrowheads). Seven precursors are formed. (G-G'') a *tin+ tj*-dsRNA-injected (*tin+tj* eRNAi) embryo (n=20/23). Weak expression of both tin and tj is detectable (G'-G''; white arrowheads) and precursors-like structures are visible. *Ofas-tj* (magenta) and *Ofas-tin* (yellow) mark somatic gonad precursors. *Ofas-inv* (cyan) marks the posterior compartment of each segment. Asterisks indicate individual gonadiole primordia. Scale bars = 50 µm.

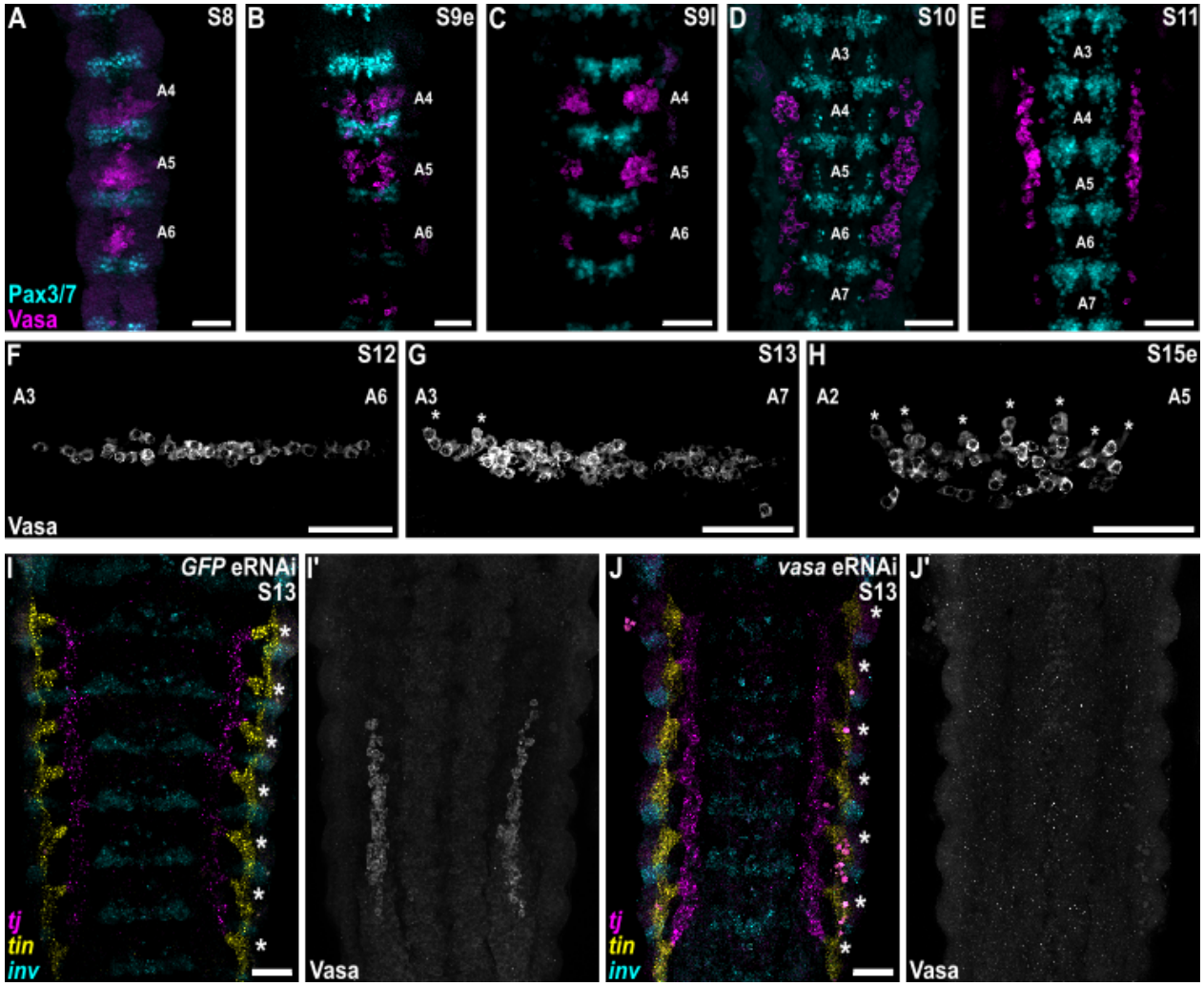


Figure 4. Germ cells begin to form seven independent clusters after the somatic gonad precursors are established. (A-H) Germ cells, labelled by Ofas-Vas (magenta in A-E; grey in F-H), across sequential stages of embryonic development. Pax3/7 (cyan) marks the posterior compartment of each segment up to S8 and segmentally iterated neuroblast clusters thereafter. **(I-J')** Representative images of selected abdominal segments of (I-I') a *GFP* dsRNA-injected embryo (*GFP* eRNAi, n=49/49); (J-J') an *Ofas-vas* dsRNA-injected embryo (*Ofas-vas* eRNAi, n=32/32).

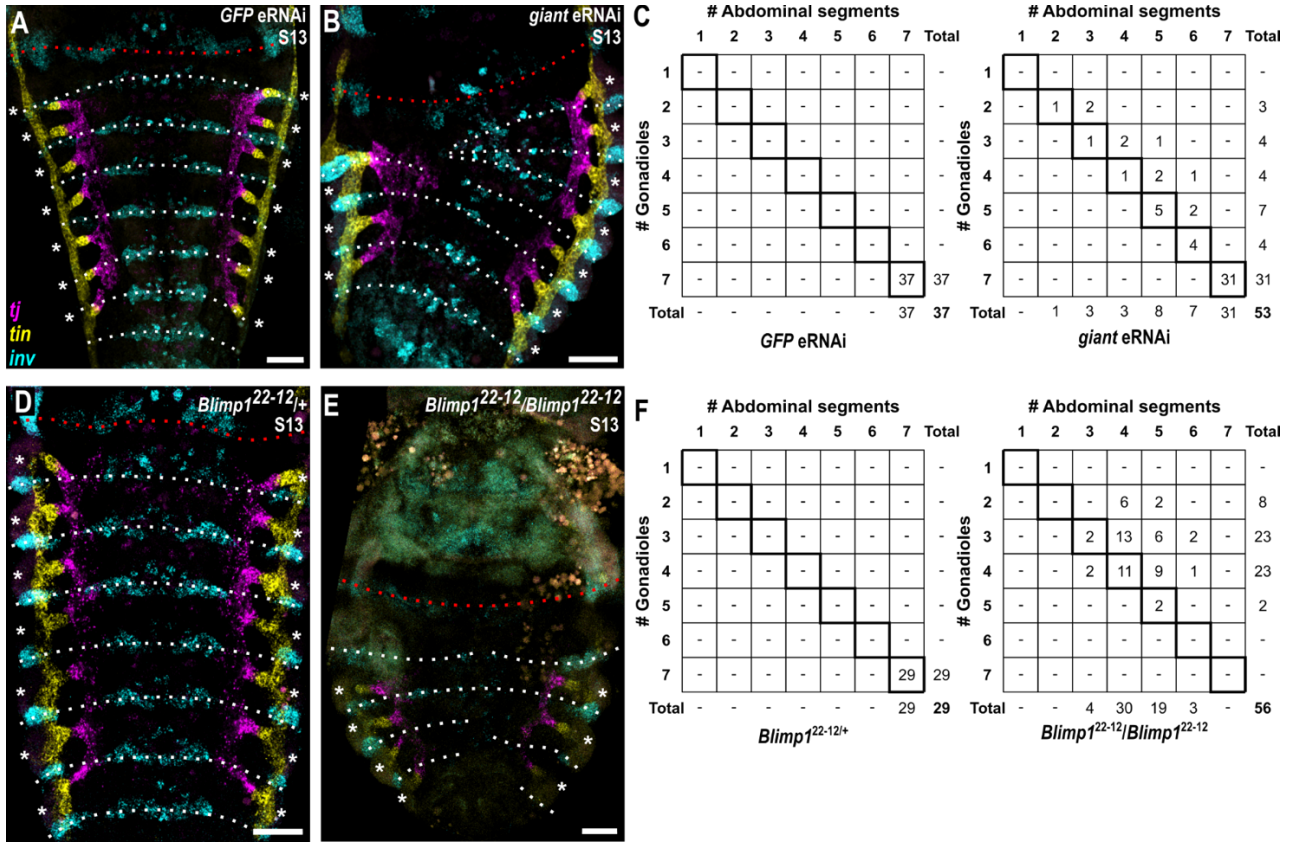


Figure 5. Reducing the number of gonadiole-producing segments decreases gonadiole number. (A-B, D-E) Representative images of selected abdominal segments of embryos (A) injected with dsRNA targeting *GFP* (*GFP* eRNAi, n=66/66); (B) injected with dsRNA targeting *Ofas-giant* (n=40/91 show a reduction in gonadiole primordium number); (D) *Ofas-Blimp1*$^{22\text{-}12}$/+ heterozygotes (n=29/29) have wild type numbers of gonadiole precursors; (E) *Ofas-Blimp1*$^{22\text{-}12}$ homozygotes (n=56/56) show a reduction in gonadiole primordium number. *Ofas-tj* (magenta) and *Ofas-tin* (yellow) mark somatic gonad precursors. *Ofas-inv* (cyan) marks the posterior compartment of each segment. Red dotted line denotes the posterior of the third thoracic segment and white dotted lines delineate the seven abdominal segments. Asterisks indicate individual gonadiole primordia. Scale bars = 50 µm. **(C, F)** Plots showing the relationship between gonadiole precursor number (y-axis) and the number of the first seven abdominal segments still present (x-axis) in (C) *GFP* eRNAi and *Ofas-giant* eRNAi embryos and (F) *Ofas-Blimp1*$^{22\text{-}12}$heterozygous and *Ofas-Blimp1*$^{22\text{-}12}$*homozygous* mutant embryos in each hemisegment. The diagonal indicates a perfect one-to-one correspondence between the total number of gonadiole primordium-producing segments and gonadiole primordia number in each hemisegment.

bioRxiv preprint doi: https://doi.org/10.64898/2026.10.09.752918; this version posted October 16, 2026. The copyright holder for this preprint (which was not certified by peer review) is the author/funder, who has granted bioRxiv a license to display the preprint in perpetuity. It is made available under a CC-BY 4.0 International license.

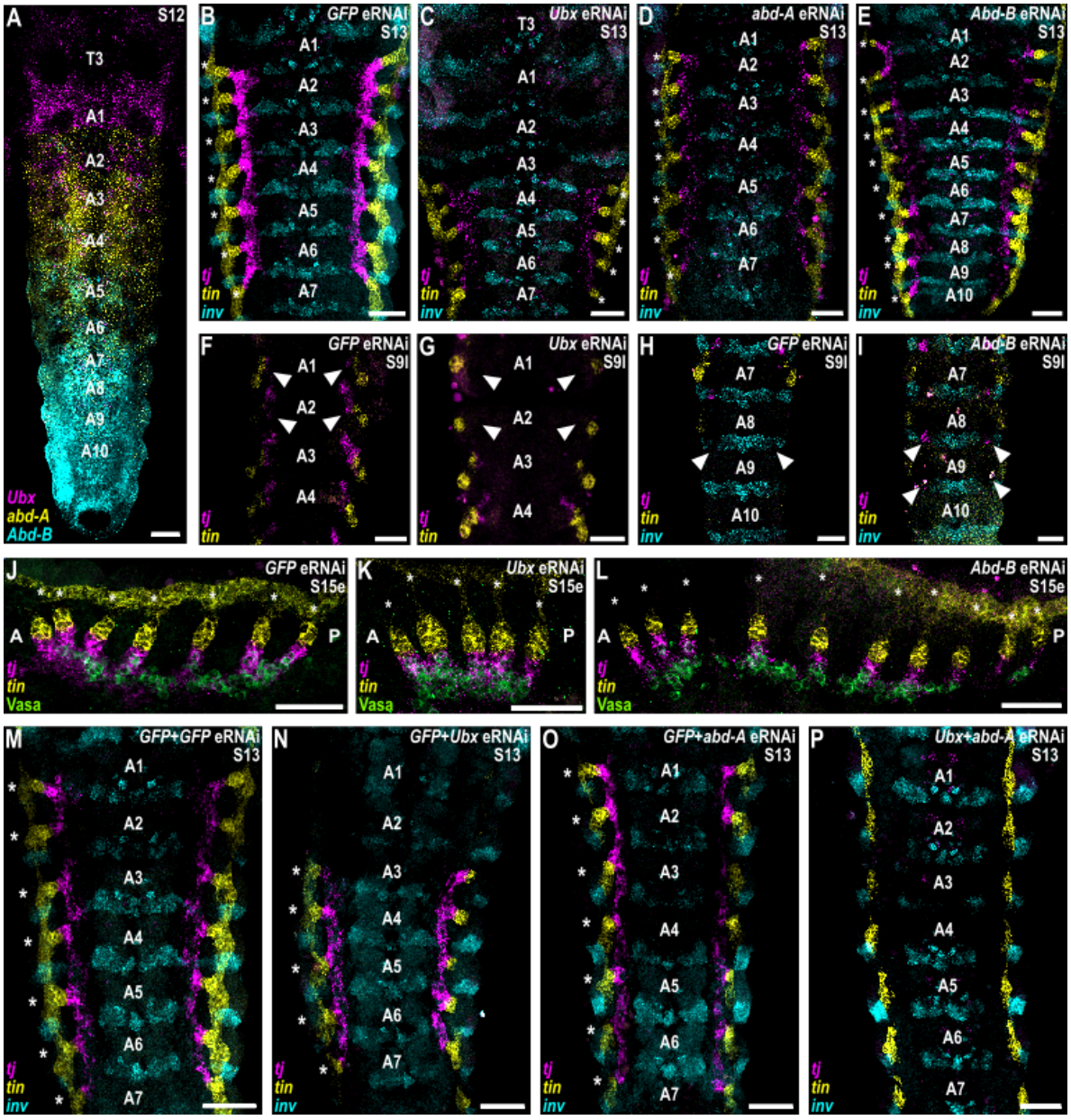


Figure 6. Posterior Hox genes regulate gonadiole primordia formation. (A) Posterior thoracic and abdominal expression of *Ofas-Ultrabithorax* (*Ubx*, magenta), *Ofas-abdominal A* (*abd-A*, yellow) and *Ofas-Abdominal B* (*abd-B*, cyan) at stage 12. Individual expression patterns are shown in Figure S5A. Scale bar = 50 µm. **(B-E)** Representative images of selected abdominal segments of embryos injected with dsRNA targeting (B) *GFP* (*GFP* eRNAi), (C) *Ofas-Ubx*, (D) *Ofas-abd-A* or (E) *Ofas-Abd-B*. *Ofas-Ubx* eRNAi embryos form only five gonadiole precursors, with the precursors missing in A1 and A2 (n=34/56). *Ofas-Abd-B* eRNAi embryos form ectopic gonadiole precursors in A8-A10 (n=32/60). *GFP* eRNAi (n=69/69) and *Ofas-abd-A* eRNAi (86/87) embryos show no change in gonadiole precursor number. **(F-G)** Neither *Ofas-tj*- nor *Ofas-tin*-expressing somatic gonad precursors are specified at stage 9 in A1 or A2 in *Ofas-Ubx* eRNAi embryos (white arrows). **(H-I)** In *Abd-B* eRNAi embryos, ectopic *Ofas-tj*- and *Ofas-tin*-expressing somatic gonad precursors are specified in segments A8-A10 in stage 9 in the same location within each segment as in the anterior abdominal segments (white arrows). **(J-L)** In *Ofas-Ubx* and *Ofas-Abd-B* eRNAi embryos, gonads coalesce normally despite having an abnormal number of gonadioles. Anterior (A) and posterior (P) are indicated on the images. **(M-P)** Representative images of selected abdominal segments of embryos from double eRNAi experiments. *Ofas-Ubx*+ *Ofas-abd-A* double eRNAi embryos have no detectable gonadiole precursors in any segment (n=102/112). Lateral secondary *Ofas-tin* domains connect to each other forming a contiguous expression domain. *GFP*+ *GFP* double eRNAi (*GFP*+*GFP* eRNAi n=98/98) and *GFP*+ *Ofas-abd-A* double eRNAi (n=79/79) embryos show no change in gonadiole precursor number, whereas *GFP*+ *Ofas-Ubx* double eRNAi embryos have only five precursors (n=89/102). In panels (B-P), *Ofas-tj* is shown in magenta, *Ofas-tin* in yellow, *Ofas-inv* in cyan, and *Ofas*-Vas in green. Asterisks denote individual gonadiole primordia. Scale bars = 50 µm.

bioRxiv preprint doi: https://doi.org/10.64898/2026.10.09.752918; this version posted October 16, 2026. The copyright holder for this preprint (which was not certified by peer review) is the author/funder, who has granted bioRxiv a license to display the preprint in perpetuity. It is made available under a CC-BY 4.0 International license.

Supplemental Information for

The Hox code abolishes anatomical variation in an insect gonad

Jonchee A. Kao, Tarun Kumar, Daniella A. Haber, Cassandra G. Extavour

Figures S1 through S6

Tables S1 through S9

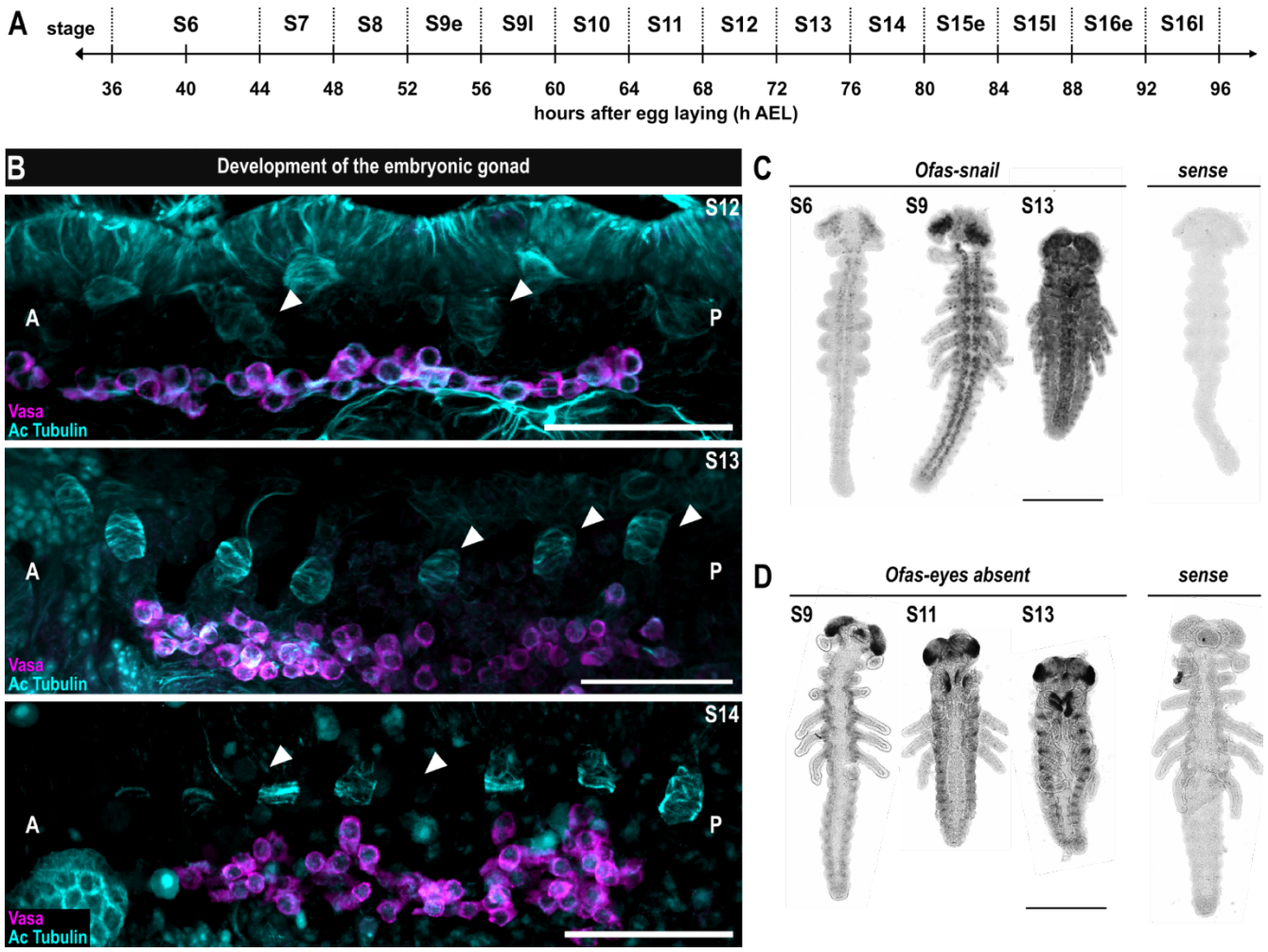


Figure S1. Acetylated Tubulin is expressed strongly in the presumptive embryonic somatic gonad primordia and weakly in the germ cells. (**A**) Embryonic stages used in this study, indicating ranges of developmental time (hours after egg laying (h AEL) spanned by each stage. (See also Table S2). (**B**) Cells in seven lateral abdominal domains expressing acetylated Tubulin (Ac Tubulin, cyan) are shown associated with the germ cells expressing Ofas-Vas (magenta) across three sequential stages of embryonic development. White arrowheads point to individual gonad precursors. A and P depict the anteroposterior axis of the embryo. Scale bars = 50 µm. (**C-D**) Colorimetric *in situ* hybridisation of (C) *Ofas-snail* (*snail*) and (D) *Ofas-eyes absent* (*eya*) across three stages of embryonic development. Scale bars = 1000 µm.

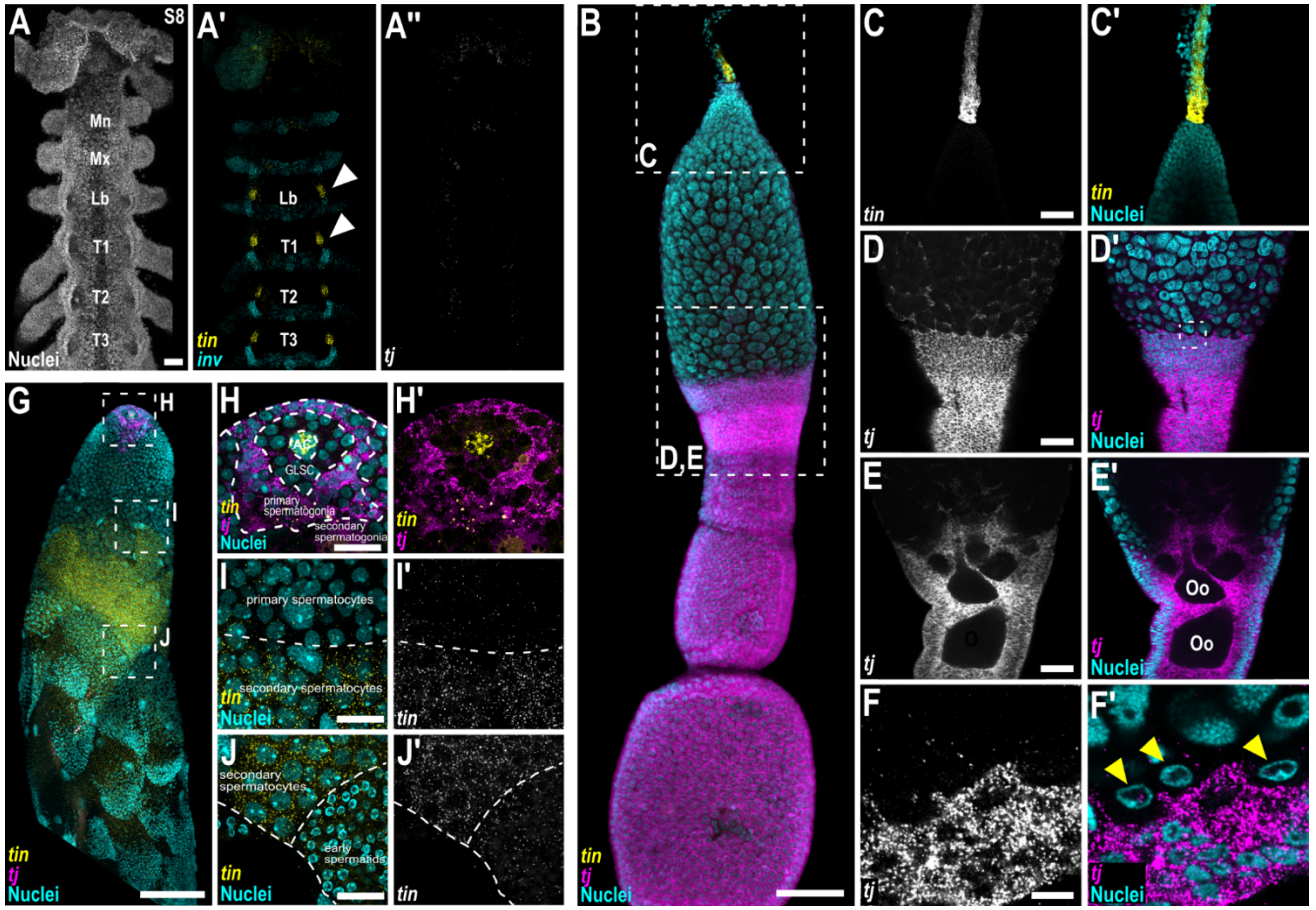


Figure S2. *Ofas-tj* and *Ofas-tin* are expressed in the adult gonads. (A) Head and thoracic segments of a stage 8 embryo. (**A'**) *Ofas-tin* (yellow) marks heart precursors in all segments including and posterior to the labial segment. *Ofas-inv* (cyan) marks the posterior compartment of each segment. (**A''**) *Ofas-tj* (magenta) expression is not detected in the head or thoracic segments. Abdominal expression of *Ofas-tj* and *Ofas-tin* at this stage is shown in Figure 2A. Nuclei stained with Hoechst 33342 (grey) show embryonic morphology. Segment identity is indicated in each panel. Scale bar = 50 µm. **(B)** In adult ovaries, *Ofas-tj* was expressed in follicle cells surrounding developing oocytes throughout oogenesis, whereas *Ofas-tin* expression was detected in the terminal filament of each ovariole. Scale bar = 100 µm. **(C-E)** Higher magnification of boxed regions in (B) showing *Ofas-tin* and *Ofas-tj* expression in distinct regions of the ovariole: *Ofas-tin* is expressed in the terminal filament (**C-C'**). *Ofas-tj* is expressed in follicle cells of both the tropharium (**D-D'**) and developing oocytes (**E-E'**; Oo). Scale bars = 25 µm. *Ofas-tj* expression is not detected in late-stage oocytes (E-E') or early oocytes (**F-F'**; yellow arrowheads). Scale bar = 50 µm. **(G)** In adult testes, *Ofas-tin* was expressed in the apical complex of each testiole, whereas *Ofas-tj* was detected in the somatic cells surrounding the primary spermatogonia. In addition to its apical expression, *Ofas-tin* was strongly expressed in a discrete region near the middle of the testiole corresponding to the secondary spermatocytes. Scale bar = 100 µm. **(H-J)** Higher magnification of insets in (G) showing *Ofas-tin* and *Ofas-tj* expression in distinct regions of the testioles. *Ofas-tj* is expressed in the region surrounding the germline stem cells (GLSC) where both presumptive gonialblasts and cyst progenitor cells can be found, whereas *Ofas-tin* is expressed in the apical complex and in secondary spermatocytes. The stages of spermatogenesis [171,172] are labelled. Scale bars = 25 µm.

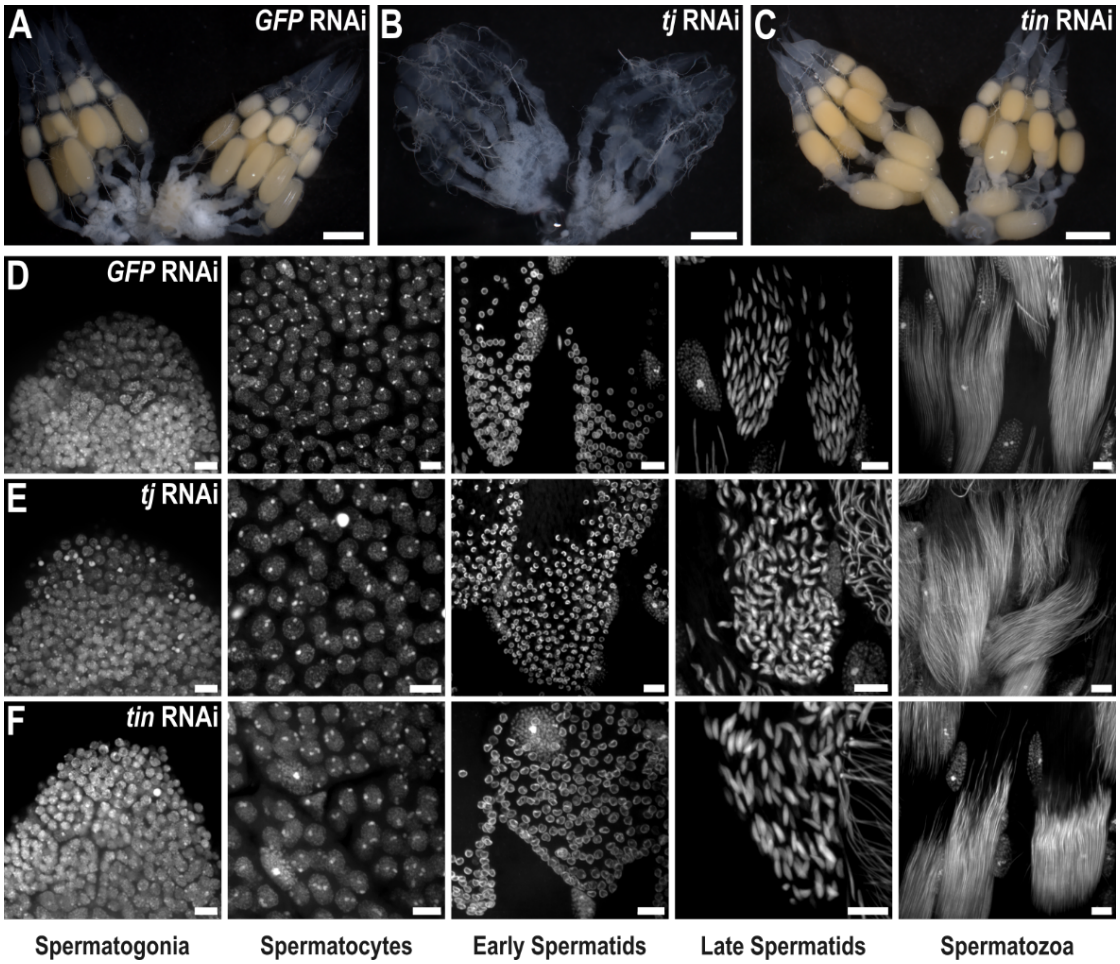


Figure S3. *Ofas-tj* is required for oogenesis. We performed RNAi against *Ofas-tin* and *Ofas-tj* in adult females and males. Reduction of *Ofas-tin* produced no readily detectable defects in oogenesis (A, C), whereas *Ofas-tj* RNAi resulted in a failure of oogenesis (B), suggesting a requirement for *Ofas-tj* during female gametogenesis under these conditions. **(A-C)** Representative ovaries, five days after injection, from adult females injected with (A) *GFP* dsRNA (*GFP* RNAi, n=12), (B) *Ofas-tj* dsRNA (*tj* RNAi, n=16) or (C) *Ofas-tin* dsRNA (*tin* RNAi, n=18). Scale bars = 1000 μm. By contrast, neither *Ofas-tin* nor *Ofas-tj* RNAi produced an overt defect in spermatogenesis: all morphological stages of spermatogenesis remained detectable in dsRNA-injected males. **(D-F)** Representative testes from adult males injected with (D) dsRNA targeting *GFP* (*GFP* RNAi, n=24), (E) *Ofas-tj* (*tj* RNAi, n=37), or (F) *Ofas-tin* (*tin* RNAi, n=29). Testes were stained with Hoechst 33342 (grey) to visualise the stages of spermatogenesis, which appear unaffected by either *Ofas-tj* or *Ofas-tin* RNAi. Scale bars = 10 μm.

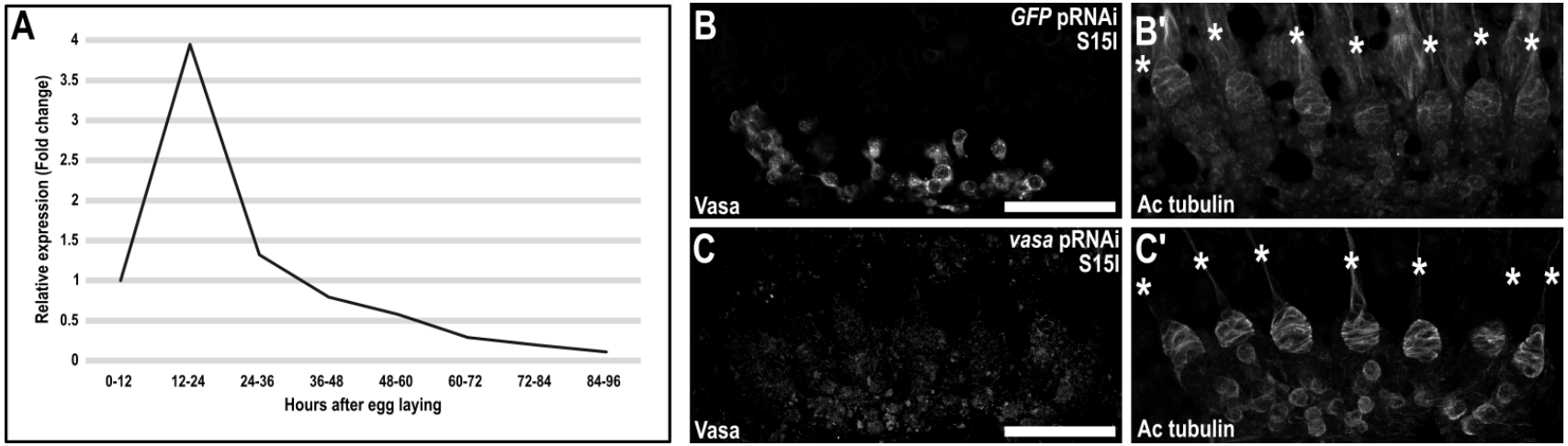
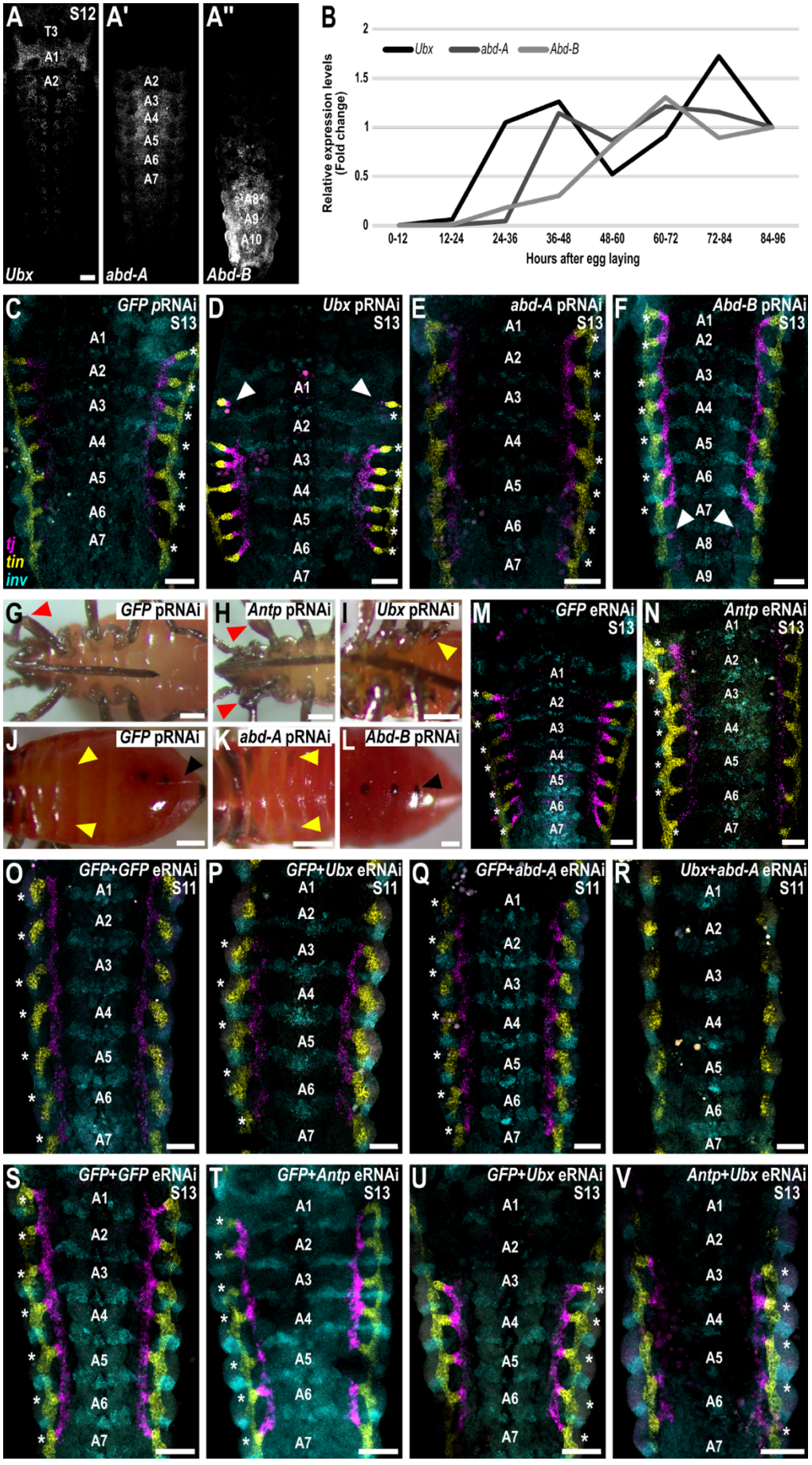


Figure S4. Maternal *Ofas-vas* RNAi reduces *Ofas-vas* expression but does not prevent formation of gonadiole primordia. (A) Relative *Ofas-vas* expression levels across sequential stages of wild type embryonic development quantified by qPCR and presented as fold change relative to embryos collected 0-12 hours after egg laying. **(B-C')** Representative gonads in stage 15 embryos laid by mothers injected with (B-B') *GFP* dsRNA (*GFP* pRNAi) or (C-C') *Ofas-vas* dsRNA (*vasa* pRNAi), stained with anti-Ofas-Vasa (grey) to detect Ofas-Vas protein levels, Acetylated Tubulin (Ac Tubulin, green) to highlight somatic gonadal structures and germ cells. Asterisks indicate individual gonadiole primordia. Scale bars = 50 μm.

bioRxiv preprint doi: https://doi.org/10.64898/2026.10.09.752918; this version posted October 16, 2026. The copyright holder for this preprint (which was not certified by peer review) is the author/funder, who has granted bioRxiv a license to display the preprint in perpetuity. It is made available under a CC-BY 4.0 International license.



bioRxiv preprint doi: https://doi.org/10.64898/2026.10.09.752918; this version posted October 16, 2026. The copyright holder for this preprint (which was not certified by peer review) is the author/funder, who has granted bioRxiv a license to display the preprint in perpetuity. It is made available under a CC-BY 4.0 International license.

Figure S5. Posterior Hox genes regulate gonadiole primordia formation (previous page). (A) Expression of *Ofas-Ultrabithorax* (*Ubx*), *Ofas-abdominal A* (*abd-A*) and *Ofas-Abdominal B* (*Abd-B*) in the stage 12 embryo shown in Figure 5A, displayed as individual channels. **(B)** Relative *Ofas-Ubx, Ofas-abd-A* and *Ofas-Abd-B* expression levels across sequential stages of embryonic development, quantified by qPCR and presented as fold change relative to expression in eggs collected 84-96 hours after egg laying. **(C-F)** Representative images of selected abdominal segments of stage 13 embryos from adult females injected with (C) dsRNA targeting *GFP* (*GFP* pRNAi), (D) *Ofas-Ubx* (*Ubx* pRNAi), (E) *Ofas-abd-A* (*abd-A* pRNAi), or (F) *Ofas-Abd-B* (*Abd-B* pRNAi). In *Ofas-Ubx* pRNAi embryos, the A1 gonadiole appears to form (white arrowheads) but does not connect to the rest of the gonad (n=11/25). In *Ofas-Abd-B* pRNAi embryos, *Ofas-tj* is expressed ectopically in A8 (red arrowheads, n=5/16). *GFP* eRNAi (n=42/42) and *Ofas-abd-A* pRNAi (n=30/30) embryos show no change in somatic gonad precursor specification. Asterisks indicate individual gonadiole primordia. Scale bars = 50 µm. **(G-I)** Segment transformations in nymphs hatched from eggs laid by adult females injected with (G) dsRNA targeting *GFP* (*GFP* pRNAi, n=30/30), (H) *Ofas-Antp* (*Antp* pRNAi; n=5/11) and (I) *Ofas-Ubx* (*Ubx* pRNAi; n=4/11). Ventral views are shown with the anterior to the left. Red arrowheads indicate the distal femur of the first leg, and yellow arrowheads indicate ectopic leg-like appendages. Scale bars = 200 µm. **(J-L)** Segment transformation in nymphs hatched from eggs laid by adult females injected with *dsRNA* targeting (J) *GFP* (*GFP* pRNAi, n=30/30), (K) *Ofas-abd-A* (*abd-A* pRNAi; n=3/11) and (L) *Ofas-Abd-B* (*Abd-B* pRNAi; n=2/20). Dorsal views of the abdomen are shown with the anterior to the left. Yellow arrowheads indicate abdominal segment A3, and black arrowheads indicate abdominal segment A7. Scale bars = 200 µm. **(M-N)** Representative images of selected abdominal segments of stage 13 embryos injected with dsRNA targeting (M) *GFP* (*GFP* eRNAi, n=69/69) and (N) *Ofas-Antp* (*Antp* eRNAi; n=35/35). There is no apparent change in gonadiole formation in either condition. **(O-R)** Representative images of selected abdominal segments of stage 11 embryos injected with dsRNA targeting (O) *GFP*+ *GFP* double eRNAi (*GFP*+*GFP* eRNAi), (P) *GFP* + *Ofas-Ubx* (2 µg/µl each), (Q) *GFP*+ *Ofas-abd-A* (2 µg/µl each) and (R) *Ofas-Ubx*+ *Ofas-abd-A* (2 µg/µl each). **(S-V)** Representative images of selected abdominal segments of stage 13 embryos injected with dsRNA targeting (S) *GFP*+ *GFP* double eRNAi (*GFP*+*GFP* eRNAi), (T) *GFP*+ *Ofas-Antp* (2 µg/µl each), (U) *GFP*+*Ofas-Ubx* (2 µg/µl each) and (V) *Ofas-Antp*+ *Ofas-Ubx* (2 µg/µl each). Additional knockdown against *Ofas-Antp* does not change the *Ofas-Ubx* knockdown phenotype. In panels **(C-F; M-V)**, *Ofas-tj* (magenta) and *Ofas-tin* (*y*ellow) mark somatic gonad precursors. *Ofas-inv* (cyan) marks the posterior compartment of each segment. Scale bars = 50 µm.

bioRxiv preprint doi: https://doi.org/10.64898/2026.10.09.752918; this version posted October 16, 2026. The copyright holder for this preprint (which was not certified by peer review) is the author/funder, who has granted bioRxiv a license to display the preprint in perpetuity. It is made available under a CC-BY 4.0 International license.

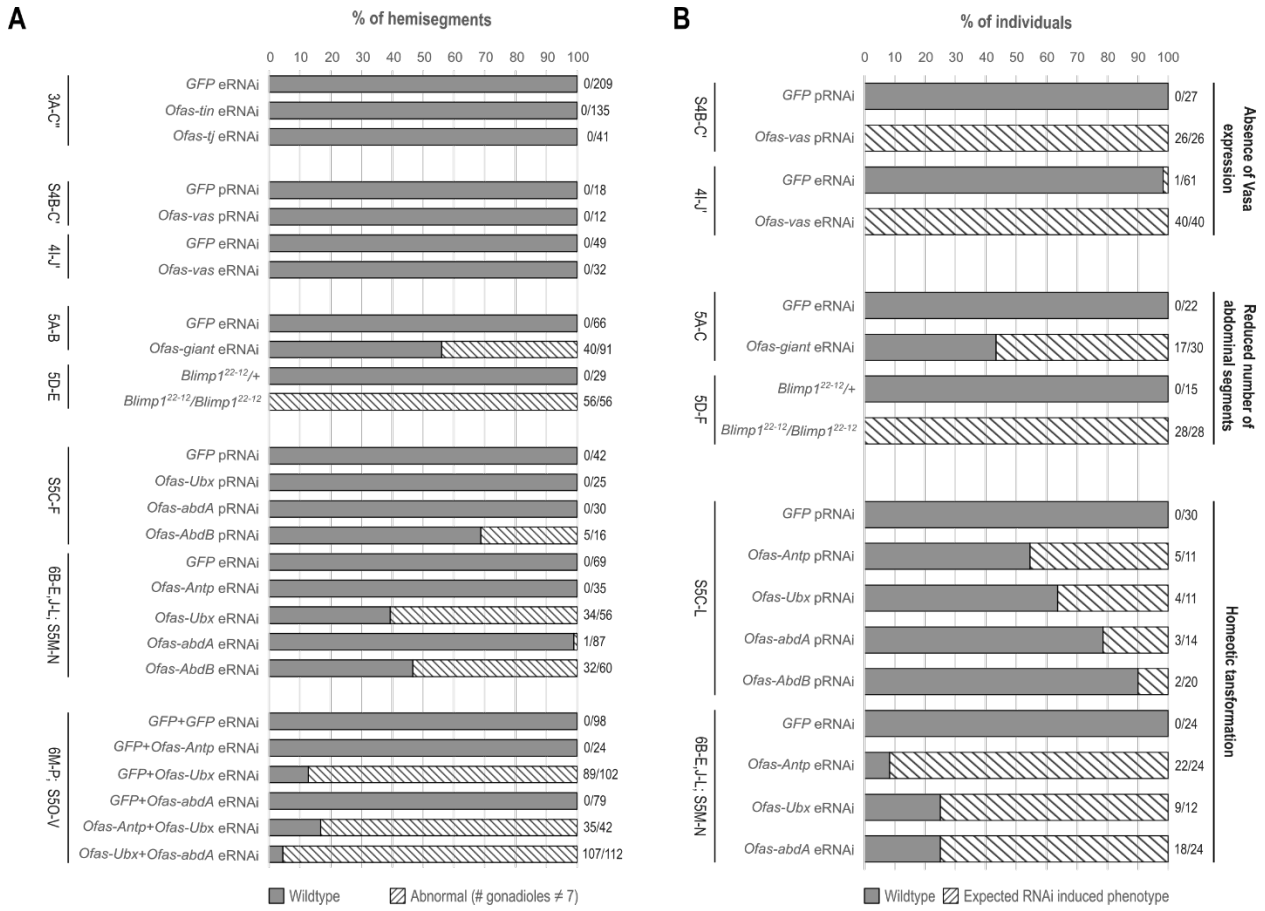


Figure S6. Phenotypic penetrance of dsRNA-induced phenotypes. (A) Bar plots showing the percentage of hemisegments containing an abnormal number of gonadioles (n ≠ 7) for each experimental manipulation. The corresponding figure number is indicated to the left of each plot, and the ratio of abnormal hemisegments to the total number of hemisegments analysed is indicated to the right. Abnormal hemisegments are shown as a hatched bar while wild type hemisegments are shown as a solid grey bar. **(B)** Bar plots showing the penetrance of expected dsRNA induced phenotypes as a percentage of the total number of individuals examined. The efficacy of dsRNA was assessed as the percentage of embryos lacking detectable Ofas-Vas protein expression in the germ cells (absence of Ofas-Vas expression; Figure 4I-J', Figure S4B-C'). The efficacy of *Ofas-gt* dsRNA and the penetrance of the *Ofas-Blimp1*$^{22\text{-}12}$ homozygous phenotype were assessed as the percentage of embryos with a reduced number of abdominal segments (Reduced number of abdominal segments; Figure 5A-D). The efficacy of Hox gene dsRNA was assessed as the percentage of embryos exhibiting homeotic transformations, as described in Table S6. Efficacy was not quantified following embryonic injection of *Ofas-Abd-B* dsRNA because the injected embryos did not hatch and lacked an easily identifiable embryonic phenotype. The corresponding figure number is indicated to the left of each plot, and the ratio of individuals with expected dsRNA phenotypes to the total number of individuals analysed is indicated to the right. dsRNA-induced phenotypes are shown as a hatched bar; wild type individuals are shown as a solid grey bar.

Table S1. References for gonadial numbers presented in Figure 1A. This list includes the literature sources from which ovariole and testiole numbers were obtained.

Species	Ovariole references	Testiole references
Thermobia domestica	57,173–175	57,173,176
Cloeon dipterum	177–179	180
Gryllus campestris	181	182
Gryllus assimilis	183	183
Periplaneta americana	184	185
Oncopeltus fasciatus	60,61	60,61
Nasonia vitripennis	186	187
Tribolium castaneum	188–191	192–195
Bombyx mori	196,197	196,198
Anopheles gambiae	199	200
Aedes aegypti	201,202	203,204
Drosophila sechellia	19,31,38,39,205,206	207
Drosophila melanogaster	19,31,38	207,208
Drosophila virilis	209	210

Table S2. Staging table for stages of wild type *O. fasciatus* embryonic development considered in this study. Descriptions of embryonic stages, adapted from [63] with corresponding descriptions of somatic gonad development, through to 100 hours after egg laying (h AEL). All times correspond to wild type development at 28°C and 70% relative humidity.

Stage	h AEL	Stage description	Somatic gonad development
1	0	Freshly laid egg.	Not yet specified.
2	20-26	Uniform blastoderm.	Not yet specified.
3	26-28	An indentation appears at the posterior end of the egg, called the posterior pit.	Not yet specified.
4	28-32	The germ band has invaginated into the posterior pit and extends toward the anterior. The orientation of the germ band is reversed with respect to the egg; i.e., the posterior end of the germ band is closer to the anterior of the egg.	Not yet specified.
5	32-36	The thorax region is wider than the abdomen region (mediolaterally), but limb buds are not yet distinct. Segments have been specified up to A5-A7 based on gene expression, but are not yet morphologically distinguishable.	Not yet specified.
6	36-44	Limb buds are now distinct semicircles. Segments have been specified up to A7-A9 based on gene expression, but are not yet morphologically distinguishable.	Not yet specified.
7	42-50	Segments start to become visibly distinct in the anterior abdomen around the time A9 is specified. Posterior tip is still round. Neural groove has formed at most up to A3.	Not yet specified.
8	48-54	Legs and gnathal appendages are triangular rather than semicircular lobes. A11 starts to thicken but the posterior tip is still mostly round.	Primary *Ofas-tin* expression domains appear at the lateral margin of each segment sequentially from anterior to posterior, from the labial segment to segment A10. Secondary *Ofas-tin* expression domains appear anterior and medial to the primary domains in segments A1-A7, at the same time as the appearance of primary *Ofas-tj* expression domains in the posterior compartments of segments A1-A6.
9	52-64	Neural groove has formed up to A8-A9. Coelomic cavities are visible as pits in all abdominal segments up to A9, though they may sometimes be obscured by germ cells, especially in A4-A6. Posterior end has folded over to form the proctodeum. Lateral margins of the germ band are thickening in the gnathal and thoracic segments.	In early stage 9 (9e), secondary *Ofas-tj* expression domains appear medial and adjacent to the secondary *Ofas-tin* domains. As the stage progresses (9l), primary and secondary *Ofas-tj* domains and secondary *Ofas-tin* domains are connected in segmentally repeated units

10	60-64	Lateral margins of the germ band are thickening in the abdomen. Ganglia appear as two parallel rectangles in each segment, separated at the midline. Coelomic cavities are no longer distinct.	*Ofas-tj* is expressed in a single continuous domain spanning A1-A7.
11	64-68	Midline neuroblasts appear at segmental boundaries.	*Ofas-tin* expression is continuous along the lateral margin of the embryo.
12	68-72	Abdominal cross commissures have formed. Ganglia within a segment appear as pairs of half circles facing away from each other.	Gonadiole primordia are clearly identifiable with the *Ofas-tin*-expressing portion of each gonadiole parallel to the medial-lateral axis.
13	72-76	The germ band is wider at the thorax, such that the trunk is now roughly triangular. The germ band as a whole has retracted to roughly the length of the egg, and is concave on the ventral side.	The embryonic gonad begins to condense along the AP axis, now spanning segments A2-A6. As the embryo becomes wider laterally, the lateral end of the gonadiole primordium becomes tapered.
14	76-80	The embryo undergoes katatrepsis and begins dorsal closure.	The embryonic gonad continues to condense along the AP axis.
15	80-88	The embryo continues dorsal closure.	At early stage 15 (15e), the embryonic gonad continues to condense along the AP axis. Gonadioles remain roughly parallel to the medio-lateral axis. Later on during this stage (15l), gonadiole begin to rotate to become parallel to the AP axis.
16	88-100	Abdominal ganglia start to fuse.	Gonadioles are bundled together and are no longer lined up in a single plane. By the end of this stage, the gonad is positioned almost entirely within segment A2.
	138-144	Hatching.	Gonads are morphologically distinguishable as ovaries or testes.

Table S3. List of analysed genes. Genes analysed in this study, identified by their gene ID and scaffold number in Official Gene Set 1.2 (accessed between 10 March 2022 and 14 September 2024) of the *O. fasciatus* genome [160]. The "Annotated?" column indicates whether the gene was already previously identified and named in Official Gene Set 1.2. The "RACE?" column indicates whether RACE was performed to obtain full-length coding sequence. Full-length sequences obtained through RACE were deposited to GenBank and can be accessed with the accession numbers listed in the "GenBank Accession" column.

***O. fasciatus* gene name**	**Gene ID**	**Scaffold #**	**Annotated?**	**RACE?**	**GenBank accession**
Ofas-snail (*sna*)	OFAS025184	1781	yes	yes	PZ910024
Ofas-eyes absent (eya)	OFAS018834	4793	yes	yes	PZ910023
Ofas-tinman (*tin*)	OFAS005760	212	yes	yes	PZ276395
Ofas-traffic jam (*tj*)	OFAS000984	14	no	yes	PZ276396
Ofas-invected (*inv*)	OFAS025056	112	yes	no	
Ofas-giant (*gt*)	OFAS025035	3738	yes	no	
Ofas-Antennapedia (*Antp*)	OFAS006718	307	yes	no	
Ofas-Ultrabithorax (*Ubx*)[a]	OFAS025026 OFAS004892	3423 220	yes	no	
Ofas-abdominal A (*abd-A*)	OFAS025133	1365	yes	no	
Ofas-Abdominal B (*Abd-B*)	OFAS025323	293	yes	no	
Ofas-Gapdh1	OFAS009253	1053	no	no	
Ofas-δ-Tubulin[b]	OFAS012604	982	no	no	

[a] The *Ofas-Ubx* gene model is split across two different scaffolds which have not yet been assembled together as of the most recent release. 025026 is exon 1 (5' end) and 004892 is exon 2 (3' end). The dsRNA sequence used in this study falls entirely within exon 1.
[b] The *Ofas-d-Tubulin* gene we report here, which was used for qPCR normalization (see Table S8), was amplified with primers that we previously [79] reported as amplifying Ofas-β-Tubulin, before the current genome assembly [160] was available. Based on the current genome assembly, we now believe that the primers used in this study amplify *Ofas-d-Tubulin*, as all reciprocal BLAST hits of the amplicon obtained with these primers are identified as δ-tubulin.

bioRxiv preprint doi: https://doi.org/10.64898/2026.10.09.752918; this version posted October 16, 2026. The copyright holder for this preprint (which was not certified by peer review) is the author/funder, who has granted bioRxiv a license to display the preprint in perpetuity. It is made available under a CC-BY 4.0 International license.

Table S4. Raw gonadiole counts. Gonadiole counts across various experimental conditions described in this study. For embryonic gonadiole number quantification, each data point represents the number of gonadioles on either the left or the ride side of an embryo (corresponding to the number of gonadioles that would be in one adult gonad).

			gonadiole number										
Figure		***n***	**0**	**1**	**2**	**3**	**4**	**5**	**6**	**7**	**8**	**9**	**10**
	wild type adult gonadiole number												
1B	testiole number per adult testis	20	0	0	0	0	0	0	0	20	0	0	0
	ovariole number per adult ovary	20	0	0	0	0	0	0	0	20	0	0	0
	embryonic gonadiole number per side in genetic manipulation experiments												
3A-C''	*GFP* eRNAi (2 µg/µl)	209	0	0	0	0	0	0	0	209	0	0	0
	Ofas-tj eRNAi (2 µg/µl)	41	0	0	0	0	0	0	0	41	0	0	0
	Ofas-tin eRNAi (2 µg/µl)	135	0	0	0	0	0	0	0	135	0	0	0
4I-J'	*GFP* eRNAi (2 µg/µl)	49	0	0	0	0	0	0	0	49	0	0	0
	Ofas-vas eRNAi (2 µg/µl)	32	0	0	0	0	0	0	0	32	0	0	0
S4B-C'	*GFP* pRNAi (5 µg/µl)	18	0	0	0	0	0	0	0	18	0	0	0
	Ofas-vas pRNAi (5 µg/µl)	12	0	0	0	0	0	0	0	12	0	0	0
5A-C	*GFP* eRNAi (2 µg/µl)	66	0	0	0	0	0	0	0	66	0	0	0
	Ofas-giant eRNAi (2 µg/µl)	91	0	0	5	10	8	10	7	51	0	0	0
5D-F	*Ofas-Blimp1*$^{22\text{-}12}$/+	29	0	0	0	0	0	0	0	29	0	0	0
	Ofas-Blimp1$^{22\text{-}12}$/*Ofas-Blimp1*$^{22\text{-}12}$	56	0	0	8	23	23	2	0	0	0	0	0
6B-E, J-L; S5M-N	*GFP* eRNAi (2 µg/µl)	69	0	0	0	0	0	0	0	69	0	0	0
	Ofas-Antp eRNAi (2 µg/µl)	35	0	0	0	0	0	0	0	35	0	0	0
	Ofas-Ubx eRNAi (2 µg/µl)	56	0	0	0	0	0	34	0	22	0	0	0
	Ofas-abd-A eRNAi (2 µg/µl)	87	0	0	0	0	0	1	0	86	0	0	0
	Ofas-Abd-B eRNAi (2 µg/µl)	60	0	0	0	0	0	0	0	28	4	5	23
6M-P; S5O-V	*GFP* eRNAi (4 µg/µl)	98	0	0	0	0	0	0	0	98	0	0	0
	GFP + *Ofas-Antp* eRNAi (2 µg/µl each)	24	0	0	0	0	0	0	0	24	0	0	0
	GFP + *Ofas-Ubx* eRNAi (2 µg/µl each)	102	0	0	0	0	0	89	0	13	0	0	0
	GFP + *Ofas-abd-A* eRNAi (2 µg/µl each)	79	0	0	0	0	0	0	0	79	0	0	0
	Ofas-Antp + *Ofas-Ubx* eRNAi (2 µg/µl each)	42	0	0	0	0	0	35	0	7	0	0	0
	Ofas-Ubx + *Ofas-abd-A* eRNAi (2 µg/µl each)	112	102	0	0	2	1	2	0	5	0	0	0
S5C–F	*GFP* pRNAi (1 µg/µl)	42	0	0	0	0	0	0	0	42	0	0	0
	Ofas-Ubx pRNAi (1 µg/µl)	25	0	0	0	0	0	0	0	25	0	0	0
	Ofas-abd-A pRNAi (1 µg/µl)	30	0	0	0	0	0	0	0	30	0	0	0
	Ofas-Abd-B pRNAi (1 µg/µl)	16	0	0	0	0	0	0	0	11	0	0	5

bioRxiv preprint doi: https://doi.org/10.64898/2026.10.09.752918; this version posted October 16, 2026. The copyright holder for this preprint (which was not certified by peer review) is the author/funder, who has granted bioRxiv a license to display the preprint in perpetuity. It is made available under a CC-BY 4.0 International license.

Table S5. Embryonic injection statistics. Survival statistics for embryonic injection experiments. All embryos were injected at 0-4 hours after egg laying. An embryo was scored as "survived" if it was still intact 24 hours after injection.

Figure	dsRNA	Concentration (µg/µl)	# injected	# survived	% survival
3A-C''	*GFP*	2	444	357	80.41
	Ofas-tj	2	114	67	58.77
	Ofas-tin	2	470	388	82.55
3D-G"	*GFP*	4	106	86	81.13
	GFP + *Ofas-tin*	2 each	105	104	99.05
	GFP + *Ofas-tj*	2 each	104	103	99.04
	Ofas-tin + Ofas-tj	2 each	159	147	92.45
4I-J'	*GFP*	2	119	117	98.32
	Ofas-vas	2	114	89	78.07
5A-C	*GFP*	2	392	330	84.18
	Ofas-gt	2	510	465	91.18
6B-E, J-L; S5M-N	*GFP*	2	615	558	90.73
	Ofas-Antp	2	113	109	96.46
	Ofas-Ubx	2	450	397	88.22
	Ofas-abd-A	2	559	485	86.76
	Ofas-Abd-B	2	437	406	92.91
6M-P; S5O-V	*GFP*	4	355	306	86.20
	GFP + *Ofas-Antp*	2 each	123	120	97.56
	GFP + *Ofas-Ubx*	2 each	355	326	91.83
	GFP + *Ofas-abd-A*	2 each	353	344	97.45
	Ofas-Antp + *Ofas-Ubx*	2 each	128	110	85.94
	Ofas-Ubx + *Ofas-abd-A*	2 each	354	337	95.20

Table S6. Penetrance of dsRNA-induced phenotypes. Phenotypes scored in addition to gonadiole primordia number in embryos and hatchlings following dsRNA treatments. For Hox gene knockdown experiments, representative images of homeotic transformations are included in Figure S5G–H", and are consistent with those described in previous reports [86].

Figure	Condition	# embryos analysed	# displaying phenotype	% penetrance	Observed phenotype
4I-J'	*GFP* eRNAi (2 µg/µl)	61	1	1.64	NA
	Ofas-vas eRNAi (2 µg/µl)	40	40	100.00	Absence of Vasa expression
S4B-C'	*GFP* pRNAi (5 µg/µl)	27	0	0.00	NA
	Ofas-vas pRNAi (5 µg/µl)	26	26	100.00	Absence of Vasa expression in laid embryos
5A-C	*GFP* eRNAi (2 µg/µl)	22	0	0.00	NA
	Ofas-gt eRNAi (2 µg/µl)	30	17	56.67	Reduction in the total number of abdominal segments
5D-F	*Ofas-Blimp1*$^{22\text{-}12}$/+	15	0	0.00	NA
	Ofas-Blimp1$^{22\text{-}12}$/*Ofas-Blimp1*$^{22\text{-}12}$	28	28	100.00	Reduction in the total number of abdominal segments
6B-E,J-L; S5M-N	*GFP* eRNAi (2 µg/µl)	24	0	0.00	NA
	Ofas-Antp eRNAi (2 µg/µl)	24	22	91.67	Complete transformation of all thoracic limbs to antennae
	Ofas-Ubx eRNAi (2 µg/µl)	12	9	75.00	Legs on segment A1
	Ofas-abd-A eRNAi (2 µg/µl)	24	18	75.00	Ectopic appendages on segments A2–A8
	Ofas-Abd-B eRNAi (2 µg/µl)	NA	NA	NA	No visible embryonic phenotype prior to hatching; embryos do not hatch
S5C-L	*GFP* pRNAi (1 µg/µl)	30	0	0.00	NA
	Ofas-Antp pRNAi (1 µg/µl)	11	5	45.45	Swelling of the distal femur
	Ofas-Ubx pRNAi (1 µg/µl)	11	4	36.36	Partial legs on segment A1
	Ofas-abd-A pRNAi (1 µg/µl)	14	3	21.43	Pigmentation in A5/A6
	Ofas-Abd-B pRNAi (1 µg/µl)	20	2	10.00	Ectopic pigmentation on segment A7

bioRxiv preprint doi: https://doi.org/10.64898/2026.10.09.752918; this version posted October 16, 2026. The copyright holder for this preprint (which was not certified by peer review) is the author/funder, who has granted bioRxiv a license to display the preprint in perpetuity. It is made available under a CC-BY 4.0 International license.

Table S7. Adult injection statistics. Survival statistics for adult injection experiments. An individual was scored as "survived" if it was still living ten days after injection.

Figure	dsRNA	Concentration (µg/µl)	sex	# injected	# survived	% survival
S3	*GFP*	1	females	27	13	48.15
	Ofas-tin	1	females	15	9	60.00
	Ofas-tj	1	females	14	8	57.14
	GFP	1	males	31	15	48.39
	Ofas-tin	1	males	21	4	19.05
	Ofas-tj	1	males	16	11	68.75
S4B-C'	*GFP*	5	females	6	6	100.00
	Ofas-vas	5	females	10	8	80.00
S5C-L	*GFP*	1	females	10	4	40.00
	Ofas-Antp	1	females	10	6	60.00
	Ofas-Ubx	1	females	10	6	60.00
	Ofas-abd-A	1	females	10	4	40.00
	Ofas-abd-B	1	females	20	9	45.00

Table S8. Primers used. Primers used in this study for experiments indicated in the headers. qPCR amplification efficiency for each primer pair was calculated from the slope of a standard curve generated by plotting C_g values against the logarithm of the input cDNA concentration for four serial dilutions [211].

RACE				
Ofas-tj	forward (3' RACE)	CAGCCGTTAGACCTGAGGCCACACTGTGCC		
	reverse (5' RACE)	GGCACAGTGTGGCCTCAGGTCTAACGGCTG		
Ofas-tin	forward (3' RACE)	GGTCTGCATGCCACACAAGCCCACTGAGAG		
	reverse (5' RACE)	CTCTCAGTGGGCTTGTGTGGCATGCAGACC		
dsRNA synthesis			**dsRNA size (bp)**	
GFP	forward	GGGTCCATGCCGAGAGTGATCC	482	
	reverse	TCGTCCATGCCGAGAGTGATCC		
Ofas-vas	forward	GGACTGGCAATGATGGTAGAGAAG	495	
	reverse	GGAAATTTGCACATGGTTCTACTCTTA		
Ofas-tin	forward	GGAGCGGAAGGGTACTCACCGT	467	
	reverse	GGCTTGTGTGGCATGCAGACCT		
Ofas-tj	forward	ATGACATGGTCTGGATGCCCCA	537	
	reverse	GGCCGTTCGGGTCTACCATCCT		
Ofas-gt	forward	GTTCTCTGCCCCCAAACCGCTC	460	
	reverse	CTCCCACCTTGCTGCTGCTTCC		
Ofas-Antp	forward	AACGGCCACCAGACGCCAGT	306	
	reverse	GAGAGGGCTGGGTAGGTTGGAGTTG		
Ofas-Ubx	forward	TTTCGAGCAGACGGGATTCTACGGT	512	
	reverse	TGGTGTTCAGACTGCACTGGTTCCA		
Ofas-abd-A	forward	GCACGGCGACTAACAACAGTTCCTC	374	
	reverse	AGCTGATACCTGTGTCGTGCAGGAG		
Ofas-Abd-B	forward	ACGAGCAGCCGTCCATAAAGACGTC	371	
	reverse	CCAGGAGTTCCCGAACGACTGATGG		
qPCR			**Amplicon size (bp)**	**Primer efficiency (%)**
Ofas-δ-Tubulin	forward	CCCGCAAGGAAATCACTCT	199	99

	reverse	TGATCCCTTACCTCGACACA		
Ofas-GapDH1	forward	TGGCAAACTAACTGGCATGGCA	171	98
	reverse	ACAACCTGGTCATCAGTGTACGCCA		
Ofas-vas	forward	TTGCATAGCCTATGGTGGGACAGT	209	118
	reverse	GCAGCAACATCTTCTCAACCGC		
Ofas-Ubx	forward	CAGACGCTGGAGCTGGAGAAGGA	169	99
	reverse	CGTTCAGCTCCTTGATCGCCTGG		
Ofas-abd-A	forward	TCTACGGACTGCACCACCAGAAC	226	98
	reverse	AACGGGCTCATCCAATCGGTGA		
Ofas-Abd-B	forward	TCTCCACATGCCATCAGTCGTT	263	98
	reverse	CGTCCATTCCAGGGGGTTGTTA		
colorimetric *in situ* hybridisation				
Of-sna	forward	AAGATCACCACCGGCCACTGGA	667	
	reverse	TGGAGATGGGCTCGGAGGTTGG		
Of-eya	forward	CACCACCAGACTGGCAGGCATG	926	
	reverse	GGAGCCAGTGAGCAAGCTGTGG		

Table S9. Sequences of oligos used in hybridisation chain reaction (HCR) experiments. All HCR probes except for that for *Ofas-inv* were designed using HCR Probe Maker (Özpolat lab, Washington University Saint Louis [167]) and ordered from Integrated DNA Technologies as oPools (oligo pools). The *Ofas-inv* probes were obtained from Molecular Instruments by submitting a partial cDNA sequence (shown below).

Sequences for pool name B1_Of-tin_20_Dla0
GAGGAGGGCAGCAAACGGaaTTTATTCAGTTCCTGGGTTACAGAC
AAAATAAAGGCAGGAAAATCTGCTTtaGAAGAGTCTTCCTTTACG
GAGGAGGGCAGCAAACGGaaTATCACTCTTCATTAATTACTTGTA
TTTTATATAACTTTCTTTGACTTCTtaGAAGAGTCTTCCTTTACG
GAGGAGGGCAGCAAACGGaaAATGACTGATTAAACAGAATGGGAC
TACAAATCTATGGAAACAAAATAAAtaGAAGAGTCTTCCTTTACG
GAGGAGGGCAGCAAACGGaaTTTATTCCTATCATAATTTTAAAAC
AAGCGTAATTATTATTAATAATTTAtaGAAGAGTCTTCCTTTACG
GAGGAGGGCAGCAAACGGaaTGTAGAGATCTCTTCTTAGGGCTTT
AATATTTGTAAATTAACACTCATGAtaGAAGAGTCTTCCTTTACG
GAGGAGGGCAGCAAACGGaaCACAGCAGCTACTATTTTCACAATT
TTTTCTACAGTGCGCTTTAGTTAAGtaGAAGAGTCTTCCTTTACG
GAGGAGGGCAGCAAACGGaaAAATCACATACGCTAACTTAAAGAA
AGAATCTCTAGGAGATAAGTTATAAtaGAAGAGTCTTCCTTTACG
GAGGAGGGCAGCAAACGGaaCCTCAGAATAGTGAGGGTGAGGGAT
TCCAATTAGGGTCATGAGTGAGGAGtaGAAGAGTCTTCCTTTACG
GAGGAGGGCAGCAAACGGaaTGGTTGTTGATAAAAGGATTGGTAC
TGGAAGGGTTGGCTGAAAGGTTAGTtaGAAGAGTCTTCCTTTACG
GAGGAGGGCAGCAAACGGaaTACCAGTAGTTACTCTCAGTGGGCT
GGTTGACTTGGGTCCTCCATACTTGtaGAAGAGTCTTCCTTTACG
GAGGAGGGCAGCAAACGGaaCTCCAGGCTCAGATTTAACAACAAT
GTGGCATGCAGACCTTGGTTACTTCtaGAAGAGTCTTCCTTTACG
GAGGAGGGCAGCAAACGGaaCCTTCTGTTTTGAAACCAAATTTTA
ATCACTCTTCATCCGCTTCACTTTGtaGAAGAGTCTTCCTTTACG
GAGGAGGGCAGCAAACGGaaGCCATCACCTCTCGTTCTGAGGCAG
TGTGTGGAAGTTAGTTTGATTGCGTtaGAAGAGTCTTCCTTTACG
GAGGAGGGCAGCAAACGGaaCCAATTCATATACTTGAGCCTGAGT

AATATCGCTGCTGCTTGAATCTCCTtaGAAGAGTCTTCCTTTACG
GAGGAGGGCAGCAAACGGaaCTGTTTAGAATCTTTCTTGTTATCA
TAATATTCTAGGCTTTCTTTTCCCAtaGAAGAGTCTTCCTTTACG
GAGGAGGGCAGCAAACGGaaTTGACTGTGGAGGAGACCTGTGGAG
TCTCGTGATCTATGCTTTAGGGGAAtaGAAGAGTCTTCCTTTACG
GAGGAGGGCAGCAAACGGaaACTCGCCCCAGTCCAGCGGGTAGCC
GTGTCTGTGCGAGATCGGTCCATGCtaGAAGAGTCTTCCTTTACG
GAGGAGGGCAGCAAACGGaaGAGGTTCAGAATGTCCTTCACCGAG
TAGCTCGAGGGGTTCCATTTCTCCAtaGAAGAGTCTTCCTTTACG
GAGGAGGGCAGCAAACGGaaTACATCGCTACCATAACCCCTGCAA
GGTGAGTACCCTTCCGCTCCGTAGCtaGAAGAGTCTTCCTTTACG
GAGGAGGGCAGCAAACGGaaACGAATCAACTGATATCAAGCTCTG
GAGGCAATGGTAGTTGTAAGAAGAGtaGAAGAGTCTTCCTTTACG
GTCCCTGCCTCTATATCTttTTTATTCAGTTCCTGGGTTACAGAC
AAAATAAAGGCAGGAAAATCTGCTTttCCACTCAACTTTAACCCG
GTCCCTGCCTCTATATCTttTATCACTCTTCATTAATTACTTGTA
TTTTATATAACTTTCTTTGACTTCTttCCACTCAACTTTAACCCG
GTCCCTGCCTCTATATCTttAATGACTGATTAAACAGAATGGGAC
TACAAATCTATGGAAACAAAATAAAttCCACTCAACTTTAACCCG
GTCCCTGCCTCTATATCTttTTTATTCCTATCATAATTTTAAAAC
AAGCGTAATTATTATTAATAATTTAttCCACTCAACTTTAACCCG
GTCCCTGCCTCTATATCTttTGTAGAGATCTCTTCTTAGGGCTTT
AATATTTGTAAATTAACACTCATGAttCCACTCAACTTTAACCCG
GTCCCTGCCTCTATATCTttCACAGCAGCTACTATTTTCACAATT
TTTTCTACAGTGCGCTTTAGTTAAGttCCACTCAACTTTAACCCG
GTCCCTGCCTCTATATCTttAAATCACATACGCTAACTTAAAGAA
AGAATCTCTAGGAGATAAGTTATAAttCCACTCAACTTTAACCCG
GTCCCTGCCTCTATATCTttCCTCAGAATAGTGAGGGTGAGGGAT
TCCAATTAGGGTCATGAGTGAGGAGttCCACTCAACTTTAACCCG
GTCCCTGCCTCTATATCTttTGGTTGTTGATAAAAGGATTGGTAC
TGGAAGGGTTGGCTGAAAGGTTAGTttCCACTCAACTTTAACCCG
GTCCCTGCCTCTATATCTttTACCAGTAGTTACTCTCAGTGGGCT
GGTTGACTTGGGTCCTCCATACTTGttCCACTCAACTTTAACCCG

GTCCCTGCCTCTATATCTttCTCCAGGCTCAGATTTAACAACAAT
GTGGCATGCAGACCTTGGTTACTTCttCCACTCAACTTTAACCCG
GTCCCTGCCTCTATATCTttCCTTCTGTTTTGAAACCAAATTTTA
ATCACTCTTCATCCGCTTCACTTTGttCCACTCAACTTTAACCCG
GTCCCTGCCTCTATATCTttGCCATCACCTCTCGTTCTGAGGCAG
TGTGTGGAAGTTAGTTTGATTGCGTttCCACTCAACTTTAACCCG
GTCCCTGCCTCTATATCTttCCAATTCATATACTTGAGCCTGAGT
AATATCGCTGCTGCTTGAATCTCCTttCCACTCAACTTTAACCCG
GTCCCTGCCTCTATATCTttCTGTTTAGAATCTTTCTTGTTATCA
TAATATTCTAGGCTTTCTTTTCCCAttCCACTCAACTTTAACCCG
GTCCCTGCCTCTATATCTttTTGACTGTGGAGGAGACCTGTGGAG
TCTCGTGATCTATGCTTTAGGGGAAttCCACTCAACTTTAACCCG
GTCCCTGCCTCTATATCTttACTCGCCCCAGTCCAGCGGGTAGCC
GTGTCTGTGCGAGATCGGTCCATGCttCCACTCAACTTTAACCCG
GTCCCTGCCTCTATATCTttGAGGTTCAGAATGTCCTTCACCGAG
TAGCTCGAGGGGTTCCATTTCTCCAttCCACTCAACTTTAACCCG
GTCCCTGCCTCTATATCTttTACATCGCTACCATAACCCCTGCAA
GGTGAGTACCCTTCCGCTCCGTAGCttCCACTCAACTTTAACCCG
GTCCCTGCCTCTATATCTttACGAATCAACTGATATCAAGCTCTG
GAGGCAATGGTAGTTGTAAGAAGAGttCCACTCAACTTTAACCCG

Sequences for pool name B5_Of-tj_32_Dla0

CTCACTCCCAATCTCTATaaTCAAGTATTTATTGCTTATTCCAAT
ATTGTACAATTGATATGGTGTAATCaaCTACCCTACAAATCCAAT
CTCACTCCCAATCTCTATaaTTTAGTAAAACTTATTACCAAAAGT
ATCTATGGAAGCTAAAATATTTACAaaCTACCCTACAAATCCAAT
CTCACTCCCAATCTCTATaaCTATTCGAAAATTATCAGCTTAAAT
AAAAGTTATTTACAAAATTACAGTCaaCTACCCTACAAATCCAAT
CTCACTCCCAATCTCTATaaATTGACCCGTTTTGTGACTTGTTTG
AATAACTCATGAACGTGTTGTAATTaaCTACCCTACAAATCCAAT
CTCACTCCCAATCTCTATaaGACAGAACTTCCTGGCAAGGAGAGG
GGAATGGAGAAGGAAACCAGCTGTAaaCTACCCTACAAATCCAAT
CTCACTCCCAATCTCTATaaAGGTACTGAGTAACTATGGTCAGTT

TTTTCATGAATCTATTTGTATTCTAaaCTACCCTACAAATCCAAT
CTCACTCCCAATCTCTATaaTCTTTAAAATGAAAACAATATATTT
TTTGGAATGCAATCTATATGTATGCaaCTACCCTACAAATCCAAT
CTCACTCCCAATCTCTATaaCTATAAAACAATAATCTTATTGCAA
AAAATTATACTTTAAACATTATTAAaaCTACCCTACAAATCCAAT
CTCACTCCCAATCTCTATaaCGAAGAGGCGGTCATGATATGATAA
AAAATATTGTCCCTCATCTTTCACTaaCTACCCTACAAATCCAAT
CTCACTCCCAATCTCTATaaATAATACTCTACAATAACGATTCTA
TTTTCAATGTAACTGACACATCAGTaaCTACCCTACAAATCCAAT
CTCACTCCCAATCTCTATaaTCATTTTATATAAATGTACAATAGC
AGTAGTAAAATATTTGAAACCTCTCaaCTACCCTACAAATCCAAT
CTCACTCCCAATCTCTATaaTACTCGTCAGATACTGCTACGAAAT
TAAGAGAGCTTATGTTAAATATAATaaCTACCCTACAAATCCAAT
CTCACTCCCAATCTCTATaaTGTACATAACAGCCTAAACAGGCGT
AACATTTACAGCGTAGATCAAAGTTaaCTACCCTACAAATCCAAT
CTCACTCCCAATCTCTATaaAATATATATATATTATATTATATAT
TAAATTAAATCTTCATATTATATATaaCTACCCTACAAATCCAAT
CTCACTCCCAATCTCTATaaGTTACACGAATCAAACTAAAGACTG
ATATATATCTTCATATAAATCTCCAaaCTACCCTACAAATCCAAT
CTCACTCCCAATCTCTATaaCATGTAAACATCCTGGCCGTTCGGG
CCTCTAGAGCTGGGATTACCTGTGTaaCTACCCTACAAATCCAAT
CTCACTCCCAATCTCTATaaGCTTCCAACTTCTGTTTGTAGAGAT
ACCATCCTCTCTCTCTTCCTGAGAAaaCTACCCTACAAATCCAAT
CTCACTCCCAATCTCTATaaACTTCAGCGTGTGGATCTCTCTCTG
GTTCGCAGGATACGTTGTTCAAATCaaCTACCCTACAAATCCAAT
CTCACTCCCAATCTCTATaaCCGCTGGTGCAGCCTCTTGCTGCGA
CTCCCTGTTCATCATCTCCAGCTCGaaCTACCCTACAAATCCAAT
CTCACTCCCAATCTCTATaaGTCCGTCGCTTCTGCTTCAATTTGA
TTCTGGGCGTATCCGCGGTTCTTCAaaCTACCCTACAAATCCAAT

Sequences for pool name B1_Of-Antp_12_Dla0

GAGGAGGGCAGCAAACGGaaCCGAGGTCTCCCTTCGTCTTATTCT
GGGGATAAGTCGCTTCCTTCGTTGGtaGAAGAGTCTTCCTTTACG

GAGGAGGGCAGCAAACGGaaACCAGATCTTGATCTGCCGCTCGGT
TCTTCCACTTCATCCTCCTGTTCTGtaGAAGAGTCTTCCTTTACG
GAGGAGGGCAGCAAACGGaaCCGCCTCCTCGTCAGGTACCTGTTG
GCAGAGGGCGTGGGCTATCTCTATCtaGAAGAGTCTTCCTTTACG
GAGGAGGGCAGCAAACGGaaTGGTACCTCGTGTAGGTCTGCCGCC
TGGAACTCCTTCTCCAGCTCCAGCGtaGAAGAGTCTTCCTTTACG
GAGGAGGGCAGCAAACGGaaAGGGGTAGAGAGGGCTGGGTAGGTT
TCTTCCTCTCGAACTGACTCCTCATtaGAAGAGTCTTCCTTTACG
GAGGAGGGCAGCAAACGGaaTCATGGTGTGCTGGGGCTGGGGCTG
GGGGTGGTGGGGCCCCGTTGTTGTAtaGAAGAGTCTTCCTTTACG
GAGGAGGGCAGCAAACGGaaCATGTGGTGACCCTGGTGGTGATGG
CTGGGCGGCCGCGTGGTGGCTCTGGtaGAAGAGTCTTCCTTTACG
GAGGAGGGCAGCAAACGGaaGGCCCGCCAATGCCGTTGCCGACGG
TTCATGTCCATCTCCGGAGGGCTCTtaGAAGAGTCTTCCTTTACG
GAGGAGGGCAGCAAACGGaaCTGGCGTCTGGTGGCCGTTCTGGCC
CCTGGAGCTTGCAAGAAGCGTACACtaGAAGAGTCTTCCTTTACG
GAGGAGGGCAGCAAACGGaaGCGAGTCCGCCCGGTAGTCCATGCC
CCCCGCCACCGCCGCCCATGGAGGCtaGAAGAGTCTTCCTTTACG
GAGGAGGGCAGCAAACGGaaGCCCACCGCTGCGTAGTGGTGCTGC
GGGGTCGCAAGCGGTGGGGTCCTCGtaGAAGAGTCTTCCTTTACG
GAGGAGGGCAGCAAACGGaaCCGTTACGCAGGTCCGGCATGTACG
TGAGGGTGTTCGGCCGGCACCACACtaGAAGAGTCTTCCTTTACG

Sequnces for pool name B5_Of-Ubx_16_Dla0

CTCACTCCCAATCTCTATaaTGCCGCTGCCGCTGCGGCCTTCTGC
CTAGTGGTCCTGCTGCTGAGCGACCaaCTACCCTACAAATCCAAT
CTCACTCCCAATCTCTATaaTCCTTGATCGCCTGGATCTCCTTCT
TGCGCCTGCTTCTCCTGCTCGTTCAaaCTACCCTACAAATCCAAT
CTCACTCCCAATCTCTATaaTCTTGATCTGCCGCTCGGTGAGGCA
GCTTCATCCTCCTGTTCTGGAACCAaaCTACCCTACAAATCCAAT
CTCACTCCCAATCTCTATaaCCTCGTGAGGTAGTGGTTCGTGTGG
GGCGTGGGCCATCTCTATCCTCCGCaaCTACCCTACAAATCCAAT
CTCACTCCCAATCTCTATaaCTCGTGTAGGTCTGTCGTCCGCGCC

TCCTTCTCCAGCTCCAGCGTCTGGTaaCTACCCTACAAATCCAAT
CTCACTCCCAATCTCTATaaCCATCCATGGGTAAAATGTGTGATT
GGAGGCCGTTCGCTCCTGCTGCAATaaCTACCCTACAAATCCAAT
CTCACTCCCAATCTCTATaaCTGGGTGGCAGTGGTGTTCAGACTG
AGGCTGTTGATGGAGTTGTCCTGCCaaCTACCCTACAAATCCAAT
CTCACTCCCAATCTCTATaaGCCGAGGAAGTCCTGCTCACCGCAC
TGGTTCCAGGAGGCAGGAGCGAGGGaaCTACCCTACAAATCCAAT
CTCACTCCCAATCTCTATaaTGTCTGGAGTGCAGGCGGCCGGTCG
GACTCCCATCCCCGCCGAGATAACGaaCTACCCTACAAATCCAAT
CTCACTCCCAATCTCTATaaGGCCGCCGACTGCCAGACGTCTTTG
CAAGGGATTGGCCGAGGGAGTGCCCaaCTACCCTACAAATCCAAT
CTCACTCCCAATCTCTATaaCCGTTCTGGTGGGTGGCGGGCTCCG
GCGGCGGCTGCCACAACAGCGGCATaaCTACCCTACAAATCCAAT
CTCACTCCCAATCTCTATaaAGTTGACGCTGGTCTGGTTCTCGCC
TGGAGCAGTCCGGCTTCGTGGTGGAaaCTACCCTACAAATCCAAT
CTCACTCCCAATCTCTATaaGACGGAGGCGTCGTACGGCGAGTCC
GGCCGAGGAGTACAGCTTGCAGGCGaaCTACCCTACAAATCCAAT
CTCACTCCCAATCTCTATaaTGGTGGTGGTGCTGCGTCGAGGCGT
GGCGGCCTCGACTGGTGCAGTGAGTaaCTACCCTACAAATCCAAT
CTCACTCCCAATCTCTATaaTGTACGCCGCGGCCGTCTGGTCATG
GCGACATGCCTATGCCCAAGGGGAAaaCTACCCTACAAATCCAAT
CTCACTCCCAATCTCTATaaTGAACCGTAGAATCCCGTCTGCTCG
GGCCGCCGTGGCGCTCTGATGGTGAaaCTACCCTACAAATCCAAT

Sequnces for pool name B3_Of-abd-A_16_Dla0

GTCCCTGCCTCTATATCTttTTTGAGGAGGTCGGCTCCCGTGCCC
CTATGTCTGCACTTTGGTGACGACAttCCACTCAACTTTAACCCG
GTCCCTGCCTCTATATCTttGTTCTGTGGGTTCTGGGGCTGTTCC
GGGGTCGTGTATCTGGTGGTGCTGTttCCACTCAACTTTAACCCG
GTCCCTGCCTCTATATCTttTCCTGTTCCTCCCGTTCCCTCCTCG
TTCTGCTGCTTCTCCTTGTTCATCCttCCACTCAACTTTAACCCG
GTCCCTGCCTCTATATCTttGCTCCTTCTTCAGCTTCATCCTCCT
GCTCGTTTATCTCCTTCACCGCCCTttCCACTCAACTTTAACCCG

GTCCCTGCCTCTATATCTttGGTGAGGCAGAGGGCGTGGGCTATC
CTGGAACCAGATCTTGATCTGCCGCttCCACTCAACTTTAACCCG
GTCCCTGCCTCTATATCTttTTAAAGTGAAATTCCTTTTCCAGCT
ATCCTCCGCCTCCTCGTCAGGTAGTttCCACTCAACTTTAACCCG
GTCCCTGCCTCTATATCTttGGCCTCTTCGTCGTGGGCAGCCGTT
GTGTCTGGAATCGGGTGTAGGTCTGttCCACTCAACTTTAACCCG
GTCCCTGCCTCTATATCTttGAACGGGCTCATCCAATCGGTGATG
TCCTGGTAACATACATACGACTCTGttCCACTCAACTTTAACCCG
GTCCCTGCCTCTATATCTttATGGGCTGGCCAGCGGCCGCGGCAG
ATCCAGGGGTAGCGAGGGATGTCGGttCCACTCAACTTTAACCCG
GTCCCTGCCTCTATATCTttCTGGTGGTAGAACTGAGCCGCCGCT
GGGGTCGGCGGCAGAAGCCGCAGCCttCCACTCAACTTTAACCCG
GTCCCTGCCTCTATATCTttGCCGCCGACGCCCCGTTCTGGTGGT
ATGGAAGCCGATGCCGCCGACACCGttCCACTCAACTTTAACCCG
GTCCCTGCCTCTATATCTttAGCCCGTGTACCTGCAGGACTTGTC
GTCCGTAGACGGGGTCTGTCGTGGCttCCACTCAACTTTAACCCG
GTCCCTGCCTCTATATCTttGTTGGTGGTGGTGGTGTGCGGCCAC
CCCCGGCTCCCGCGAACAGTCCCTGttCCACTCAACTTTAACCCG
GTCCCTGCCTCTATATCTttGAGTGACGGTGGAGGCGAGGAAGAC
CGGGTACATCCTCGAGGCGGAACTGttCCACTCAACTTTAACCCG
GTCCCTGCCTCTATATCTttCTGTAATTCACTGCTGACGGACTGT
GAGGAACTGTTGTTAGTCGCCGTGCttCCACTCAACTTTAACCCG
GTCCCTGCCTCTATATCTttGCTGATGATGATACTGCTGGTGGTA
AACTCGTCGTGATCACTGGGTTCAAttCCACTCAACTTTAACCCG

Sequences for pool name B4_Of-Abd-B_16_Dla0

CCTCAACCTACCTCCAACaaGGGAGGGTGATGGGGTACCATCTGA
TCACTGGTGGTGTTTCATGGCTCCAatTCTCACCATATTCGCTTC
CCTCAACCTACCTCCAACaaTTGTTCGCGGCGCTGCTGTTGTTGT
GGAGGGTGGTGAGCGTGGTGGTTGGatTCTCACCATATTCGCTTC
CCTCAACCTACCTCCAACaaTGTTCTTCTTGTTCTTCATCCGTCT
TGGCGGCCTGGGCCGCCTGCCGCTGatTCTCACCATATTCGCTTC
CCTCAACCTACCTCCAACaaGGTCAGGTTGAGGTTCCTCGCCAGC

CTGGAACCAGATCTTCACCTGCCGCatTCTCACCATATTCGCTTC
CCTCAACCTACCTCCAACaaTTGAAGAGGAACTCCTTCTCCAGCT
CACCTCTTCTGCTTAGAGACGTAGGatTCTCACCATATTCGCTTC
CCTCAACCTACCTCCAACaaGCTTCTTCCTCACCGTCACCTGGCC
GGGTCTGGAACTTGGAGTAGGGCTTatTCTCACCATATTCGCTTC
CCTCAACCTACCTCCAACaaACCTGGTGGAGGGTAAGGGGTGGAC
CCCCATGCCGGGCATCCCCACACCAatTCTCACCATATTCGCTTC
CCTCAACCTACCTCCAACaaAAGTCGTGGCCGAATCCGGGGCCAG
ACGGGTTCGGGCGGAGGGTAGTTCCatTCTCACCATATTCGCTTC
CCTCAACCTACCTCCAACaaCCGTCGAAGGCAGGTAGCCGGGCTC
ACCCGTCACTCATCGCTCGCCGCTCatTCTCACCATATTCGCTTC
CCTCAACCTACCTCCAACaaGTAGCCGCACCAGGAGTTCCCGAAC
GTGATGTCGTCCGGCAGAGTAGGGCatTCTCACCATATTCGCTTC
CCTCAACCTACCTCCAACaaGCCGATGTCCCGGGAGTCACCGTCG
TGATGGCATGTGGAGACCGCCGGATatTCTCACCATATTCGCTTC
CCTCAACCTACCTCCAACaaTCCAGAAGAGGCTCGACTTGCGGTC
TGTACTTGTACTCCTGAGAGGCCGGatTCTCACCATATTCGCTTC
CCTCAACCTACCTCCAACaaCTGGGCGGGGTAGTCCGAGTACTCG
CCCGTCCGGCAGGTTGTAGTAGGTGatTCTCACCATATTCGCTTC
CCTCAACCTACCTCCAACaaTGGCGTATCACCCCGCCCGAGCCCT
GAGTAGTTCCAGTGGCCGTGGTGAGatTCTCACCATATTCGCTTC
CCTCAACCTACCTCCAACaaGGATGTGGAGAGGCCCGCTCTGACT
CGCACTCGTAGCCCAGTCTCTTGGCatTCTCACCATATTCGCTTC
CCTCAACCTACCTCCAACaaGGTGGTGACCGGTGTCGAGCTGGGC
CACCGGCGAGGTGGACGAGGCCGAAatTCTCACCATATTCGCTTC

Sequence for B4 Of-inv

GAGCGCAGGCCGTCGGCCTTCCACAGGATCGAGCTGTTAACGCTGAAAGAGCCCGCGGTGGAGCCTTCAGCACTCCCCTTCTCGGTGGA
CAACATCCTGCGACCGGAGTTCGGACGGCGGGTGCGACCTCCATTGGTCGCCGAGGAGCAGGACGAAGGACCTCCGCCGAACAAGATTG
ACCCACCCATTCCTGATGAACCGAATGGTCCTGTCTGGCCGGCCTGGGTCTACTGCACCCGCTACTCGGACAGGCCCAGCTCAGGAGGTA
GGAGACCCCGATCTCGAAGGATCAAGAGGAAAGACAAGAGCAAGGAAGACAAGAGGCCGAGGACGGCATTCAGCGGCGAACAGCTGGCC
AGACTCAAGACAGAGTTCAGCATCAACAGGTATCTTACTGAGCGACGGCGTCAAGCGTTGGCCTCCGAGCTTGGGCTGAACGAGGCTCAG
ATCAAGATCTGGTTCCAGAACAAGCGAGCCAAGATCAAGAAGGCCTCCGGGAACCGGAACCCTCTGGCACTCCAGCTGATGGCCCAGGGA
CTGTACAACCACTCGACGGTGCCCATGTCGGACGAGGAGTGCGACGAGAACACCAACTCCAACGGCCACTGACTGAGCGGGCTTCCTGAA

GAGCGTTCCCACGTGTCTCAGCACGGCTCCAGAGGAAGTCAGAGTCTTCGGCCATCCAGAACTTCCAAAGGAAACAATGAGAAATTCCATT
CAGACATTGGTTACATTATTATTGTAATCTTATAAAATTATTTGTTAATCGTTATCTTTGAGAACACACTTGATGTCTTTTCCACTGAAGGATGT
CATAATGGCAAGAACCGTTGCCGAAAAATTCAAGCGAAGCAACAATGATCAACCCCCCAACATAGACTTTGCATTGACACGAAGAGTAGATG
TGATTGCGGATTGGGCTTTGAAAAGAAATGAAACTCTGCATCATATTATGTCCGACTGCCTCTGTACCCAATGTCCATAGAGATTCTTCTAAT
GACAAATAATAATAATTGTCGTTGTTTAGCGGTAACTGCTTTACACTAACTTTAAACAATTAACGTTGAAAAAAGTGGATGGGAACTCATTACA
AGCTTTCTTCGATAACCAAGTATATTTTGGAAAGGGATACTACTCTTTAAAACGTTAAGATACATAAAAACTACATTTAAAGTTCGATAAACTT
CCTTAATTCCTAAAATGCTCTCAGAACAAAAGAAATGTAGAAGGAATGTACATCATCCAGAGAATTGACTGGTAAGCTCCTCTTCTGTCTTCT
AATCGTCTTCTGTGATGGGAAAGATATTCATGGCATGAAGTTTATGAAAGTAGAAGATTCATCTGTAGCCTGAATATTTCTTGCTTGAGATTT
GTGGAAGATACTTTCTGTTGAAGCCTTGAAACTCTCTTGGATAATATGATGACAAATACTCACCAGAATCACCCGACGAAGGATTTAAACAAA
GTGTGCTTAGGATTCCTAAGGGCGATTCGCCCTGTTTCGAAATAATTATTGCTTTTGAGAATTTTATTCAATCAGAGGTTTATATGTTATATGC
GAATGAAATTCCTGCTAGTTTTTCCTTAATCTCAATTTGTTTTGAGGGAGTAATTCACCTTTATGATTGGAATTTAAAGCTGTGTTTCAAATTTT
CAGCTGAGCCTCAGACTCAGACTAAGACTCAAAAGAACACTGCCAATAAAATCAACAATCCAAGAATCCGATACTCGATCATGGGATCTCAA
ATCCAAGACTGGGAAAATCCAAGAAACTGGGGCTTAATTTTGCCTTTTATTATATTATGTATTATGTTCCTATTAAGCCGTTTCTTTTTTATATT
ATTCTCAAGAGAAGGATTTGCATCATTATTAACTCTACATTTCCTTAGGTAGCTGATATTTTCAGTGAGTGATTTTAGTCCGTAAAGATGTTAA
AGGAAGAAAACAACTTGATAAGAAGAATAAAACAACTCGCATGAATAATCCAATAACAACTGATTGCAAAGTTGGTTAAAAAGCAGACATAAA
ATTGTTTGAATGTGTATTGTTTCTTTCTCTTCCTTAATGTCTGACTAGAGGCCCTCACAGATCAAATACTCGAA